Stochastic response determination and spectral identification of complex dynamic structural systems

Olga Brudastova

Submitted in partial fulfillment of the
requirements for the degree of
Doctor of Philosophy
in the Graduate School of Arts and Sciences

Columbia University
2018

This page is intentionally left blank.

© 2018
Olga Brudastova
All rights reserved

This page is intentionally left blank.

ABSTRACT

Stochastic response determination and spectral identification of complex dynamic structural systems

Olga Brudastova

Uncertainty propagation in engineering mechanics and dynamics is a highly challenging problem that requires development of analytical/numerical techniques for determining the stochastic response of complex engineering systems. In this regard, although Monte Carlo simulation (MCS) has been the most versatile technique for addressing the above problem, it can become computationally daunting when faced with high-dimensional systems or with computing very low probability events. Thus, there is a demand for pursuing more computationally efficient methodologies. Further, most structural systems are likely to exhibit nonlinear and time-varying behavior when subjected to extreme events such as severe earthquake, wind and sea wave excitations. In such cases, a reliable identification approach is of paramount importance for subsequent developments of diagnostic methods for fault/damage detection, monitoring of the structural system dynamic behavior and for assessing its reliability.

Current work addresses two research themes in the field of stochastic engineering dynamics related to the above challenges.

In the first part of the dissertation, the recently developed Wiener Path Integral (WPI) technique for determining the joint response probability density function (PDF) of nonlinear systems subject to Gaussian white noise excitation is generalized herein to account for non-white, non-Gaussian, and non-stationary excitation processes. Specifically, modeling the excitation process as the output of a filter equation with Gaussian white noise as its input, it is possible to define an augmented response vector process to be considered in the WPI solution technique. A significant advantage relates to the fact that the technique is still applicable even for arbitrary excitation power spectrum

forms. In such cases, it is shown that the use of a filter approximation facilitates the implementation of the WPI technique in a straightforward manner, without compromising its accuracy necessarily. Further, in addition to dynamical systems subject to stochastic excitation, the technique can also account for a special class of engineering mechanics problems where the media properties are modeled as non-Gaussian and non-homogeneous stochastic fields. Several numerical examples pertaining to both single- and multi-degree-of-freedom systems are considered, including a marine structural system exposed to flow-induced non-white excitation, as well as a beam with a non-Gaussian and non-homogeneous Young's modulus. Comparisons with MCS data demonstrate the accuracy of the technique.

In the second part of the dissertation, a novel multiple-input/single-output (MISO) system identification technique is developed for parameter identification of nonlinear time-variant multi-degree-of-freedom oscillators with fractional derivative terms subject to incomplete non-stationary data. The technique utilizes a representation of the nonlinear restoring forces as a set of parallel linear subsystems. In this regard, the oscillator is transformed into an equivalent MISO system in the wavelet domain. Next, a recently developed L_1-norm minimization procedure based on compressive sampling theory is applied for determining the wavelet coefficients of the available incomplete non-stationary input-output (excitation-response) data. Finally, these wavelet coefficients are utilized to determine appropriately defined time- and frequency-dependent wavelet based frequency response functions and related oscillator parameters. A nonlinear time-variant system with fractional derivative elements is used as a numerical example to demonstrate the reliability of the technique even in cases of noise corrupted and incomplete data.

Contents

List of Tables

This page is intentionally left blank.

List of Figures

Acknowledgements

The graduate program was a challenging experience for me, yet I am honored and grateful to have been a part of it. The journey was made attainable by the many people in my life who provided their constant support and encouragement.

First, I would like to thank my academic advisor, Prof. Ioannis A. Kougioumtzoglou, for giving me an opportunity to carry through my graduate studies, and for being a mentor who inspires and cares about their students' success. I got to learn from amazing faculty at Columbia who truly make this institution world-class, and I would like to extend special thanks to Prof. George Deodatis for providing mentorship outside the classroom. It has been my great pleasure to work with other graduate students and postdoctoral researchers in and outside Columbia, and to learn from them and with them. Further, I would like to acknowledge the work of the support staff of the CEEM department for their continuous assistance and help.

None of this would have been possible without the mental health professionals who sustained me throughout the past five years. Moreover, I am forever thankful to the Graduate Workers of Columbia for providing the sense of community that I could not always find in the academic environment.

My immense gratitude goes to all of my friends for letting me be myself.

Lastly, I would like to thank my parents, Olga Maksyutina and Yury Brudastov, for accepting my decision to live so far away from them.

This page is intentionally left blank.

Organization of the Thesis

The thesis consiststs of two parts followed by the list of cited references. Each part presents an independent research topic and provides a complete presentation of that research effort which includes an introductory section followed by the analytical derivations, verified by numerical example(s), and concluded with remarks and suggestions for future work.

The first part is dedicated to developing a Wiener Path Integral (WPI) based technique for response determination of nonlinear single- and multi-degree-of-freedom (SDOF and MDOF) engineering systems subject to non-white, non-Gaussian, and non-stationary stochastic excitations. The technique also allows to account for a class of systems with stochastic medium properties/parameters subject to deterministic excitations.

Chapter 1 serves as an introduction to the problem of interest, describes motivation and objectives for the study.

Chapter 2 provides an overview of the WPI framework, starting with Chapman-Kolmogorov (C-K) and Fokker-Planck (F-P) equations describing the associated Markov process, followed by the corresponding stochastic differential equation (SDE) and the derivation of the transition probability density function (PDF) for the studied process. A notion of a Lagrangian functional of a system is also introduced in this chapter.

In Chapter 3, the WPI technique is further generalized to account for non-white and non-Gaussian excitation processes via a filter approximation technique that allows to reproduce excita-

tions not readily available in the time domain, but rather described in the frequency domain in the form of the associated power spectrum. The full derivation of the Lagrangian and the path integral follows; calculus of variations is further used to obtain the appropriate Euler-Lagrange (E-L) equations and the boundary conditions to define the set of boundary value problems (BVPs) to be solved. The non-stationary nature of excitation processes is addressed in the next section of the current chapter through considering time-modulated power spectra. An appropriate modification to the WPI technique implementation is introduced in the context of the idea of a "switch" adopted, for example, from standard statistical linearization technique implementations. In addition, computational aspects regarding addressing both of those challenges (non-white/non-Gaussian and non-stationary processes) are discussed in this chapter.

In Chapter 4, several numerical examples pertaining to both SDOF and MDOF systems are considered, including a marine structural system exposed to flow-induced non-white excitation, as well as a bending beam with a non-Gaussian and non-homogeneous Young's modulus. Comparisons with Monte Carlo simulations (MCS) data demonstrate accuracy and reliability of the technique.

Chapter 5 concludes the first part of the thesis with remarks on the results and applicability of the proposed herein technique, as well as potential direction for the future work.

The second part of the current work describes a parameter identification technique utilizing the Generalized Harmonic Wavelet Transform (GHWT) suitable to treat nonlinear time-variant MDOF oscillators with fractional derivative elements subject to incomplete/limited data.

Chapter 6 provides introductory remarks, including motivation and goals, for the research project.

Chapter 7 addresses two major challenges in the field of system identification, namely, the non-stationary nature of the real-life data and its limited/incomplete availability. The first challenge can be approached via generalized harmonic wavelets transformation (GHWT) which allows to con-

sider signals exhibiting both time- and frequency-varying behavior. The incomplete data analysis is accomplished through the compressive sensing (CS) approach; a signal processing technique able to reconstruct signals recorded at the maximum frequency greater than half of the signal's sampling rate.

In Chapter 8, a system parameter identification technique is developed to treat nonlinear time-varying engineering systems with fractional derivative elements. The technique utilizes the generalized harmonic wavelet (GHW) treatment of the non-stationary signals and is based on the reverse multiple-input/single-output (MISO) approach well established in literature. The chapter presents full derivation of the method and is concluded with an algorithm outlining the procedure for parameter identification.

Chapter 9 presents numerical validation of the developed identification technique and considers a time-variant MDOF Duffing oscillator with fractional derivative elements. The reliability and robustness of the technique are shown in determining unknown system parameters, both time-varying and constant.

Chapter 10 provides concluding remarks on the second part of the dissertation and suggests directions for further implementation and development of the technique.

This page is intentionally left blank.

Part I

Wiener Path Integral based response determination of nonlinear systems subject to non-white, non-Gaussian, and non-stationary stochastic excitation

This page is intentionally left blank.

Chapter 1

Introduction

Uncertainty propagation in engineering mechanics and dynamics is a highly challenging problem that requires development of analytical/numerical techniques for determining the stochastic response of complex engineering systems. In this regard, although MCS has been the most versatile technique for addressing the above problem (e.g., [Rubinstein and Kroese, 2007, Spanos and Zeldin, 1998]), it can become computationally daunting when faced with high-dimensional systems or with computing very low probability events. Thus, there is a demand for pursuing more computationally efficient methodologies. In the field of stochastic engineering dynamics, a number of alternative techniques, such as stochastic averaging (e.g., [Roberts and Spanos, 1986, Spanos et al., 2011, Zhu, 1996]), statistical linearization (e.g., [Fragkoulis et al., 2016, Roberts and Spanos, 2003, Spanos and Kougioumtzoglou, 2012]), as well as methodologies based on Markov approximations and related Fokker-Planck equations [Lin, 1976], have been developed over the past few decades with varying degrees of accuracy.

More recently, a WPI technique, whose origins can be found in theoretical physics [Chaichian and Demichev, 2001], has been developed in the field of engineering dynamics for determining the response transition PDF of oscillators subject to Gaussian white noise excitation [Kougioumtzoglou and Spanos, 2012]. The idea of a path integral was first presented by Wiener within the

Brownian motion theory [Wiener, 1921], and later rediscovered and generalized by Feynman in quantum mechanics [Feynman, 1948]. The technique found a great variety of applications in the field of theoretical physics; e.g. theories of superfluidity, of unified electromagnetic and weak interactions, and of quantum chromodynamics. More specifically, it presented a valuable tool in determining system transition PDF for a great variety of stochastic processes via the Feynman-Kac formula [Feynman, 1948, Kac, 1949]. Moreover, both analytical and approximate numerical treatments of path integrals can be found in literature (e.g., [Brush, 1961, Feng et al., 1992, Gelfand and Yaglom, 1960, Wiegel, 1975]).

Despite the wide use of the WPI approach in various fields of theoretical physics, its application to engineering dynamics problems has been considered only recently by [Kougioumtzoglou and Spanos, 2012]. The WPI technique has been further generalized to account for MDOF systems and diverse nonlinear/hysteretic system modeling [Kougioumtzoglou and Spanos, 2014], as well as for systems endowed with fractional derivative terms [Di Matteo et al., 2014]. Next, the technique has been enhanced from a computational efficiency perspective by relying on its localization capabilities and invoking appropriate expansions for the response PDF [Kougioumtzoglou et al., 2015]. Moreover, it has been shown by [Kougioumtzoglou, 2017] that the technique can also address a special class of engineering mechanics problems where media properties are modeled as stochastic fields, while preliminary efforts on quantifying the error of the technique can be found in [Meimaris et al., 2018]. The latest improvement of the technique has been introduced by [Psaros et al., 2018b], where the computational efficiency has been improved by exploiting CS procedures in combination with group sparsity concepts and appropriate optimization algorithms. The technique also found a new area of application in the field of energy harvesting; more specifically, it was recently utilized in stochastic response determination and optimization of a class of nonlinear electromechanical energy harvesters [Petromichelakis et al., 2018]. Nevertheless, the WPI technique has been limited so far to treating Gaussian white noise excitation processes only.

The presented herein research is specifically aimed at developing a novel WPI based technique for response statistics determination of nonlinear MDOF systems subject to non-white, non-Gaussian and non-stationary excitation processes. The "filter" approximation [Spanos, 1986] is utilized to model such excitations as an output to a filter equation with a Gaussian white noise input. The resulting augmented response vector process is then considered in the WPI formulation. Moreover, the approach allows to account for the excitations not readily available in the time domain, but rather represented by power spectra in the frequency domain; this serves as a noticeable advantage and makes the technique widely applicable in the field of engineering dynamics. Finally, several numerical examples are presented , including a marine structure subject to flow-induced forces and a Euler-Bernoulli beam with a non-Gaussian and non-homogeneous Young's modulus. The results are then compared to the MCS data; the comparisons demonstrate accuracy and reliability of the technique for the wide variety of structural dynamics problems.

This page is intentionally left blank.

Chapter 2

WPI Formalism

2.1 Fokker-Planck equation

The derivation of the path integral departs from the definition of a Markov process, whose most prominent property is that "at a given instant, given all past observations, [conditional probability distributions of a Markov process] depend only upon the most recent past" [Soong and Grigoriu, 1993]; a rigorous study of such processes can be found in [Doob, 1953, Kolmogorov, 1931, Loéve, 1963, Stratonovich, 1968] among other publications.

Consider a Markov stochastic vector process $\boldsymbol{\alpha}(t) = [\alpha_1(t), \ldots, \alpha_n(t)]$ for which the C-K equation for any $t_{l+1} \geq t_l \geq t_{l-1}$ takes the form (e.g., [Soong and Grigoriu, 1993])

$$p(\boldsymbol{\alpha}_{l+1}, t_{l+1} | \boldsymbol{\alpha}_{l-1}, t_{l-1}) = \int_{-\infty}^{\infty} p(\boldsymbol{\alpha}_{l-1}, t_{l-1} | \boldsymbol{\alpha}_l, t_l) p(\boldsymbol{\alpha}_l, t_l | \boldsymbol{\alpha}_{l+1}, t_{l+1}) \, \mathrm{d}\boldsymbol{\alpha}_l, \tag{2.1}$$

where $p(\boldsymbol{\alpha}_{l+1}, t_{l+1} | \boldsymbol{\alpha}_{l-1}, t_{l-1})$ is the transition PDF of the process from the state $\boldsymbol{\alpha}_{l-1}$ at a time instance t_{l-1} to the state $\boldsymbol{\alpha}_{l+1}$ at a time t_{l+1}.

The sample paths of a Markov process are continuous functions of t with probability one if the

Lindeberg condition is satisfied (e.g., [Gihman and Skorohod, 1972])

$$\lim_{\Delta t\to 0}\frac{1}{\Delta t}\int\limits_{|\boldsymbol{\alpha}_{l+1}-\boldsymbol{\alpha}_l|>\varepsilon} p(\boldsymbol{\alpha}_{l+1},t_{l+1}|\boldsymbol{\alpha}_l,t_l)\mathrm{d}\boldsymbol{\alpha}_{l+1}=0 \quad \forall\varepsilon>0, \tag{2.2}$$

where $\Delta t = t_{l+1}-t_l$. Such a process is defined as a diffusion process, and the components of its drift vector $\mathbf{A}(\boldsymbol{\alpha}_l,t_l)=[A_j(\boldsymbol{\alpha}_l,t_l)]_{n\times 1}$ and of its diffusion matrix $\mathbf{B}(\boldsymbol{\alpha}_l,t_l)=[B_{jk}(\boldsymbol{\alpha}_l,t_l)]_{n\times n}$ can be defined as (e.g., [Gardiner, 2009])

$$A_j(\boldsymbol{\alpha}_l,t_l)=\lim_{\Delta t\to 0}\frac{\mathbb{E}\left[\alpha_{jl+1}-\alpha_{jl}\right]}{\Delta t} \tag{2.3}$$

and

$$B^2_{jk}(\boldsymbol{\alpha}_l,t_l)=\lim_{\Delta t\to 0}\frac{\mathbb{E}\left[(\alpha_{jl+1}-\alpha_{jl})(\alpha_{kl+1}-\alpha_{kl})\right]}{\Delta t}, \tag{2.4}$$

respectively.

Further, the well-known F-P equation can be obtained through employing the C-K Eqn. (2.1) (e.g., [Arnold, 1974, Grigoriu, 2002])

$$\frac{\partial p}{\partial t}=-\sum_j\frac{\partial}{\partial\alpha_j}\left(A_j(\boldsymbol{\alpha},t)p\right)+\frac{1}{2}\sum_j\sum_k\frac{\partial}{\partial\alpha_j}\frac{\partial}{\partial\alpha_k}\left(\widetilde{B}_{jk}(\boldsymbol{\alpha},t)p\right), \tag{2.5}$$

where $p=p(\boldsymbol{\alpha}_{l+1},t_{l+1}|\boldsymbol{\alpha}_l,t_l)$, and $\widetilde{\mathbf{B}}(\boldsymbol{\alpha},t)=\mathbf{B}(\boldsymbol{\alpha},t)\mathbf{B}^T(\boldsymbol{\alpha},t)$.

The F-P Eqn. (2.5) is related to a first-order SDE of the form

$$\dot{\boldsymbol{\alpha}}=\mathbf{A}(\boldsymbol{\alpha},t)+\mathbf{B}(\boldsymbol{\alpha},t)\boldsymbol{\eta}(t), \tag{2.6}$$

where $\boldsymbol{\eta}(t)$ is a zero-mean delta-correlated process of intensity one, i.e., $\mathbb{E}\left[\eta_j(t)\right]=0$ and $\mathbb{E}\left[\eta_j(t_l)\eta_k(t_{l+1})\right]=\delta_{jk}\delta(t_l-t_{l+1})$, $j,k\in\{1,\ldots,n\}$, with δ_{jk} being the Kronecker delta, and $\delta(t)$ representing the Dirac delta function. Eqn. (2.6) is also widely known as the diffusion or Itô equation (e.g., [Grigoriu, 2002]).

2.2 WPI formulation

The transition PDF has been shown to admit a Gaussian distribution at the limit $\Delta t \to 0$ (e.g., [Gardiner, 2009, Risken, 1996])

$$p(\boldsymbol{\alpha}_{l+1}, t_{l+1} | \boldsymbol{\alpha}_l, t_l) = \left[\sqrt{(2\pi\Delta t)^n \det \left[\widetilde{\mathbf{B}}(\boldsymbol{\alpha}_l, t_l) \right]} \right]^{-1} \dots$$
$$\exp\left(-\frac{1}{2} \frac{[\boldsymbol{\alpha}_{l+1} - \boldsymbol{\alpha}_l - \Delta t \mathbf{A}(\boldsymbol{\alpha}_l, t_l)]^T \left[\widetilde{\mathbf{B}}(\boldsymbol{\alpha}_l, t_l) \right]^{-1} [\boldsymbol{\alpha}_{l+1} - \boldsymbol{\alpha}_l - \Delta t \mathbf{A}(\boldsymbol{\alpha}_l, t_l)]}{\Delta t} \right). \quad (2.7)$$

Note here that the choice of the Gaussian distribution of the form of Eqn. is not restrictive, and non-Gaussian distributions can also be utilized (e.g., [Langouche et al., 1979, Naess and Moe, 1996]). As a matter of fact, Eqn. (2.7) together with the C-K Eqn. (2.1) have been the starting point of the alternative purely numerical schemes, typically refered in literature as numerical path integral schemes, for propagating the response PDF in short time steps [Alevras and Yurchenko, 2016, Di Paola and Santoro, 2008, Naess and Johnsen, 1993, Wehner and Wolfer, 1983]. Despite these schemes being highly accurate since the only approximation is related to discretizing the C-K Eqn. (2.1), they have proven to be computationally demanding. This is caused by the fact that a multi-dimensional convolution integral has to be calculated numerically for each time step, while the time step is kept short.

It is assumed in Eqn. (2.7) that $\widetilde{\mathbf{B}}$ is a non-singular matrix and its inverse exists.

In addition, the probability that the stochastic process $\boldsymbol{\alpha}$ follows a specific path, $\boldsymbol{\alpha}(t)$, can be interpreted as the probability of a compound event, i.e., as a product of probabilities of the form of

Eqn. (2.7) (e.g., [Chaichian and Demichev, 2001, Risken, 1996])

$$\mathrm{P}[\boldsymbol{\alpha}(t)] = \lim_{\substack{\Delta t\to 0\\ N\to\infty}} \left\{ \left[\prod_{l=0}^{N-1} \left(\left[\sqrt{(2\pi\Delta t)^n \det\left[\widetilde{\mathbf{B}}(\boldsymbol{\alpha}_l,t_l)\right]} \right]^{-1} \prod_{j=1}^{n} \mathrm{d}\alpha_{jl} \right) \right] \dots \right.$$
$$\left. \exp\left(-\sum_{l=0}^{N-1} \frac{1}{2} \frac{[\boldsymbol{\alpha}_{l+1} - \boldsymbol{\alpha}_l - \Delta t\mathbf{A}(\boldsymbol{\alpha}_l,t_l)]^T \left[\widetilde{\mathbf{B}}(\boldsymbol{\alpha}_l,t_l)\right]^{-1} [\boldsymbol{\alpha}_{l+1} - \boldsymbol{\alpha}_l - \Delta t\mathbf{A}(\boldsymbol{\alpha}_l,t_l)]}{\Delta t} \right) \right\}, \quad (2.8)$$

where the time discretization assumes N points Δt apart, and the path $\boldsymbol{\alpha}(t)$ is represented by its values $\boldsymbol{\alpha}_l$ at the discrete time instances t_l, $l \in \{0,\dots,N-1\}$. Moreover, $\mathrm{d}\alpha_{jl}$ represent the (infinite in number) infinitesimal "gates" through which the path propagates. Eqn. (2.8) roughly represents the probability of the process to propagate through the infinitesimally thin tube around the path $\boldsymbol{\alpha}(t)$. However, if the diffusion matrix $\mathbf{B}(\boldsymbol{\alpha},t)$ is diagonal, Eqn. (2.8) can be written in a compact form [Chaichian and Demichev, 2001]

$$\mathrm{P}[\boldsymbol{\alpha}(t)] = \exp\left(-\int_{t_i}^{t_f} \frac{1}{2} \sum_{j=1}^{n} \frac{[\dot{\alpha}_j - A_j(\boldsymbol{\alpha},t)]^2}{\widetilde{B}_{jj}(\boldsymbol{\alpha},t)}\, \mathrm{d}t \right) \prod_{j=1}^{n} \prod_{t=t_i}^{t_f} \frac{\mathrm{d}\alpha_j(t)}{\sqrt{2\pi\widetilde{B}_{jj}(\boldsymbol{\alpha},t)\,\mathrm{d}t}}. \quad (2.9)$$

Consider next an initial state $\boldsymbol{\alpha}_i$ at time t_i and a final state $\boldsymbol{\alpha}_f$ at time t_f. Then, the total probability that the path $\boldsymbol{\alpha}$ will follow from $\boldsymbol{\alpha}_i$ to $\boldsymbol{\alpha}_f$ takes the form of a functional integral that "sums up" the respective probabilities of each path that the process can possibly follow (see, e.g., [Chaichian and Demichev, 2001, Feynman et al., 2010]). Denoting the set of all such paths from $\boldsymbol{\alpha}_i$ to $\boldsymbol{\alpha}_f$ by $C\{\boldsymbol{\alpha}_i,t_i;\boldsymbol{\alpha}_f,t_f\}$, the transition PDF becomes

$$p(\boldsymbol{\alpha}_f,t_f|\boldsymbol{\alpha}_i,t_i) = \int\limits_{C\{\boldsymbol{\alpha}_i,t_i;\boldsymbol{\alpha}_f,t_f\}} \exp\left(-\int_{t_i}^{t_f} L[\boldsymbol{\alpha},\dot{\boldsymbol{\alpha}}]\,\mathrm{d}t \right) \prod_{j=1}^{n} \mathcal{D}[\alpha_j(t)], \quad (2.10)$$

where $L[\boldsymbol{\alpha},\dot{\boldsymbol{\alpha}}]$ denotes the Lagrangian functional of the system of the form

$$L[\boldsymbol{\alpha},\dot{\boldsymbol{\alpha}}] = \frac{1}{2} \sum_{j=1}^{n} \frac{[\dot{\alpha}_j - A_j(\boldsymbol{\alpha},t)]^2}{\widetilde{B}_{jj}(\boldsymbol{\alpha},t)}, \quad (2.11)$$

and $\mathcal{D}[\alpha_j(t)]$, $j \in \{1,\ldots,n\}$, is a functional measure given as

$$\mathcal{D}[\alpha_j(t)] = \prod_{t=t_i}^{t_f} \frac{\mathrm{d}\alpha_j(t)}{\sqrt{2\pi \widetilde{B}_{jj}(\boldsymbol{\alpha},t)\mathrm{d}t}}. \tag{2.12}$$

The aforementioned concepts allowed Kougioumtzoglou and coworkers to develop recently a novel WPI based technique for determination of the response tranasition PDF of stochastically excited SDOF and MDOF nonlinear systems [Kougioumtzoglou and Spanos, 2012]. The technique has been shown to be versatile in addressing various engineering systems, including ones with fractional derivative elements [Di Matteo et al., 2014] or exhibiting hysteretic behavior [Kougioumtzoglou and Spanos, 2014]. Nonetheless, it has been applied so far to Gaussian white noise excitation stochastic processes only.

This page is intentionally left blank.

Chapter 3

Mathematical Formulation

3.1 WPI technique generalization: non-white and non-Gaussian excitation process

3.1.1 Theoretical formulation

Consider a MDOF nonlinear oscillator governed by the following equation

$$\mathbf{M}\ddot{\mathbf{x}} + \mathbf{C}\dot{\mathbf{x}} + \mathbf{K}\mathbf{x} + \mathbf{g}(\mathbf{x}, \dot{\mathbf{x}}) = \boldsymbol{\xi}(t), \tag{3.1}$$

where $\mathbf{x}(t) = [x_1, \ldots, x_m]^T$ is the displacement vector process; $\mathbf{M}$, $\mathbf{C}$, $\mathbf{K}$ are the $m \times m$ mass, damping and stiffness matrices, respectively; and $\mathbf{g}(\mathbf{x}, \dot{\mathbf{x}})$ is an arbitrary nonlinear vector function. $\boldsymbol{\xi}(t)$ represents a non-white non-Gaussian excitation stochastic process, which can be modeled as a response to a nonlinear "filter" equation (e.g., [Roberts and Spanos, 2003])

$$\mathbf{P}\ddot{\boldsymbol{\xi}} + \mathbf{Q}\dot{\boldsymbol{\xi}} + \mathbf{R}\boldsymbol{\xi} + \mathbf{u}(\boldsymbol{\xi}, \dot{\boldsymbol{\xi}}) = \mathbf{w}(t), \tag{3.2}$$

where $\mathbf{P}$, $\mathbf{Q}$, $\mathbf{R}$ are coefficient matrices; $\mathbf{u}(\boldsymbol{\xi}, \dot{\boldsymbol{\xi}})$ is an arbitrary nonlinear vector function; and $\mathbf{w}(t) = [w_1, \ldots, w_m]^T$ is a white noise stochastic vector process with the power spectrum matrix of

the form

$$\mathbf{S_w} = \begin{bmatrix} S_0 & \dots & 0 \\ \vdots & \ddots & \vdots \\ 0 & \dots & S_0 \end{bmatrix}. \tag{3.3}$$

Various non-white excitation processes often employed in engineering dynamics models (e.g., the Kanai-Tajimi excitation process in earthquake engineering [Kanai, 1957, Tajimi, 1960]) can be defined via the filter Eqn. (3.2). As a matter of fact, the filter equation can be understood as the time-domain representation of those excitation processes that are typically described in the frequency domain by their power spectra [Li and Chen, 2009]. More importantly, it has been shown [Chai et al., 2015, Spanos, 1986] that a filter approximation of the form of Eqn. (3.2) can generate satisfactory accuracy for practical applications even for the cases of excitations not readily available in the time domain as a response to such a filter. Eqn. (3.2) also allows to account for non-Gaussian excitation models via the nonlinear vector function $\mathbf{u}(\boldsymbol{\xi}, \dot{\boldsymbol{\xi}})$.

Next, differentiating Eqn. (3.1) and substituting into Eqn. (3.2) yields the fourth-order SDE

$$\mathbf{\Lambda}_4\mathbf{x}^{(4)} + \mathbf{\Lambda}_3\mathbf{x}^{(3)} + \mathbf{\Lambda}_2\ddot{\mathbf{x}} + \mathbf{\Lambda}_1\dot{\mathbf{x}} + \mathbf{\Lambda}_0\mathbf{x} + \mathbf{h}(\mathbf{x}, \dot{\mathbf{x}}, \ddot{\mathbf{x}}, \mathbf{x}^{(3)}) = \mathbf{w}(t), \tag{3.4}$$

where

$$\begin{cases} \mathbf{\Lambda}_4 = \mathbf{PM} \\ \mathbf{\Lambda}_3 = \mathbf{PC} + \mathbf{QM} \\ \mathbf{\Lambda}_2 = \mathbf{PK} + \mathbf{QC} + \mathbf{RM} \\ \mathbf{\Lambda}_1 = \mathbf{QK} + \mathbf{RC} \\ \mathbf{\Lambda}_0 = \mathbf{RK}, \end{cases} \tag{3.5}$$

and

$$\mathbf{h}(\mathbf{x}, \dot{\mathbf{x}}, \ddot{\mathbf{x}}, \mathbf{x}^{(3)}) = \mathbf{P}\ddot{\mathbf{g}}(\mathbf{x}, \dot{\mathbf{x}}) + \mathbf{Q}\dot{\mathbf{g}}(\mathbf{x}, \dot{\mathbf{x}}) + \mathbf{R}\mathbf{g}(\mathbf{x}, \dot{\mathbf{x}}) + \mathbf{u}(\mathbf{x}, \dot{\mathbf{x}}, \ddot{\mathbf{x}}, \mathbf{x}^{(3)}). \tag{3.6}$$

A state variable formulation can be applied to the Eqn. (3.4) [Einchcomb and McKane, 1995, McKane et al., 1990, Risken, 1996] to yield an equation of the form of Eqn. (2.6) with

$$\boldsymbol{\alpha} = [\mathbf{x}, \mathbf{y}_1, \mathbf{y}_2, \mathbf{y}_3]^T, \tag{3.7}$$

$$\mathbf{A}(\boldsymbol{\alpha}, t) = \begin{bmatrix} \mathbf{y}_1 \\ \mathbf{y}_2 \\ \mathbf{y}_3 \\ \boldsymbol{\Lambda}_4^{-1} \left(-\boldsymbol{\Lambda}_3 \mathbf{y}_3 - \boldsymbol{\Lambda}_2 \mathbf{y}_2 - \boldsymbol{\Lambda}_1 \mathbf{y}_1 - \boldsymbol{\Lambda}_0 \mathbf{x} - \mathbf{h}(\mathbf{x}, \mathbf{y}_1, \mathbf{y}_2, \mathbf{y}_3)\right) \end{bmatrix}, \tag{3.8}$$

and

$$\mathbf{B}(\boldsymbol{\alpha}, t) = \begin{bmatrix} \mathbf{0}_{3m \times 3m} & \mathbf{0}_{3m \times m} \\ \mathbf{0}_{m \times 3m} & \sqrt{2\pi} \boldsymbol{\Lambda}_4^{-1} \mathbf{S}_{\mathbf{w}}{}^{1/2} \end{bmatrix}. \tag{3.9}$$

This way, the m-dimensional fourth-order SDE of Eqn. (3.4) becomes a $4m$-dimensional first-order SDE for the process $\boldsymbol{\alpha} = [\mathbf{x}, \mathbf{y}_1, \mathbf{y}_2, \mathbf{y}_3]^T$.

Notice that the diffusion matrix $\mathbf{B}(\boldsymbol{\alpha}, t)$ (as well as $\widetilde{\mathbf{B}}(\boldsymbol{\alpha}, t) = \mathbf{B}(\boldsymbol{\alpha}, t)\mathbf{B}^T(\boldsymbol{\alpha}, t)$) in Eqn. (3.9) is singular and requires a different treatment than directly employing Eqn. (2.10). The challenge of encountering singular diffusion matrices in path integral formulations has been repeatedly addressed in literature [Colet et al., 1989, Donoso et al., 1999, Drozdov and Talkner, 1998, Einchcomb and McKane, 1995, Hänggi, 1989, Machlup and Onsager, 1953, McKane et al., 1990, Newman et al., 1990, Wio et al., 1989]. The ensuing analysis bypasses singularity of the matrix $\mathbf{B}(\boldsymbol{\alpha}, t)$ by utilizing delta-functionals in the path integral formulation [Chaichian and Demichev, 2001, Wio, 2013], which enforce the compatibility equations ($\dot{\mathbf{x}} = \mathbf{y}_1$, $\dot{\mathbf{y}}_1 = \mathbf{y}_2$, and $\dot{\mathbf{y}}_2 = \mathbf{y}_3$). In this ragard, the transition PDF of $\boldsymbol{\alpha} = [\mathbf{x}, \mathbf{y}_1, \mathbf{y}_2, \mathbf{y}_3]^T$ can be expressed as [Chaichian and Demichev, 2001]

$$p(\boldsymbol{\alpha}_f, t_f | \boldsymbol{\alpha}_i, t_i) = \int\limits_{C\{\boldsymbol{\alpha}_f, t_f; \boldsymbol{\alpha}_i, t_i\}} \exp\left(-\int\limits_{t_i}^{t_f} \frac{1}{2} \mathbf{S}^T \widetilde{\mathbf{B}}_{ns}^{-1} \mathbf{S} \, \mathrm{d}t \right) \ldots$$

$$\delta[\dot{\mathbf{y}}_2 - \mathbf{y}_3] \delta[\dot{\mathbf{y}}_1 - \mathbf{y}_2] \delta[\dot{\mathbf{x}} - \mathbf{y}_1] \mathcal{D}[\mathbf{x}(t)] \mathcal{D}[\mathbf{y}_1(t)] \mathcal{D}[\mathbf{y}_2(t)] \mathcal{D}[\mathbf{y}_3(t)], \tag{3.10}$$

where

$$\mathbf{S} = \mathbf{\Lambda}_4\dot{\mathbf{y}}_3 + \mathbf{\Lambda}_3\mathbf{y}_3 + \mathbf{\Lambda}_2\mathbf{y}_2 + \mathbf{\Lambda}_1\mathbf{y}_1 + \mathbf{\Lambda}_0\mathbf{x} + \mathbf{h}(\mathbf{x}, \mathbf{y}_1, \mathbf{y}_2, \mathbf{y}_3), \tag{3.11}$$

and

$$\widetilde{\mathbf{B}}_{ns} = \begin{bmatrix} 2\pi S_0 & \dots & 0 \\ \vdots & \ddots & \vdots \\ 0 & \dots & 2\pi S_0 \end{bmatrix}. \tag{3.12}$$

Integrating over paths $\mathbf{y}_1(t)$, $\mathbf{y}_2(t)$ and $\mathbf{y}_3(t)$ [Wio, 2013] transforms Eqn. (3.10) into

$$p\left(\mathbf{x}_f, \dot{\mathbf{x}}_f, \ddot{\mathbf{x}}_f, \mathbf{x}_f^{(3)}, t_f | \mathbf{x}_i, \dot{\mathbf{x}}_i, \ddot{\mathbf{x}}_i, \mathbf{x}_i^{(3)}, t_i\right) = \int\limits_{C\{\mathbf{x}_i, \dot{\mathbf{x}}_i, \ddot{\mathbf{x}}_i, \mathbf{x}_i^{(3)}, t_i; \mathbf{x}_f, \dot{\mathbf{x}}_f, \ddot{\mathbf{x}}_f, \mathbf{x}_f^{(3)}, t_f\}} \exp\left(-\int_{t_i}^{t_f} L\left[\mathbf{x}, \dot{\mathbf{x}}, \ddot{\mathbf{x}}, \mathbf{x}^{(3)}, \mathbf{x}^{(4)}\right] \mathrm{d}t\right) \mathcal{D}[\mathbf{x}(t)], \tag{3.13}$$

where the Lagrangian-like functional $L\left[\mathbf{x}, \dot{\mathbf{x}}, \ddot{\mathbf{x}}, \mathbf{x}^{(3)}, \mathbf{x}^{(4)}\right]$ is given by

$$L\left[\mathbf{x}, \dot{\mathbf{x}}, \ddot{\mathbf{x}}, \mathbf{x}^{(3)}, \mathbf{x}^{(4)}\right] = \frac{1}{2}\left[\mathbf{\Lambda}_4\mathbf{x}^{(4)} + \mathbf{\Lambda}_3\mathbf{x}^{(3)} + \mathbf{\Lambda}_2\ddot{\mathbf{x}} + \mathbf{\Lambda}_1\dot{\mathbf{x}} + \mathbf{\Lambda}_0\mathbf{x} + \mathbf{h}\left(\mathbf{x}, \dot{\mathbf{x}}, \ddot{\mathbf{x}}, \mathbf{x}^{(3)}\right)\right]^T \dots \widetilde{\mathbf{B}}_{ns}^{-1}\left[\mathbf{\Lambda}_4\mathbf{x}^{(4)} + \mathbf{\Lambda}_3\mathbf{x}^{(3)} + \mathbf{\Lambda}_2\ddot{\mathbf{x}} + \mathbf{\Lambda}_1\dot{\mathbf{x}} + \mathbf{\Lambda}_0\mathbf{x} + \mathbf{h}\left(\mathbf{x}, \dot{\mathbf{x}}, \ddot{\mathbf{x}}, \mathbf{x}^{(3)}\right)\right]. \tag{3.14}$$

Eqn. (3.13) provides a formal expression of the path integral and is of little practical use since its analytical or numerical evaluation is extremely challenging [Chaichian and Demichev, 2001]. Hence, the problem requires an approximate solution of the path integral, such as the "most probable path" approach (e.g., [Chaichian and Demichev, 2001, Kougioumtzoglou and Spanos, 2012]), according to which the largest contribution to the transition PDF of Eqn. (3.13) comes from the path $\mathbf{x}_c(t)$ that minimizes the integral inside the exponential. In agreement with calculus of variations (e.g., [Ewing, 1985, Lanczos, 1986]), $\mathbf{x}_c(t)$ should satisfy the extremality condition

$$\delta \int_{t_i}^{t_f} L\left[\mathbf{x}_c, \dot{\mathbf{x}}_c, \ddot{\mathbf{x}}_c, \mathbf{x}_c^{(3)}, \mathbf{x}_c^{(4)}\right] \mathrm{d}t = 0, \tag{3.15}$$

which yields the system of Euler-Lagrange (E-L) equations

$$\begin{gathered}\frac{\partial L}{\partial x_{c,1}}-\frac{\partial}{\partial t}\frac{\partial L}{\partial \dot{x}_{c,1}}+\frac{\partial^2}{\partial t^2}\frac{\partial L}{\partial \ddot{x}_{c,1}}-\frac{\partial^3}{\partial t^3}\frac{\partial L}{\partial x^{(3)}_{c,1}}+\frac{\partial^4}{\partial t^4}\frac{\partial L}{\partial x^{(4)}_{c,1}}=0\\ \vdots\\ \frac{\partial L}{\partial x_{c,m}}-\frac{\partial}{\partial t}\frac{\partial L}{\partial \dot{x}_{c,m}}+\frac{\partial^2}{\partial t^2}\frac{\partial L}{\partial \ddot{x}_{c,m}}-\frac{\partial^3}{\partial t^3}\frac{\partial L}{\partial x^{(3)}_{c,m}}+\frac{\partial^4}{\partial t^4}\frac{\partial L}{\partial x^{(4)}_{c,m}}=0,\end{gathered} \tag{3.16}$$

together with $8\times m$ boundary conditions

$$\begin{gathered}x_{c,1}(t_i)=x_{1,i},\quad \dot{x}_{c,1}(t_i)=\dot{x}_{1,i},\quad x_{c,1}(t_f)=x_{1,f},\quad \dot{x}_{c,1}(t_f)=\dot{x}_{1,f},\\ \ddot{x}_{c,1}(t_i)=\ddot{x}_{1,i},\quad x^{(3)}_{c,1}(t_i)=x^{(3)}_{1,i},\quad \ddot{x}_{c,1}(t_f)=\ddot{x}_{1,f},\quad x^{(3)}_{c,1}(t_f)=x^{(3)}_{1,f},\\ \vdots\\ x_{c,m}(t_i)=x_{m,i},\quad \dot{x}_{c,m}(t_i)=\dot{x}_{m,i},\quad x_{c,m}(t_f)=x_{m,f},\quad \dot{x}_{c,m}(t_f)=\dot{x}_{m,f},\\ \ddot{x}_{c,m}(t_i)=\ddot{x}_{m,i},\quad x^{(3)}_{c,m}(t_i)=x^{(3)}_{m,i},\quad \ddot{x}_{c,m}(t_f)=\ddot{x}_{m,f},\quad x^{(3)}_{c,m}(t_f)=x^{(3)}_{m,f}.\end{gathered} \tag{3.17}$$

Further, the most probable path $\mathbf{x}_c(t)$ can be obtained by solving the BVP of Eqs. (3.16) and (3.17) (e.g., [Agarwal and O'Regan, 2008, Shampine et al., 2003]), and the transition PDF from the initial state $\{\mathbf{x}_i,\dot{\mathbf{x}}_i,\ddot{\mathbf{x}}_i,\mathbf{x}^{(3)}_i,t_i\}$ to the final state $\{\mathbf{x}_f,\dot{\mathbf{x}}_f,\ddot{\mathbf{x}}_f,\mathbf{x}^{(3)}_f,t_f\}$ is calculated as

$$p\left(\mathbf{x}_f,\dot{\mathbf{x}}_f,\ddot{\mathbf{x}}_f,\mathbf{x}^{(3)}_f,t_f|\mathbf{x}_i,\dot{\mathbf{x}}_i,\ddot{\mathbf{x}}_i,\mathbf{x}^{(3)}_i,t_i\right)=C\exp\left(-\int_{t_i}^{t_f}L\left[\mathbf{x}_c,\dot{\mathbf{x}}_c,\ddot{\mathbf{x}}_c,\mathbf{x}^{(3)}_c,\mathbf{x}^{(4)}_c\right]\mathrm{d}t\right), \tag{3.18}$$

where the normalization constant C is determined through the condition

$$\int_{-\infty}^{\infty}\cdots\int_{-\infty}^{\infty}p\left(\mathbf{x}_f,\dot{\mathbf{x}}_f,\ddot{\mathbf{x}}_f,\mathbf{x}^{(3)}_f,t_f|\mathbf{x}_i,\dot{\mathbf{x}}_i,\ddot{\mathbf{x}}_i,\mathbf{x}^{(3)}_i,t_i\right)\mathrm{d}\mathbf{x}_f\ldots\mathrm{d}\mathbf{x}^{(3)}_f=1. \tag{3.19}$$

3.1.2 Computational aspects

The numerical implementation of the WPI technique as developed in Section 3.1.1 is dicussed next. In this respect, one can note that solving one BVP of the form of Eqs. (3.16) and (3.17) provides one point of the response transition PDF.

Consider a given time instance t_f and a corresponding effective domain of boundary values for the response transition PDF. The effective domain can be discretized with N points in each

dimension ($\mathbf{x}_f$, $\dot{\mathbf{x}}_f$, $\ddot{\mathbf{x}}_f$, $\mathbf{x}_f^{(3)}$). The brute force implementation of the technique yields the PDF being determined for each point of the mesh. For example, an m-DOF system requires solution of N^{4m} BVPs. Clearly, this quickly drives the computational cost to prohibitive for relatively high-dimensional MDOF engineering systems. However, an efficient approach, such as the ones developed by [Kougioumtzoglou et al., 2015, Psaros et al., 2018b], can be combined with the WPI technique. More specifically, one can utilize the localization property of the joint response PDF and apply an appropriate polynomial expansion to it. This approach has been shown to result in a computational effort following a power law of the form $\sim (4m)^l / l!$ (where l is the degree of the polynomial), which can be orders of magnitude smaller than N^{4m} (depending on the dimensionality of the original system of ineterest m) [Kougioumtzoglou et al., 2015]. Additionally, utilizing sparse PDF respresentations in combination with CS tools and group sparsity concepts can reduce the number of BVPs required to be solved even further [Psaros et al., 2018b].

3.2 WPI technique generalization: non-stationary excitation process

3.2.1 Theoretical formulation

In the above, Section 3.1 presents stochastic modeling that takes into account the transient phase of the filter through Eqn. (3.2), i.e., the non-white excitation process $\boldsymbol{\xi}(t)$ is non-stationary in this formulation. However, many engineering dynamics applications adopt an excitation model provided by a (time-mofulated) power spectrum [Li and Chen, 2009, Roberts and Spanos, 2003]

$$\mathbf{S}_{\mathbf{f}}(\omega,t) = \mathbf{D}(t)\mathbf{S}_{\boldsymbol{\xi}_s}(\omega)\mathbf{D}^T(t), \tag{3.20}$$

corresponding to the (non-stationary) stochastic process

$$\mathbf{f}(t) = \mathbf{D}(t)\boldsymbol{\xi}_s(t), \tag{3.21}$$

where $\mathbf{D}(t)$ is the $m \times m$ matrix of deterministic time-modulating functions.

Note that $\boldsymbol{\xi}_s(t)$ in Eqs. (3.20) and (3.21) represents the stationary reposnse of the filter of Eqn. (3.2); in other words, the output of Eqn. (3.2) after the transient phase has died out and $\boldsymbol{\xi}(t)$ has reached its stationary phase. Thus, the implementation of the WPI technique as it has been derived in Section 3.1 requires a modification to account for modeling stochastic excitation processes through Eqs. (3.20) and (3.21).

In this regard, Eqn. (3.1) becomes

$$\mathbf{M}\ddot{\mathbf{x}} + \mathbf{C}\dot{\mathbf{x}} + \mathbf{K}\mathbf{x} + \mathbf{g}(\mathbf{x}, \dot{\mathbf{x}}) = \mathbf{f}(t). \tag{3.22}$$

Considering Eqn. (3.21) with $D_{jk}(t) \neq 0 \; \forall j,k \in \{1,\ldots,m\}$ yields

$$\boldsymbol{\xi}_s(t) = \mathbf{D}^{-1}(t)\mathbf{f}(t) \tag{3.23}$$

$$\dot{\boldsymbol{\xi}}_s(t) = \mathbf{D}^{-1}(t)\left[\dot{\mathbf{f}}(t) - \dot{\mathbf{D}}(t)\boldsymbol{\xi}_s(t)\right] \tag{3.24}$$

$$\ddot{\boldsymbol{\xi}}_s(t) = \mathbf{D}^{-1}(t)\left[\ddot{\mathbf{f}}(t) - \ddot{\mathbf{D}}(t)\boldsymbol{\xi}_s(t) - 2\dot{\mathbf{D}}(t)\dot{\boldsymbol{\xi}}_s(t)\right] \tag{3.25}$$

Next, substituting Eqs. (3.22)-(3.25) into Eqn. (3.2), a SDE similar to Eqn. (3.4) can be obtained,

where

$$\begin{cases} \mathbf{\Lambda}_4 = \mathbf{P}\mathbf{D}^{-1}\mathbf{M} \\ \mathbf{\Lambda}_3 = \mathbf{P}\mathbf{D}^{-1}\left[-2\dot{\mathbf{D}}\mathbf{D}^{-1}\mathbf{M}+\mathbf{C}\right]+\mathbf{Q}\mathbf{D}^{-1}\mathbf{M} \\ \mathbf{\Lambda}_2 = \mathbf{P}\mathbf{D}^{-1}\left[\left(2\dot{\mathbf{D}}\mathbf{D}^{-1}\dot{\mathbf{D}}\mathbf{D}^{-1}-\ddot{\mathbf{D}}\mathbf{D}^{-1}\right)\mathbf{M}-2\dot{\mathbf{D}}\mathbf{D}^{-1}\mathbf{C}+\mathbf{K}\right] \\ \quad +\mathbf{Q}\mathbf{D}^{-1}\left(-\dot{\mathbf{D}}\mathbf{D}^{-1}\mathbf{M}+\mathbf{C}\right)+\mathbf{R}\mathbf{D}^{-1}\mathbf{M} \\ \mathbf{\Lambda}_1 = \mathbf{P}\mathbf{D}^{-1}\left[\left(2\dot{\mathbf{D}}\mathbf{D}^{-1}\dot{\mathbf{D}}\mathbf{D}^{-1}-\ddot{\mathbf{D}}\mathbf{D}^{-1}\right)\mathbf{C}-2\dot{\mathbf{D}}\mathbf{D}^{-1}\mathbf{K}\right] \\ \quad +\mathbf{Q}\mathbf{D}^{-1}\left(-\dot{\mathbf{D}}\mathbf{D}^{-1}\mathbf{C}+\mathbf{K}\right)+\mathbf{R}\mathbf{D}^{-1}\mathbf{C} \\ \mathbf{\Lambda}_0 = \mathbf{P}\mathbf{D}^{-1}\left(2\dot{\mathbf{D}}\mathbf{D}^{-1}\dot{\mathbf{D}}\mathbf{D}^{-1}-\ddot{\mathbf{D}}\mathbf{D}^{-1}\right)\mathbf{K} \\ \quad -\mathbf{Q}\mathbf{D}^{-1}\dot{\mathbf{D}}\mathbf{D}^{-1}\mathbf{K}+\mathbf{R}\mathbf{D}^{-1}\mathbf{K}, \end{cases} \tag{3.26}$$

and

$$\begin{aligned} \mathbf{h}(\mathbf{x},\dot{\mathbf{x}},\ddot{\mathbf{x}},\mathbf{x}^{(3)}) = {} & \mathbf{P}\mathbf{D}^{-1}\ddot{\mathbf{g}}(\mathbf{x},\dot{\mathbf{x}}) \\ & +\left(-2\mathbf{P}\mathbf{D}^{-1}\dot{\mathbf{D}}\mathbf{D}^{-1}+\mathbf{Q}\mathbf{D}^{-1}\right)\dot{\mathbf{g}}(\mathbf{x},\dot{\mathbf{x}}) \\ & +\left[\mathbf{P}\mathbf{D}^{-1}\left(2\dot{\mathbf{D}}\mathbf{D}^{-1}\dot{\mathbf{D}}\mathbf{D}^{-1}-\ddot{\mathbf{D}}\mathbf{D}^{-1}\right)\right. \\ & \left.-\mathbf{Q}\mathbf{D}^{-1}\dot{\mathbf{D}}\mathbf{D}^{-1}+\mathbf{R}\mathbf{D}^{-1}\right]\mathbf{g}(\mathbf{x},\dot{\mathbf{x}})+\mathbf{u}(\mathbf{x},\dot{\mathbf{x}},\ddot{\mathbf{x}},\mathbf{x}^{(3)}). \end{aligned} \tag{3.27}$$

Once again, one arrives at a set of BVPs (Eqs. (3.16) and (3.17)) that necessitates initial values $\left(\mathbf{x}_i,\dot{\mathbf{x}}_i,\ddot{\mathbf{x}}_i,\mathbf{x}_i^{(3)}\right)$ at time t_i and final values $\left(\mathbf{x}_f,\dot{\mathbf{x}}_f,\ddot{\mathbf{x}}_f,\mathbf{x}_f^{(3)}\right)$ at time t_f to be known. The initial displacement $\mathbf{x}_i$ and velocity $\dot{\mathbf{x}}_i$ are usually assumed to be deterministic and fixed, whereas the values of $\ddot{\mathbf{x}}_i$ and $\mathbf{x}_i^{(3)}$ are typically expressed through Eqn. (3.22) in the form of

$$\ddot{\mathbf{x}}_i = \mathbf{M}^{-1}\left(\mathbf{f}(t_i)-\mathbf{C}\dot{\mathbf{x}}_i-\mathbf{K}\mathbf{x}_i-\mathbf{g}(\mathbf{x}_i,\dot{\mathbf{x}}_i)\right), \tag{3.28}$$

$$\mathbf{x}_i^{(3)} = \mathbf{M}^{-1}\left(\dot{\mathbf{f}}(t_i)-\mathbf{C}\ddot{\mathbf{x}}_i-\mathbf{K}\dot{\mathbf{x}}_i-\dot{\mathbf{g}}(\mathbf{x}_i,\dot{\mathbf{x}}_i)\right). \tag{3.29}$$

It is easy to notice from Eqs. (3.28) and (3.29) that $\ddot{\mathbf{x}}_i$ and $\mathbf{x}_i^{(3)}$ are (correlated) random vectors, whose joint PDF $p\left(\ddot{\mathbf{x}}_i,\mathbf{x}_i^{(3)}\right)$ can be determined via the following steps:

i. Apply the WPI technique (e.g., [Kougioumtzoglou et al., 2015]) to Eqn. (3.2) to evaluate the joint PDF of $\boldsymbol{\xi}_s$ and $\dot{\boldsymbol{\xi}}_s$.

ii. $\boldsymbol{\xi}_s$ and $\dot{\boldsymbol{\xi}}_s$ are related to $\mathbf{f}$ and $\dot{\mathbf{f}}$ via Eqn. (3.21) and its differentiated version

$$\dot{\mathbf{f}}(t) = \mathbf{D}(t)\dot{\boldsymbol{\xi}}_s(t) + \dot{\mathbf{D}}(t)\boldsymbol{\xi}_s(t) \tag{3.30}$$

Thus, the joint PDF $p\left(\ddot{\mathbf{x}}_i, \mathbf{x}_i^{(3)}\right)$ can be readily evaluated by considering Eqs. (3.28), (3.29), (3.21), and (3.30) and applying standard PDF transformations between random vectors (e.g., [Ang and Tang, 2007]).

Furthermore, taking into account the fact that the initial conditions $\mathbf{x}_i$ and $\dot{\mathbf{x}}_i$ are deterministic and fixed, the response transition PDF can be written as [Wio et al., 1989]

$$p\left(\mathbf{x}_f, \dot{\mathbf{x}}_f, \ddot{\mathbf{x}}_f, \mathbf{x}_f^{(3)}, t_f | \mathbf{x}_i, \dot{\mathbf{x}}_i, t_i\right) = \int_{-\infty}^{\infty} p\left(\mathbf{x}_f, \dot{\mathbf{x}}_f, \ddot{\mathbf{x}}_f, \mathbf{x}_f^{(3)}, t_f | \mathbf{x}_i, \dot{\mathbf{x}}_i, \ddot{\mathbf{x}}_i, \mathbf{x}_i^{(3)}, t_i\right) p\left(\ddot{\mathbf{x}}_i, \mathbf{x}_i^{(3)}\right) \mathrm{d}\ddot{\mathbf{x}}_i \mathrm{d}\,\mathbf{x}_i^{(3)} \tag{3.31}$$

Eqn. (3.31) can be seen as the mean of $p\left(\mathbf{x}_f, \dot{\mathbf{x}}_f, \ddot{\mathbf{x}}_f, \mathbf{x}_f^{(3)}, t_f | \mathbf{x}_i, \dot{\mathbf{x}}_i, \ddot{\mathbf{x}}_i, \mathbf{x}_i^{(3)}, t_i\right)$ over all possible initial values $\ddot{\mathbf{x}}_i$ and $\mathbf{x}_i^{(3)}$. In general, stochastic excitation models of the form of Eqs. (3.20) and (3.21) can be accounted for with the use of the herein developed WPI based technique of Section 3.1, where $p\left(\mathbf{x}_f, \dot{\mathbf{x}}_f, \ddot{\mathbf{x}}_f, \mathbf{x}_f^{(3)}, t_f | \mathbf{x}_i, \dot{\mathbf{x}}_i, \ddot{\mathbf{x}}_i, \mathbf{x}_i^{(3)}, t_i\right)$ is computed for every pair of initial values $\left(\ddot{\mathbf{x}}_i, \mathbf{x}_i^{(3)}\right)$, followed by the integration of Eqn. (3.31). This procedure yields one point of the response transition PDF $p\left(\mathbf{x}_f, \dot{\mathbf{x}}_f, \ddot{\mathbf{x}}_f, \mathbf{x}_f^{(3)}, t_f | \mathbf{x}_i, \dot{\mathbf{x}}_i, t_i\right)$.

Interestingly, analogous modifications have been introduced in alternative stochastic dynamics techniques, such as the time-domain formulation of statistical linearization, where a "switch" allows the filter equation output to reach stationarity before being used as an input to the original governing equation of the engineering system [Roberts and Spanos, 2003].

3.2.2 Computational aspects

As discussed in Section 3.1.2, implementing the WPI technique with the brute force approach to discretizing the effective domain for the response transition PDF yields N^{4m} BVPs to be solved. Moreover, discretizing the domains of the initial values of $\ddot{\mathbf{x}}_i$ and $\mathbf{x}_i^{(3)}$ into M points in each dimension requires solving M^2 BVPs (Eqs. (3.16) and (3.17)) to determine one point of $p\left(\mathbf{x}_f, \dot{\mathbf{x}}_f, \ddot{\mathbf{x}}_f, \mathbf{x}_f^{(3)}, t_f | \mathbf{x}_i, \dot{\mathbf{x}}_i, t_i\right)$. This way, the total number of BVPs to be solved to evaluate the full PDF $p\left(\mathbf{x}_f, \dot{\mathbf{x}}_f, \ddot{\mathbf{x}}_f, \mathbf{x}_f^{(3)}, t_f | \mathbf{x}_i, \dot{\mathbf{x}}_i, t_i\right)$ becomes $M^2 N^{4m}$. Obviously, the increase in the computational effort makes it almost mandatory to use the WPI technique in combination with the computationally efficient PDF representation scheme proposed in [Kougioumtzoglou et al., 2015].

Chapter 4

Numerical Validation

In this chapter, the versatility and reliability of the developed technique are demonstrated by considering various diverse numerical examples. In the first example the technique developed in Section 3.1 is applied to a 2-DOF linear structure under non-white excitation, while to demonstrate the approach delineated in Section 3.2 the second example refers to an SDOF nonlinear oscillator subject to time-modulated non-white excitation. Further, the third example relates to a marine structure subject to flow-induced forces. This example serves to demonstrate that even in cases where the excitation power spectrum (e.g., JONSWAP [Hasselmann et al., 1973, Pierson and Moskowitz, 1964]) cannot be analytically expressed in the time domain in the form of Eqn. (3.2), a linear filter approximation [Spanos, 1986] provides satisfactory accuracy; and thus, the herein developed WPI technique can be applied in a straightforward manner. Finally, the last example pertains to a cantilever beam with the Young's modulus modeled as a non-white and non-Gaussian stochastic field. In all of the examples, comparisons with corresponding MCS data ($50,000$ realizations) demonstrate the accuracy of the developed WPI technique. To this aim, a standard fourth-order Runge-Kutta numerical integration scheme is employed for solving the governing equations of motion within the MCS context.

4.1 MDOF system subject to non-white excitation process

The first example demonstrates the WPI technique developed in Section 3.1 in application to a MDOF system exposed to non-white stochastic excitation. Particularly, the joint response PDF of a 2-DOF system is determined, where the oscillator is governed by the equation of motion of the form of Eqn. (3.1) with $\mathbf{g}(\mathbf{x},\dot{\mathbf{x}}) = \mathbf{0}$ and

$$\mathbf{M} = \begin{bmatrix} m_0 & 0 \\ m_0 & m_0 \end{bmatrix}, \tag{4.1}$$

$$\mathbf{C} = \begin{bmatrix} c & -c \\ 0 & c \end{bmatrix}, \tag{4.2}$$

$$\mathbf{K} = \begin{bmatrix} k & -k \\ 0 & k \end{bmatrix}. \tag{4.3}$$

The filter coefficients of Eqn. (3.2) are chosen as

$$\mathbf{P} = \begin{bmatrix} p & 0 \\ 0 & p \end{bmatrix}, \tag{4.4}$$

$$\mathbf{Q} = \begin{bmatrix} q & 0 \\ 0 & q \end{bmatrix}, \tag{4.5}$$

$$\mathbf{R} = \begin{bmatrix} r & 0 \\ 0 & r \end{bmatrix}. \tag{4.6}$$

Table 4.1: System parameters pertaining to Eqs. (4.1)-(4.6).

m_0	c	k	p	q	r	S_0
1	0.1	1	1	0.1	1	0.0637

The numerical values of the parameters chosen for the simulations are presented in Table 4.1. The joint PDF of displacements x_1 and x_2 is plotted for time instances $t = 1.0\,s$ and $t = 2.0\,s$ in Figs. 4.1 and 4.2, respectively. The corresponding marginal PDFs are presented in Fig. 4.3. The joint response transition PDF is approximated by a second-order polynomial [Kougioumtzoglou et al., 2015]; this way, the polynomial coefficients are obtained through solving only 37 BVPs of

the form of Eqs. (3.16) and (3.17) for any given time instance t_f. The complete PDF is then readily available at any point of the effective domain $(\mathbf{x}_f, \dot{\mathbf{x}}_f, \ddot{\mathbf{x}}_f, \mathbf{x}_f^{(3)})$.

Comparison is made with the pertinent MCS data (50,000 realizations) and included in the figures. The results obtained via the proposed technique are in very good agrrement with the MCS data and demonstrate the capability of the WPI approach to capture the prominent features of the system joint response PDF.

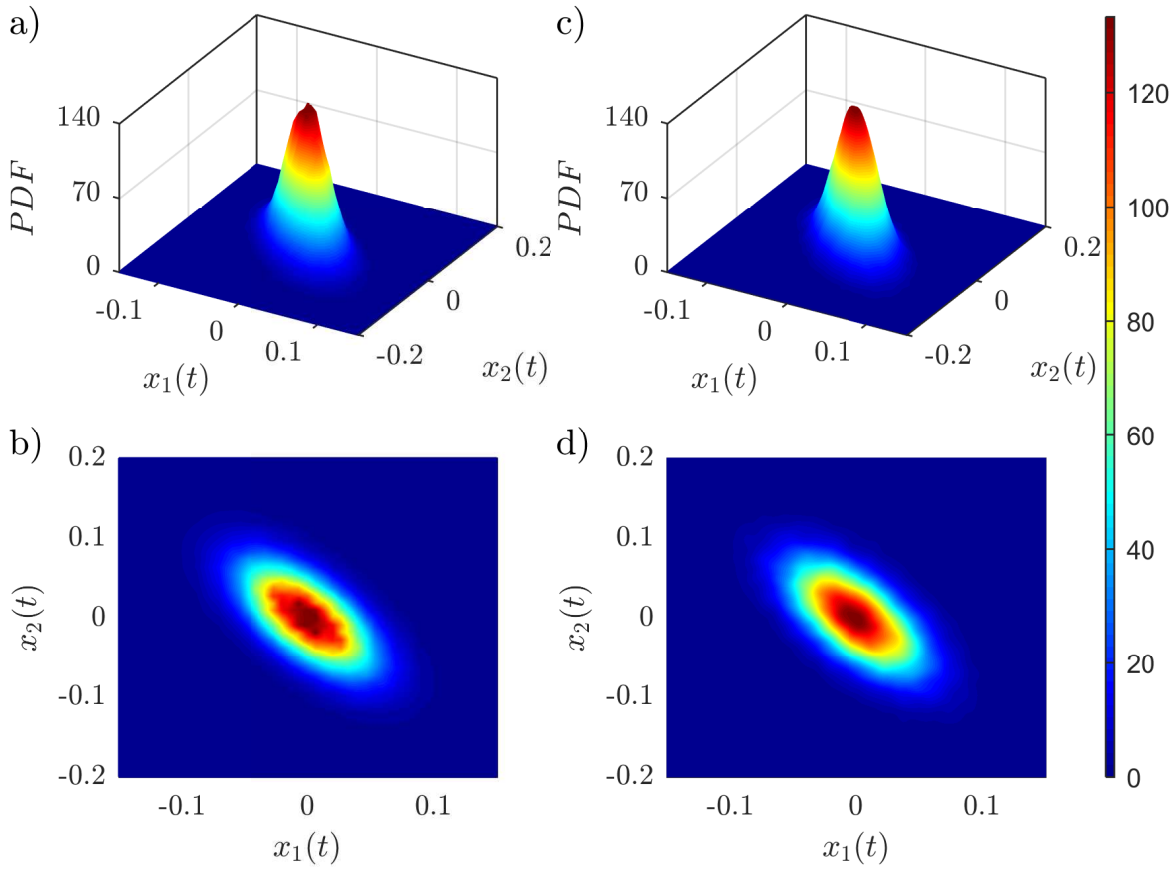

Figure 4.1: Joint PDF of $x_1(t)$ and $x_2(t)$ at time $t = 1.0\ s$, as obtained via the WPI technique (a - b); comparisons with MCS data - 50,000 realizations (c - d).

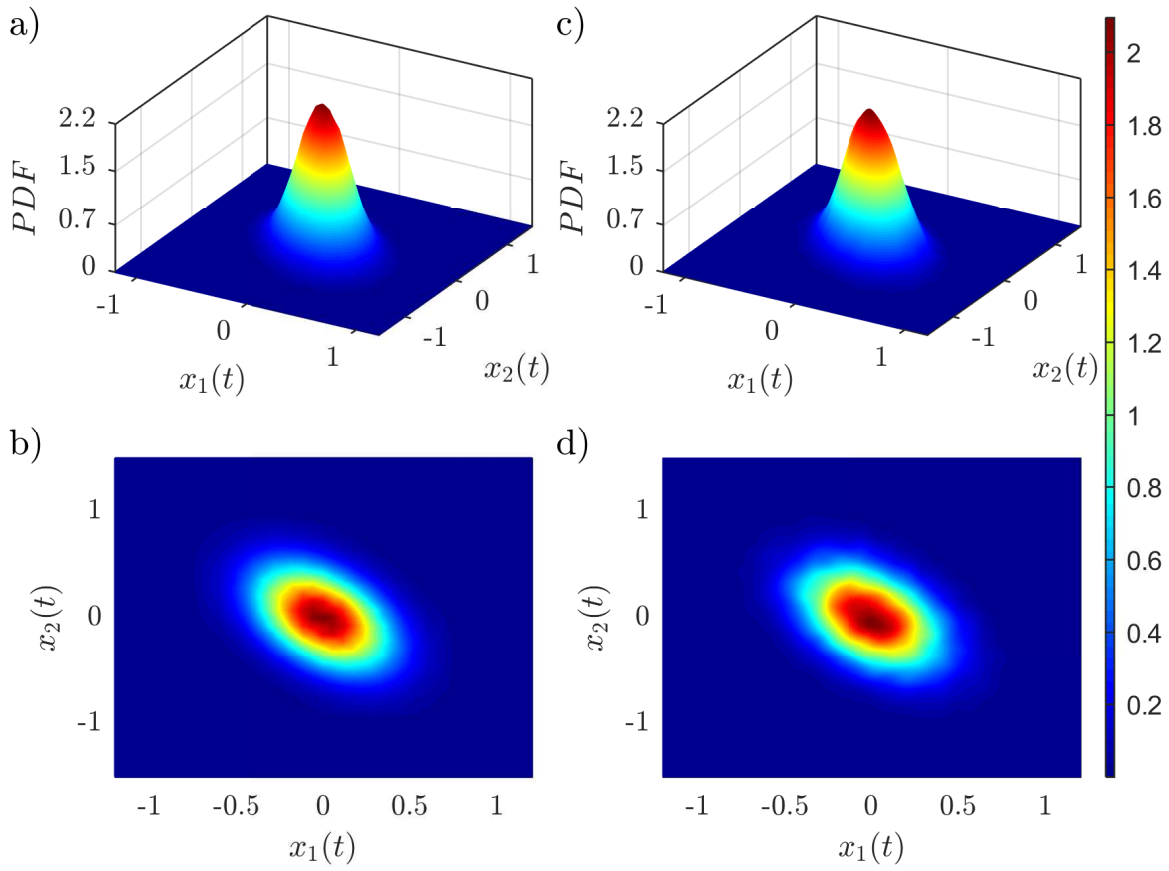

Figure 4.2: Joint PDF of $x_1(t)$ and $x_2(t)$ at time $t = 2.0\,s$, as obtained via the WPI technique (a - b); comparisons with MCS data - 50,000 realizations (c - d).

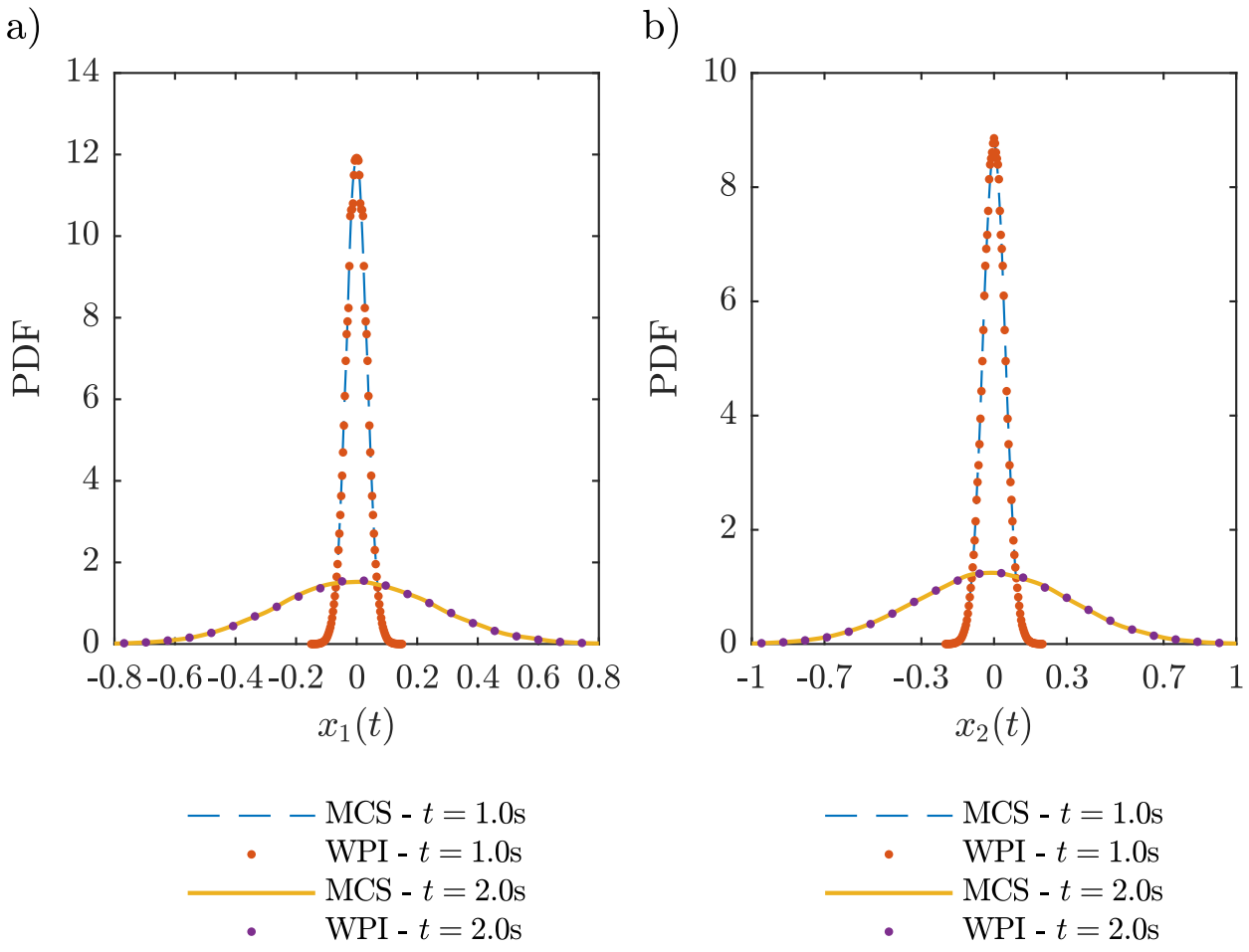

Figure 4.3: Marginal PDF of $x_1(t)$ (a) and $x_2(t)$ (b) at time instances $t = 1.0\,s$ and $t = 2.0\,s$, as obtained via the WPI technique; comparisons with MCS data (50,000 realizations).

4.2 SDOF system subject to time-modulated non-white excitation process

The modification of the technique discussed in Section 3.2 is implemented next. It allows the filter equation output to reach stationarity, and is applied below to a problem of a nonlinear SDOF oscillator. The oscillator's motion is governed by Eqn. (3.22) with $\mathbf{M} = m_0$; $\mathbf{C} = c$; $\mathbf{K} = k$; $\mathbf{g}(\mathbf{x}, \dot{\mathbf{x}}) = \varepsilon k x^3$, where ε is the magnitude of nonlinearity. The numerical values of the parameters are listed in Table 4.2.

Table 4.2: System parameters used in Section 4.2.

m_0	c	k	ε	S_0	α	β	γ	λ	q	r
1	0.1	2	1	1	1	2	10^{-4}	4	1	1

The excitation $f(t)$ is modeled in accordance with Eqs. (3.20) and (3.21) with the power spectrum expressed as

$$S_f(\omega, t) = d^2(t) S_{\xi_s}(\omega), \tag{4.7}$$

where

$$S_{\xi_s}(\omega) = \frac{S_0}{\omega^2 q^2 + r^2}, \tag{4.8}$$

and

$$d(t) = \gamma + \lambda(e^{-\alpha t} - e^{-\beta t}). \tag{4.9}$$

Note that $S_{\xi_s}(\omega)$ corresponds to the stationary output of the filter equation in the time domain

$$q\dot{\xi} + r\xi = w(t), \tag{4.10}$$

where $w(t)$ is a zero-mean white noise process with intensity S_0.

Next, $\xi_s(t)$ and $\dot{\xi}_s(t)$ can be expressed in terms of $f(t)$ via applying Eqs. (3.23) and (3.24), and

substituted into Eqn. (4.10), which yields

$$\frac{1}{d}\left[r\left(m_0\ddot{x}+c\dot{x}+kx+\varepsilon kx^3\right)\right.$$
$$\left.+q\left(m_0x^{(3)}+c\ddot{x}+k\dot{x}+3\varepsilon kx^2\dot{x}-\frac{\dot{d}}{d}\left(m_0\ddot{x}+c\dot{x}+kx+\varepsilon kx^3\right)\right)\right]=w(t). \quad (4.11)$$

The associated Lagrangian then takes the form

$$L\left[x,\dot{x},\ddot{x},x^{(3)}\right]=\frac{1}{4\pi S_0}\cdot\frac{1}{d^2}\left[r\left(m_0\ddot{x}+c\dot{x}+kx+\varepsilon kx^3\right)\right.$$
$$\left.+q\left(m_0x^{(3)}+c\ddot{x}+k\dot{x}+3\varepsilon kx^2\dot{x}-\frac{\dot{d}}{d}\left(m_0\ddot{x}+c\dot{x}+kx+\varepsilon kx^3\right)\right)\right]^2, \quad (4.12)$$

and the associated E-L Eqn. (3.16) becomes

$$\frac{\partial L}{\partial x_c}-\frac{\partial}{\partial t}\frac{\partial L}{\partial \dot{x}_c}+\frac{\partial^2}{\partial t^2}\frac{\partial L}{\partial \ddot{x}_c}-\frac{\partial^3}{\partial t^3}\frac{\partial L}{\partial x_c^{(3)}}=0, \quad (4.13)$$

together with the initial conditions for $t_i=0$

$$x_c(t_i)=x_i=0,\quad \dot{x}_c(t_i)=\dot{x}_i=0,\quad \ddot{x}_c(t_i)=\ddot{x}_i=\frac{1}{m_0}d(t_i)\xi_s(t_i). \quad (4.14)$$

It was noted in Section 3.2.1 that $\ddot{x}_i$ is a random variable. Therefore, the WPI technique [Kougioumtzoglou et al., 2015] is first utilized in conjunction with the filter Eqn. (4.10) to determine the stationary PDF $p_{\xi_s}\left(\xi_s(t_i)\right)$. The PDF $p_{\ddot{x}_i}(\ddot{x}_i)$ is then computed with the use of the following relationship [Ang and Tang, 2007]

$$p_{\ddot{x}_i}(\ddot{x}_i)=\frac{m_0}{d(t_i)}\left[p_{\xi_s}\left(\frac{m_0}{d(t_i)}\ddot{x}_i\right)\right]. \quad (4.15)$$

The domain of initial values of $\ddot{x}_i$ is discretized into $M=30$ points next. In addition, an effective domain of final values x_f, $\dot{x}_f$ and $\ddot{x}_f$ is into $N=101$ points in each dimension (see also Section 3.2.2). Therefore, each set of final values $(x_f,\dot{x}_f,\ddot{x}_f)$ requires solving $M^2=900$ BVPs of the form of Eqn. (4.13). Each such solution provides a most probable path $x_c(t)$, which can be substituted

into Eqn. (3.18) to obtain

$$p(x_f,\dot{x}_f,\ddot{x}_f,t_f|x_i,\dot{x}_i,\ddot{x}_i,t_i) = \exp\left(-\int_{t_i}^{t_f} L\left[x_c,\dot{x}_c,\ddot{x}_c,x_c^{(3)}\right] \mathrm{d}t\right) \tag{4.16}$$

Next, Eqn. (3.31) is employed to calculate a point of the PDF $p(x_f,\dot{x}_f,\ddot{x}_f,t_f|x_i,\dot{x}_i,t_i)$

$$p(x_f,\dot{x}_f,\ddot{x}_f,t_f|x_i,\dot{x}_i,t_i) = \int_{-\infty}^{\infty} p\left(x_f,\dot{x}_f,\ddot{x}_f,t_f|x_i,\dot{x}_i,\ddot{x}_i,t_i\right) p_{\ddot{x}_i}(\ddot{x}_i)\, \mathrm{d}\ddot{x}_i \tag{4.17}$$

Further, the developed approximate WPI technique is compared to the MCS data, namely, the nonstationary response displacement and velocity PDFs. The spectral representation technique [Liang et al., 2007, Shinozuka and Deodatis, 1991] is employed to generate realizations of $f(t)$ compatible with the evolutionary power spectrum of Eqn. (4.7) to be used in the MCS. The result of modeling the evolutionary power spectrum (EPS) of the excitation is shown in Fig. 4.4.

The comparison between the MCS data (50,000 realizations) and the WPI results allows to assess the performance of the new technique. Figs. 4.5 and 4.6 demonstrate the joint PDF of $x(t)$ and $\dot{x}(t)$ at times $t = 0.5\ s$ and $t = 1.0\ s$, respectively. In addition, the marginal PDFs of $x(t)$ and $\dot{x}(t)$ at times $t = 0.5\ s$ and $t = 1.0\ s$ are obtained via both approaches for comparison and plotted in Fig. 4.7. It can be observed that the results provided by the WPI technique agree very well with the MCS data; nevertheless, the computational cost can become prohibitive for relatively high dimensional MDOF systems. The suggestion is to employ an efficient numerical treatment for determining the joint response PDF, such as the one proposed by [Kougioumtzoglou et al., 2015], to reduce the computational effort.

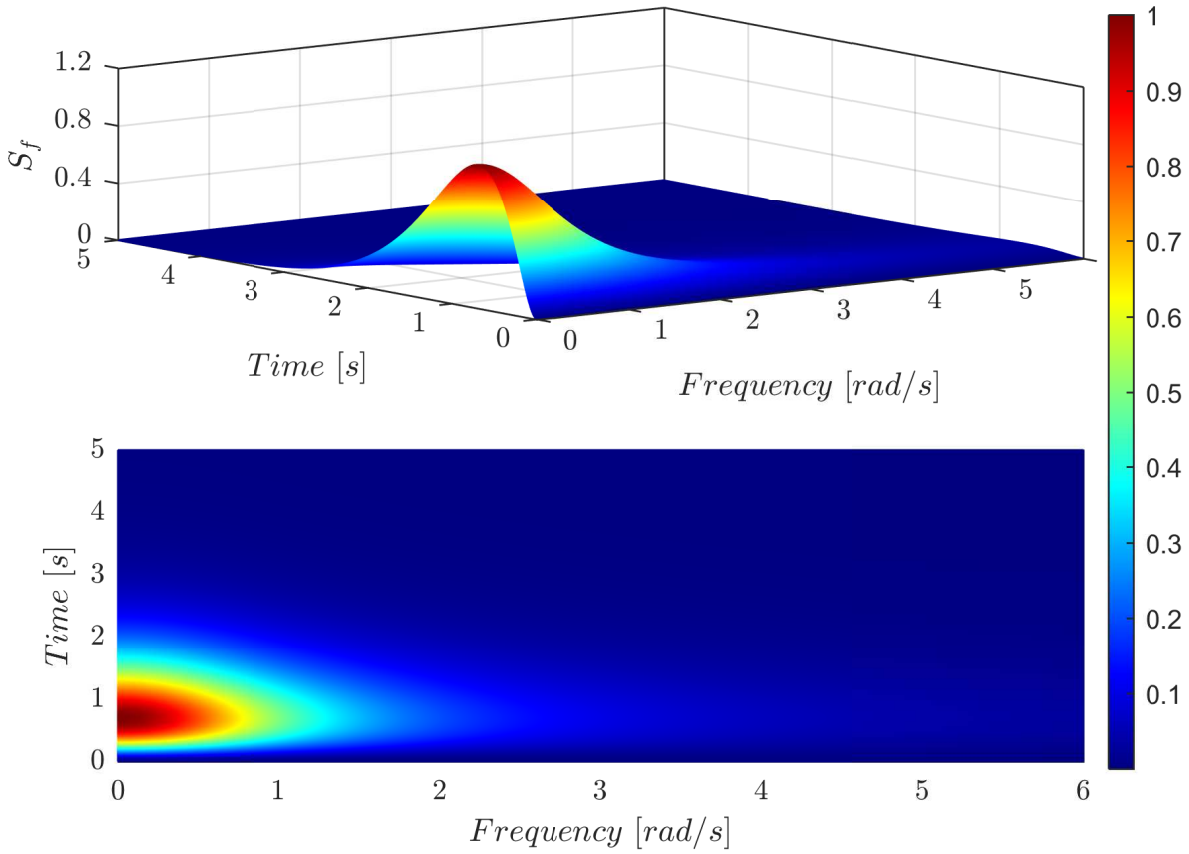

Figure 4.4: Excitation EPS, given by Eqn. (4.7) with parameter values from Table 4.2.

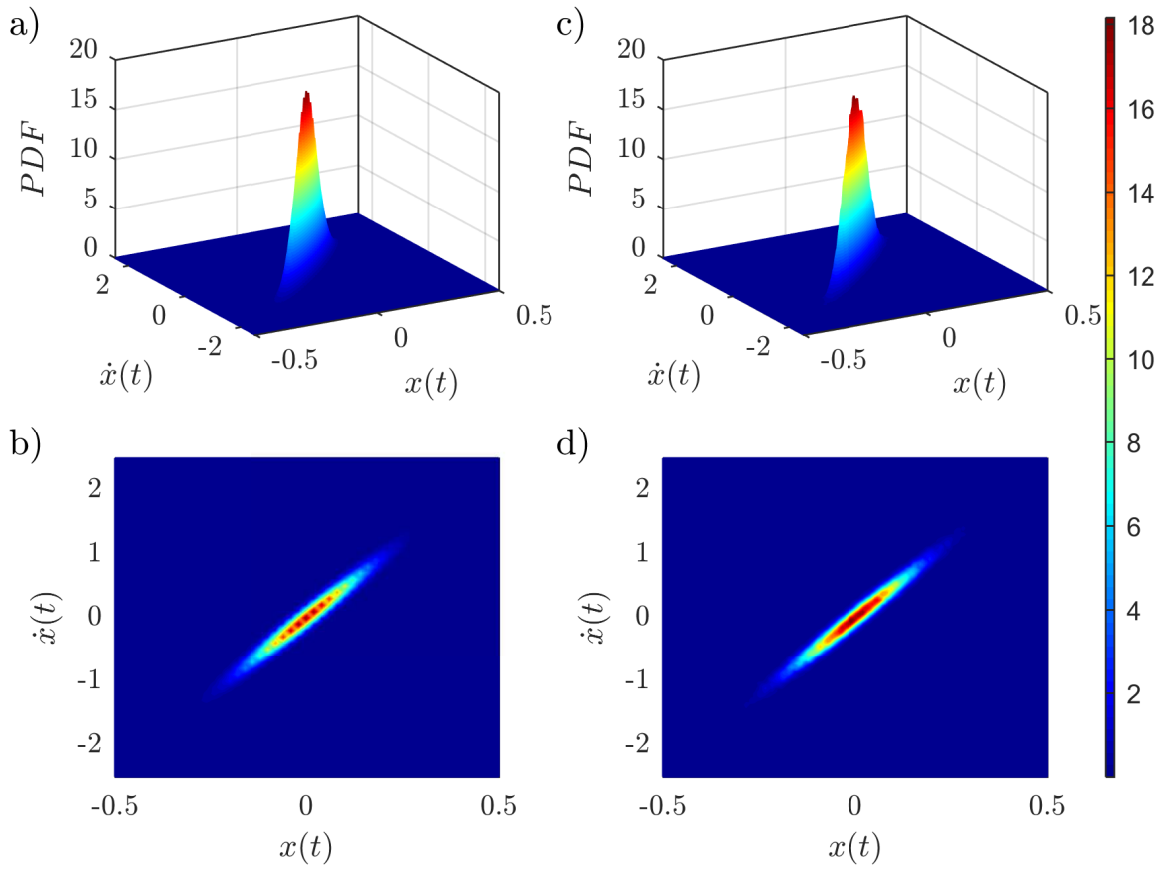

Figure 4.5: Joint PDF of $x(t)$ and $\dot{x}(t)$ at time $t = 0.5$ *s*, as obtained via the WPI technique (a - b); comparisons with MCS data - 50,000 realizations (c - d).

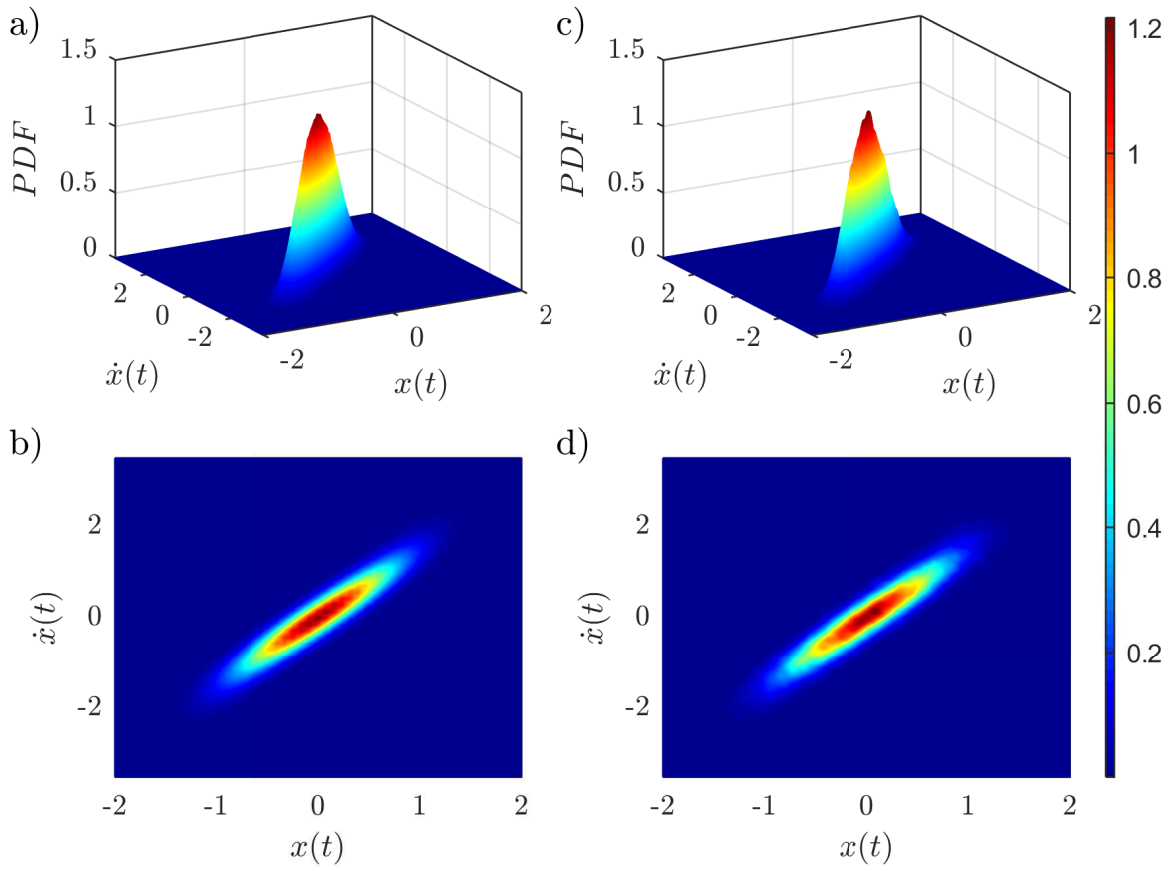

Figure 4.6: Joint PDF of $x(t)$ and $\dot{x}(t)$ at time $t = 1.0\ s$, as obtained via the WPI technique (a - b); comparisons with MCS data - 50,000 realizations (c - d).

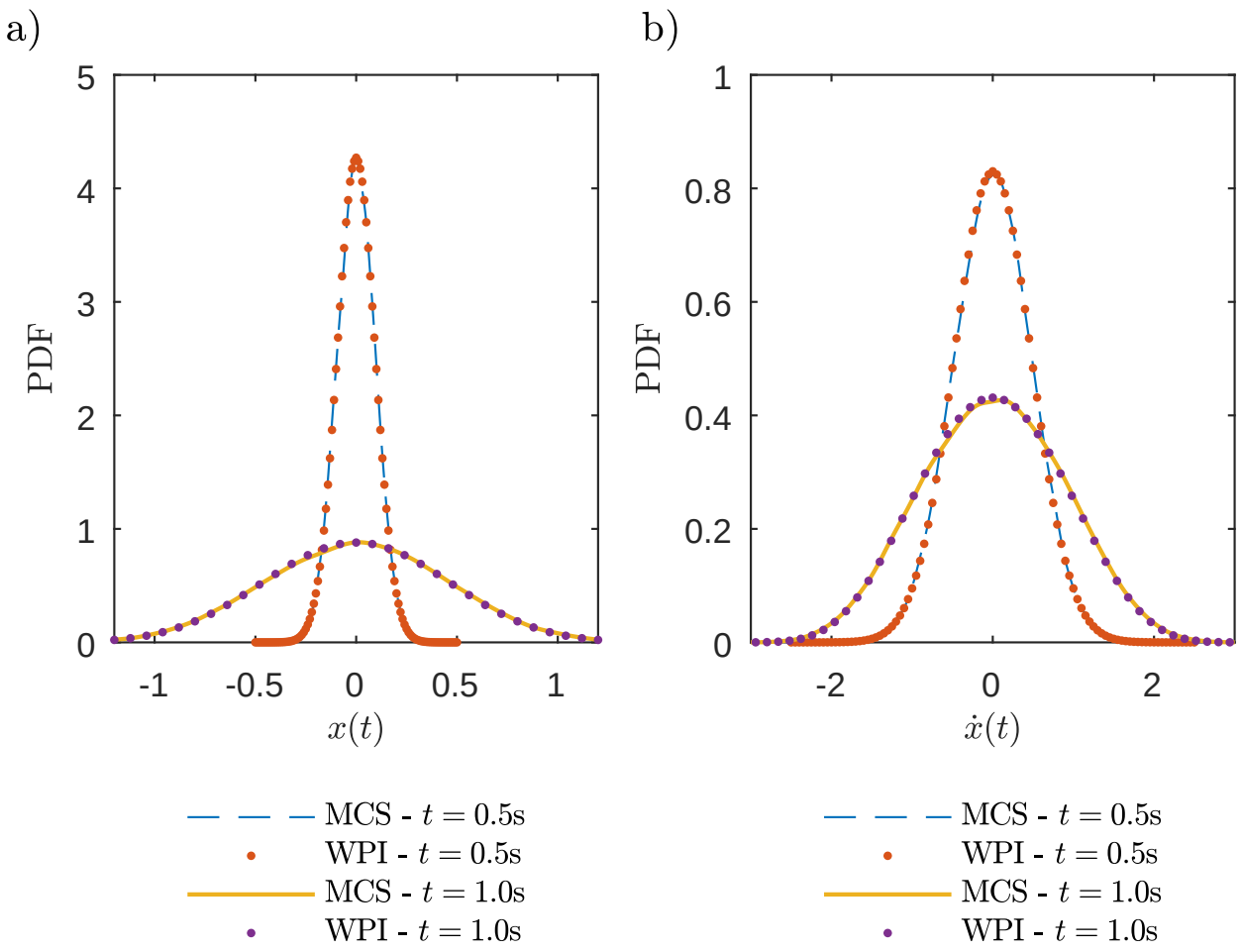

Figure 4.7: Marginal PDF of $x(t)$ (a) and $\dot{x}(t)$ (b) at time instances $t = 0.5\,s$ and $t = 1.0\,s$, as obtained via the WPI technique; comparisons with MCS data (50,000 realizations).

4.3 Structural system exposed to flow-induced forces

The next example studies a structure exposed to flow-induced forces. This is a frequently encountered problem in marine engineering applications, where structures composed with slender elements are excited by flow-induced forces described often via Morison equation [Morison et al., 1950]. The main terms of the Morison equation are the inertial force component proportional to the mass of the system and the drag-type nonlinear term dependent on the relative velocity of the structure to the water particles. Typical examples include tension leg platforms [Kim et al., 2001], the jacket structures [Naess et al., 2007] and the spar structures [Spanos et al., 2005].

It is common to characterize the stochastic excitation in this class of problems through an additional nonlinearity provided by non-white power spectra dependent on the free surface power spectrum of the underlying sea state. A number classical models of the sea wave spectra have been proposed over the last few decades; the current research utilizes the celebrated JONSWAP spectrum for modeling of the sea state [Hasselmann et al., 1973, Pierson and Moskowitz, 1964]. This way, the power spectrum of the free surface displacement can be described by the following nondimensional equation

$$S(\bar{\omega}) = \frac{S(\omega)}{S(\omega_p)} = \frac{\exp(1.25)}{\bar{\omega}^5} \exp\left(-\frac{1.25}{\bar{\omega}^4}\right) \gamma^{\mu-1}, \tag{4.18}$$

where

$$\bar{\omega} = \frac{\omega}{\omega_p}, \tag{4.19}$$

and

$$\gamma = \exp\left[-\frac{(1-\bar{\omega})^2}{2\lambda^2}\right]. \tag{4.20}$$

In this model, γ denotes the peak enhancement factor, λ the sharpness magnification factor, and ω_p is the peak frequency of the spectrum.

This numerical example considers a SDOF linear oscillator

$$m_0\ddot{x} + c\dot{x} + kx = h(t), \tag{4.21}$$

where m_0 is the mass of the engineering system; c its structural damping; k the structural stiffness; x the absolute displacement of the structure; and $h(t)$ the system excitation, which can be calculated as [Spanos and Chen, 1981]

$$h(t) = \rho A\ddot{v} + C_l\rho A(\ddot{v} - \ddot{x}) + \frac{1}{2}C_D\rho D|\dot{v} - \dot{x}|(\dot{v} - \dot{x}). \tag{4.22}$$

Here, ρ is the water density; A the cross-sectional area of the structure; D its diameter; C_l and C_D the mass and drag coefficients, respectively; and $\dot{v}$ the water particles velocity. After switching to the relative coordinates $y = x - v$, the equation of motion becomes

$$\ddot{y} + 2\omega_N\xi_N\dot{y} + \omega_N^2 y + \frac{1}{2}\frac{C_D\rho D}{M_0}|V + \dot{y}|(V + \dot{y}) = f(t), \tag{4.23}$$

where V denotes the water current (mean component of the water particle velocity); $M_0 = m_0 + C_l\rho A$; and $f(t)$ denotes the system excitation compatible with the power spectrum [Spanos and Chen, 1981]

$$S_f(\omega) = \left[\omega_N^4 + \left(2\xi_N - 2 + 2C_M\frac{\rho A}{M_0}\right)\omega_N^2\omega^2 + \left(1 - C_M\frac{\rho A}{M_0}\right)^2\omega^4\right]S(\omega), \tag{4.24}$$

with

$$C_M = 1 + C_l, \tag{4.25}$$

$$\omega_N = \omega_0\sqrt{\frac{m_0}{M_0}}, \tag{4.26}$$

$$\xi_N = c\sqrt{\frac{m_0}{M_0}}. \tag{4.27}$$

An implementation of the proposed WPI technique follows via a second-order linear filter approximation of the excitation power spectrum (4.24)

$$p\ddot{f}(t) + q\dot{f}(t) + rf(t) = w(t). \tag{4.28}$$

Thus, the dynamics of the system can be described by the system of equations

$$\begin{cases} \ddot{y} + 2\omega_N \xi_N \dot{y} + \omega_N^2 y + \dfrac{1}{2}\dfrac{C_D \rho D}{M_0} |V + \dot{y}|(V + \dot{y}) = f(t) \\ p\ddot{f}(t) + q\dot{f}(t) + rf(t) = w(t). \end{cases} \tag{4.29}$$

In this regard, the model is in no way restricted to use of a second-order linear filter. Moreover, the accuracy of the filter approximation can be enhanced to a desired level by employing higher-order filters; relevant work has been done by [Spanos, 1986] and more recently by [Chai et al., 2015] on evaluation of the filter parameters and its impact on the response determination of engineering systems.

The numerical parameters for the example take the values in Table 4.3. The free surface displacement power spectrum $S(\omega)$ is made compatible with the a mean JONSWAP spectrum with the significant wave height $H_S = 1\ m$. Further, the system is exposed to an excitation compatible with the power spectrum in Fig. 4.8; an important note is that the spectrum is bell-shaped. Fig. 4.8 also presents a comparison with the corresponding free surface displacement spectrum $S(\omega)$ which demonstrates similarity in low frequency pattern and peak frequencies, however, the free surface spectrum decays more rapidly at higher frequencies.

Table 4.3: System parameters used in Section 4.3.

ξ_N	$\rho D/M_0$	$V[m/s]$	C_D	ω_N	C_M	$A[m^2]$	$D[m]$	p	q	r	S_0
0.02	1.136	0	1	1.2566	1.25	0.073	0.3	18.98	4.59	31.39	17.18

The implementation of the technique starts with employing the second-order filter with parameters (p,q,r) to approximate the system excitation, Eqn. (4.29). The parameters are estimated via least squares numerical optimization scheme and are chosen to minimize the mean square error between the excitation spectrum and the filter approximation in the frequency domain. The resulting optimal filter parameter values are presented in Table 4.3; the corresponding power spectrum is shown in Fig. 4.9 as a dashed line.

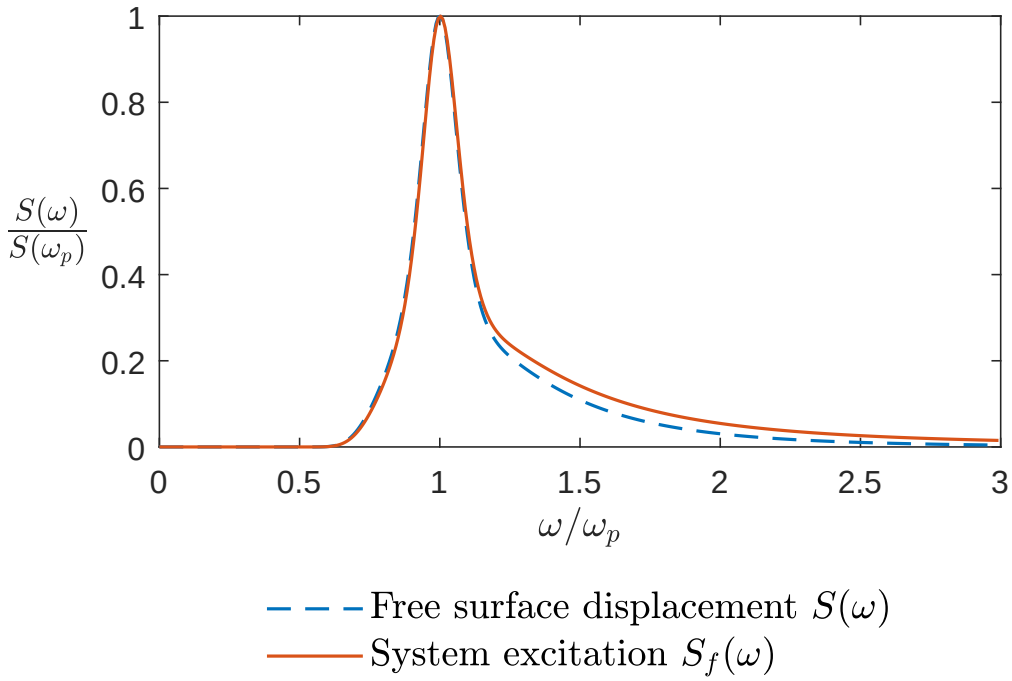

Figure 4.8: Comparison between the normalized power spectra of the free surface displacement and of the system excitation Eqn. (4.23).

Reliability of the WPI technique is assessed through comparison of the response PDF with the MCS data (50,000 realizations). The approximate WPI solution uses a domain of final values $(y_f, \dot{y}_f, \ddot{y}_f, y_f^{(3)})$ discretized into 51 points in each dimension; whereas, the initial values are assumed deterministic $(y_i = 0, \dot{y}_i = 0, \ddot{y}_i = 0, y_i^{(3)} = 0)$. The marginal PDFs are then obtained with numerical integration. The joint PDFs of the system displacement and velocity at final time instances $t = 0.5\ s$ and $t = 1.0\ s$ are demontsrated in Figs. 4.10 and 4.11, respectively. The marginal system displacement and velocity PDFs at times $t = 0.5\ s$ and $t = 1.0\ s$ can be found in Fig. 4.12. Comparison with the MCS data proves high degree of accuracy of the approximate WPI technique developed herein. Moreover, an arbitrary form of the excitation power spectrum can be facilitated in a straightforward manner due to the filter approximation.

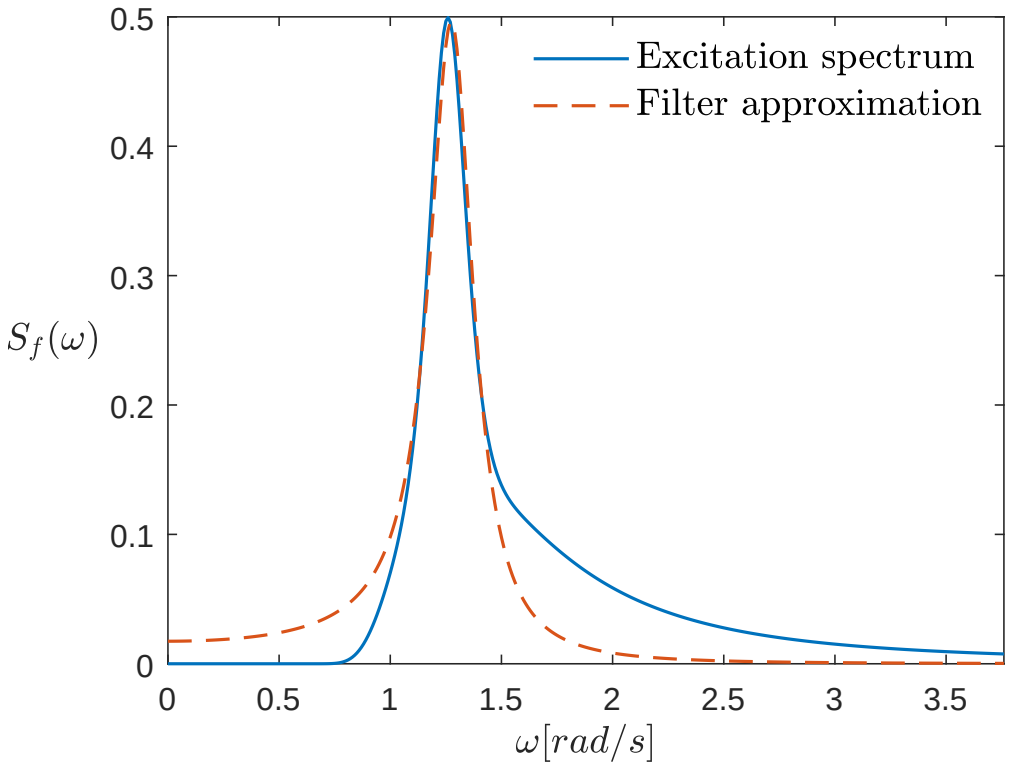

Figure 4.9: Comparison between the excitation spectrum and its filter approximation.

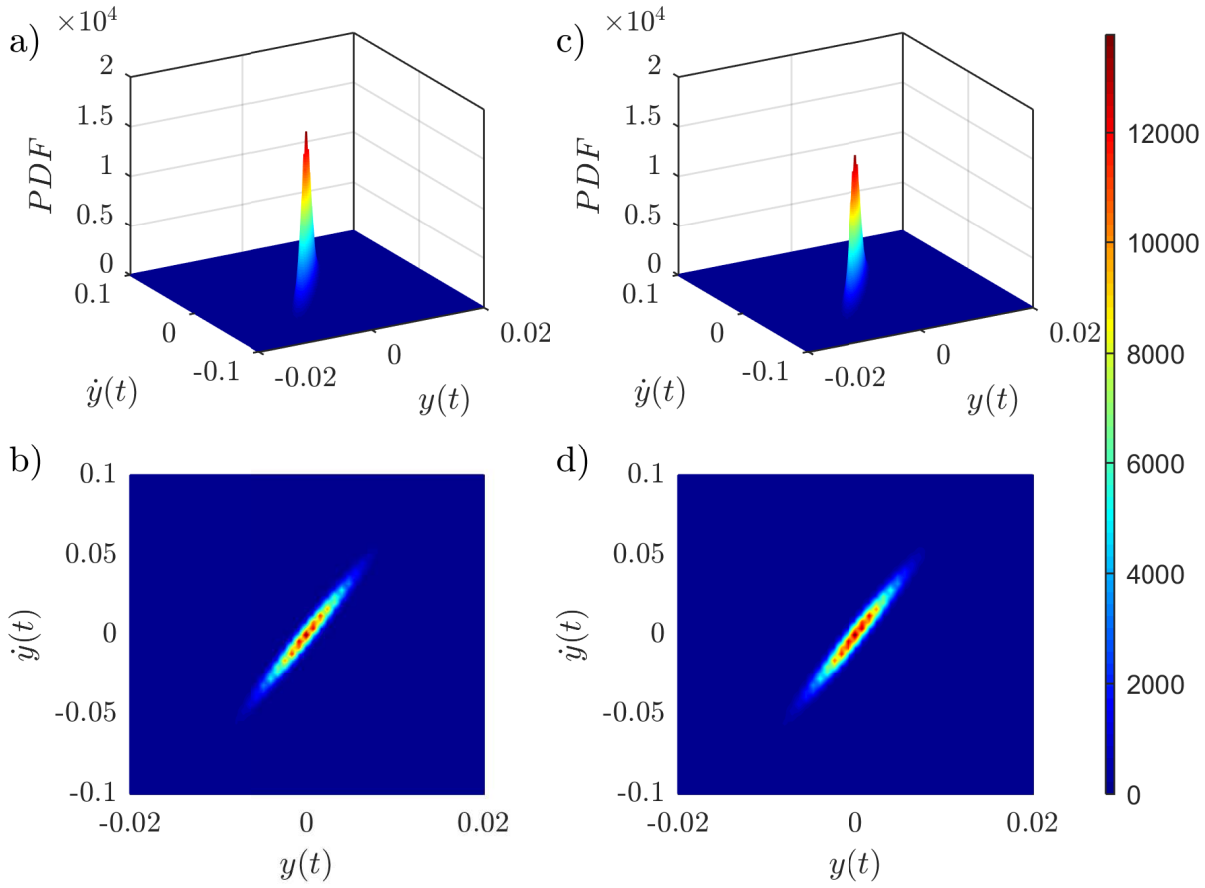

Figure 4.10: Joint PDF of $y(t)$ and $\dot{y}(t)$ at time $t = 0.5\ s$, as obtained via the WPI technique (a - b); comparisons with MCS data - 50,000 realizations (c - d).

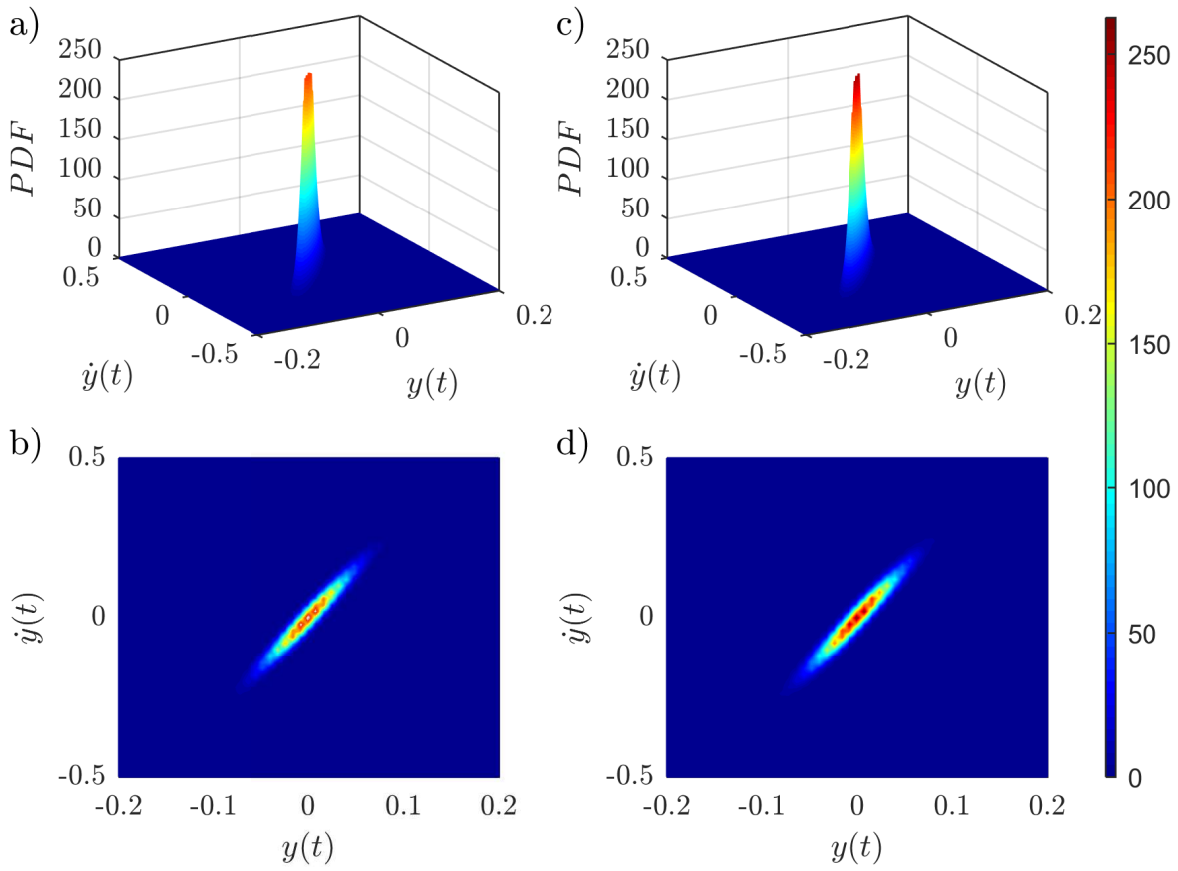

Figure 4.11: Joint PDF of $y(t)$ and $\dot{y}(t)$ at time $t = 1.0\,s$, as obtained via the WPI technique (a - b); comparisons with MCS data - 50,000 realizations (c - d).

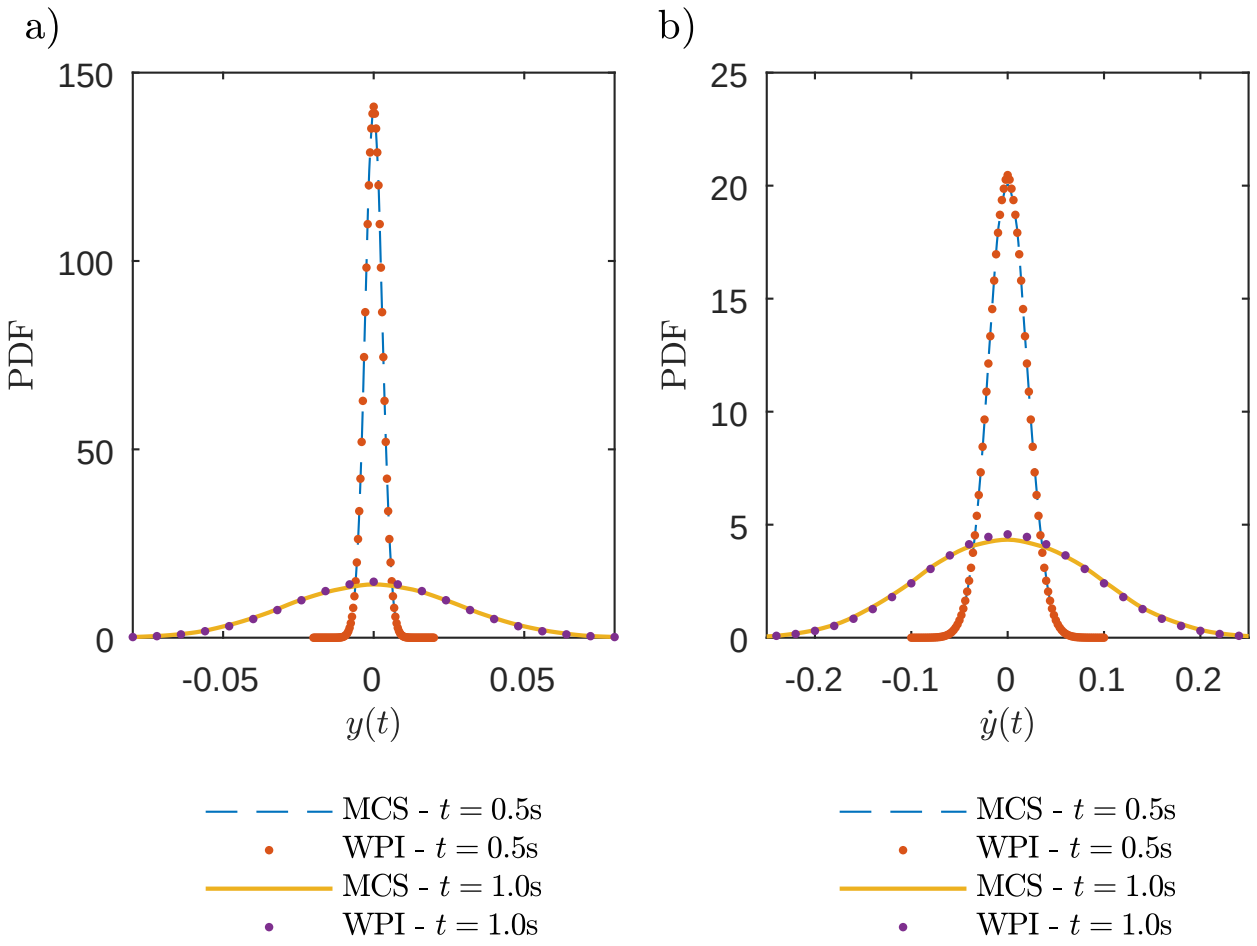

Figure 4.12: Marginal PDF of $y(t)$ (a) and $\dot{y}(t)$ (b) at time instances $t = 0.5\,s$ and $t = 1.0\,s$, as obtained via the WPI technique; comparisons with MCS data (50,000 realizations).

4.4 Beam Bending Problem with Stochastic Young's Modulus

The final example considers a statically determinate Euler-Bernoulli beam described by the following differential equation

$$\frac{\mathrm{d}^2}{\mathrm{d}z^2}\left[E(z)I\ddot{q}(z)\right] = l(z), \tag{4.30}$$

where $E(z)$ is the Young's modulus; I the constant cross-sectional moment of inertia; $q(z)$ the deflection of the beam; and $l(z)$ is a deterministic distributed force. In the current problem, the dot over a variable denotes differentiation with respect to the space coordinate z. Since the structure is statically determinate, one can integrate Eqn. (4.30) twice [Kougioumtzoglou, 2017, Shinozuka, 1987] taking into account boundary conditions $-E(z)I\ddot{q}(z) = M_0$ at $z = 0$ and $-E(z)I\ddot{q}(z) = M_L$ at $z = L$ which yields

$$-E(z)I\ddot{q}(z) = M(z), \tag{4.31}$$

where L is the length of the beam, and $M(z)$ the bending moment of the beam. Eqn. (4.31) can be also recast as

$$-\frac{M(z)}{I\ddot{q}(z)} = E(z). \tag{4.32}$$

Further, the Young's modulus is modeled as a non-Gaussian, non-white and non-homogeneous stochastic field

$$\frac{\dot{E}(z)}{E(z)} = w(z), \tag{4.33}$$

with $E(0) = E_M$, and $w(z)$ is the white noise process as defined in Eqn. (3.2). This way, Eqn. (4.33) is a standard geometric Brownian motion SDE, whose space-dependent response PDF is log-normal (e.g., [Øksendal, 2003]).

Moreover, Eqs. (4.32) and (4.33) can be combined to obtain an equation of the form of Eqn.

(3.4)

$$\frac{\dot{M}(z)}{M(z)} - \frac{q^{(3)}(z)}{\ddot{q}(z)} = w(z). \tag{4.34}$$

More specifiaclly, a cantilever beam subject to a single point moment at its free end is considered in the current example (Fig. 4.13). Thus, the bending moment $M(z)$ is constant along the length of the beam, i.e., $M(z) = M_0$; Eqn. (4.34) then becomes

$$-\frac{q^{(3)}(z)}{\ddot{q}(z)} = w(z). \tag{4.35}$$

Then, the Lagrangian from Eqn. (3.14) is

$$L\left[q, \dot{q}, \ddot{q}, q^{(3)}\right] = \frac{\left(q^{(3)}(z)\right)^2}{4\pi S_0 \left(\ddot{q}(z)\right)^2}, \tag{4.36}$$

and the E-L equation becomes

$$\frac{\partial L}{\partial q_c} - \frac{\partial}{\partial z}\frac{\partial L}{\partial \dot{q}_c} + \frac{\partial^2}{\partial z^2}\frac{\partial L}{\partial \ddot{q}_c} - \frac{\partial^3}{\partial z^3}\frac{\partial L}{\partial q_c^{(3)}} = 0, \tag{4.37}$$

with the initial conditions for $z_i = 0$, $q_c(z_i) = q_i = 0$, $\dot{q}_c(z_i) = \dot{q}_i = 0$ and $\ddot{q}_c(z_i) = -M_0/E_M I$.

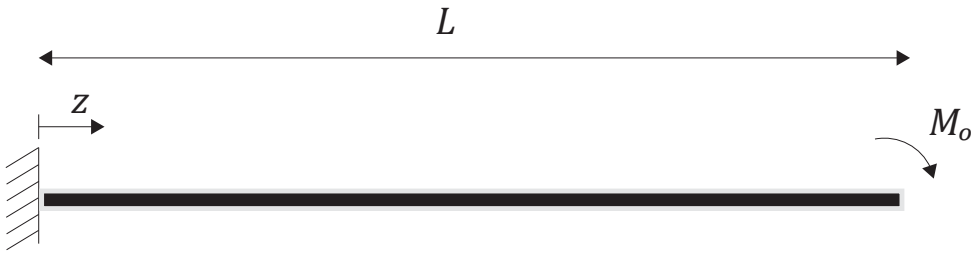

Figure 4.13: Cantilever beam subject to a single-point moment.

Table 4.4: System parameters used in Section 4.4.

E_M	I	M_0	L	S_0
10^6	10	10^5	1	0.001

The parameter values for the model are given in the Table 4.4. The joint PDFs of $q(z)$ and

$\dot{q}(z)$ at positions $z = 0.5$ and $z = 1.0$ along the length of the beam are shown in Figs. 4.14 and 4.15, respectively. Comparison with MCS data (50,000 realizations) is made as well. In addition, marginal PDFs of $q(z)$ and $\dot{q}(z)$ at positions $z = 0.5$ and $z = 1.0$ can be found in Figs. 4.16 and 4.17, respectively.

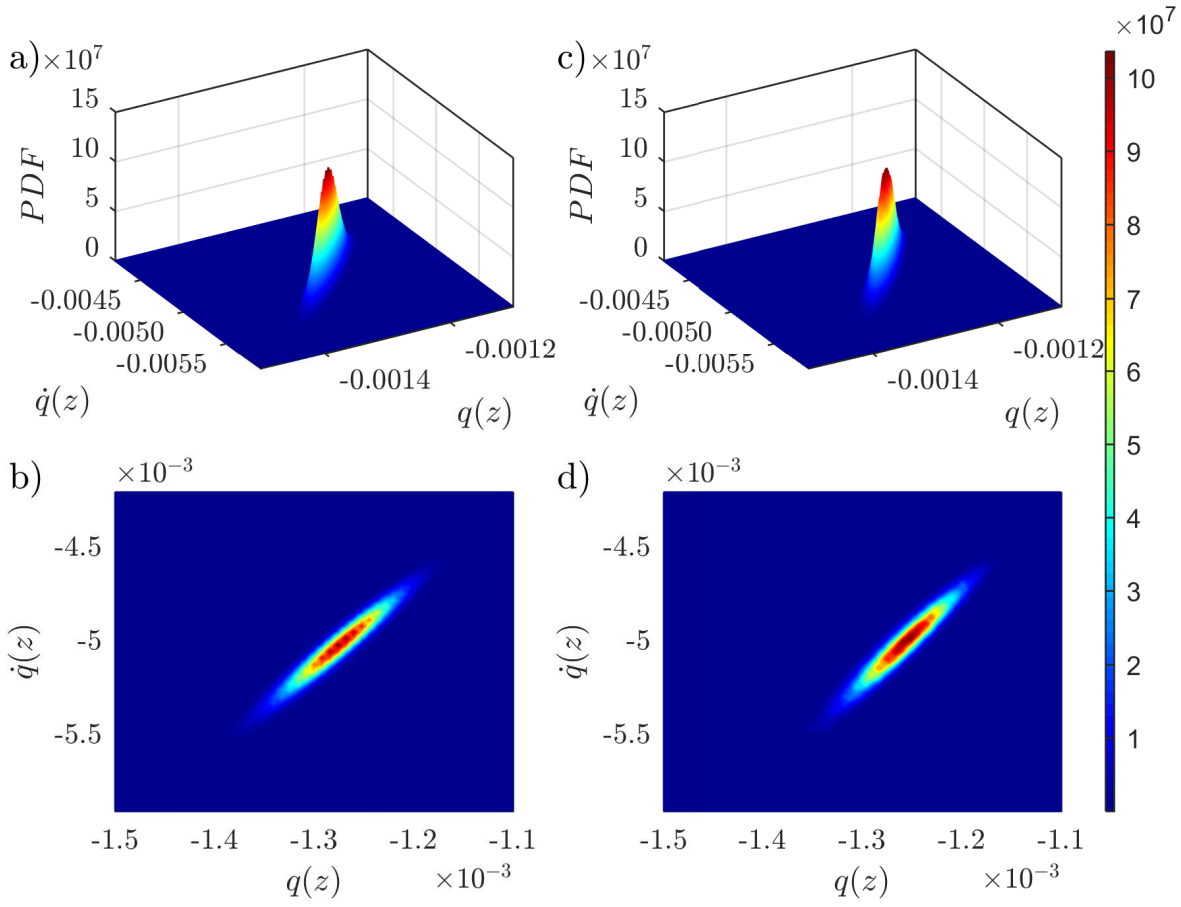

Figure 4.14: Joint PDF of $q(z)$ and $\dot{q}(z)$ at position $z = 0.5$, as obtained via the WPI technique (a - b); comparisons with MCS data - 50,000 realizations (c - d).

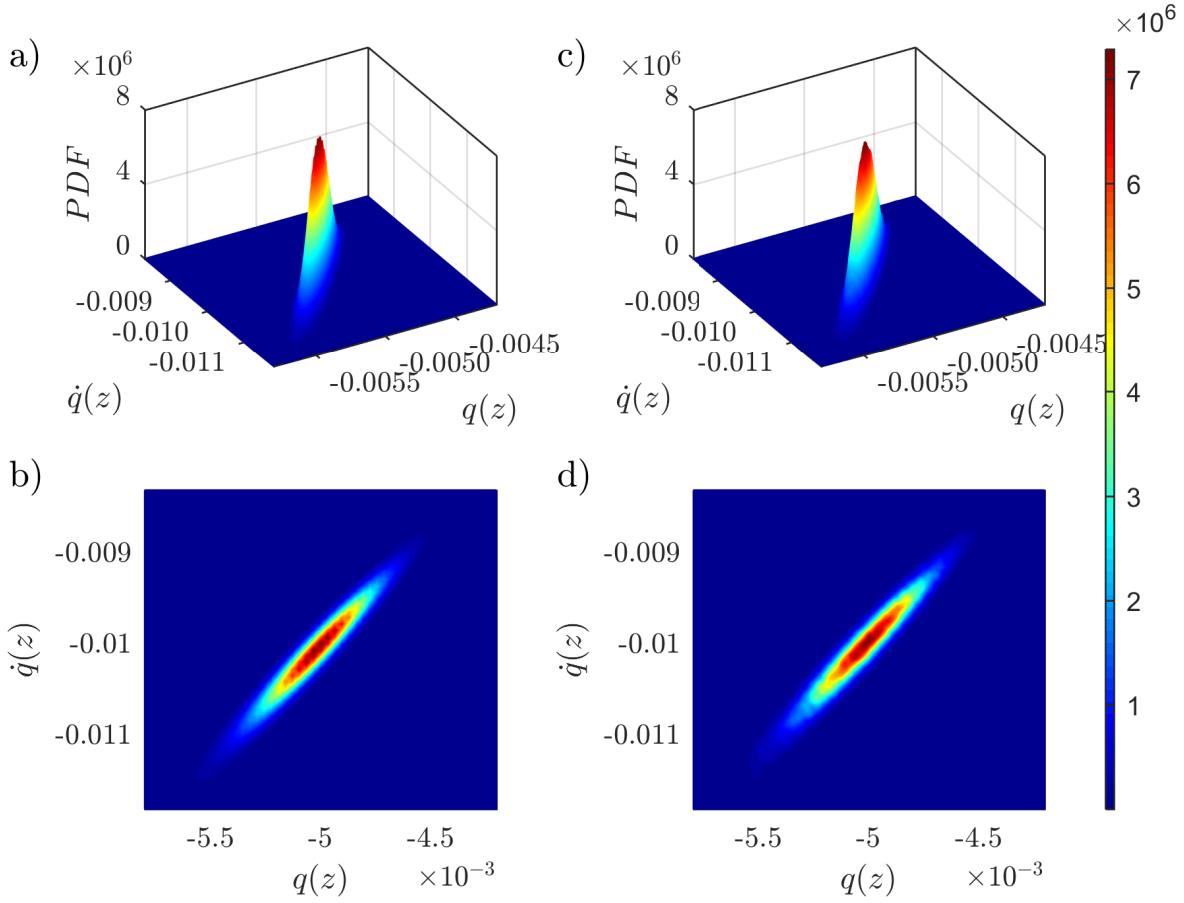

Figure 4.15: Joint PDF of $q(z)$ and $\dot{q}(z)$ at position $z = 1.0$, as obtained via the WPI technique (a - b); comparisons with MCS data - 50,000 realizations (c - d).

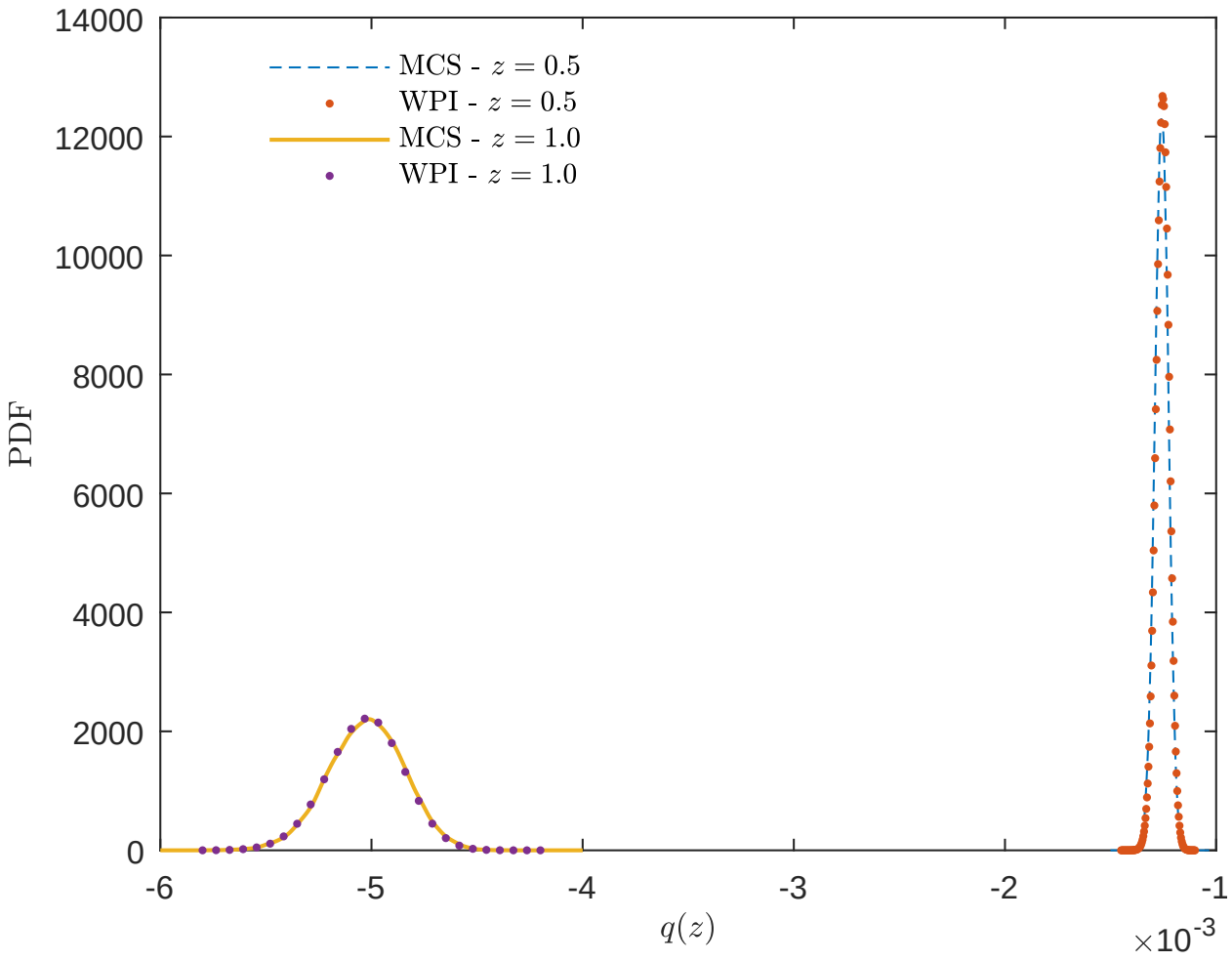

Figure 4.16: PDF of $q(z)$ at positions $z = 0.5$ and $z = 1.0$, as obtained via the WPI technique; comparisons with MCS data (50,000 realizations).

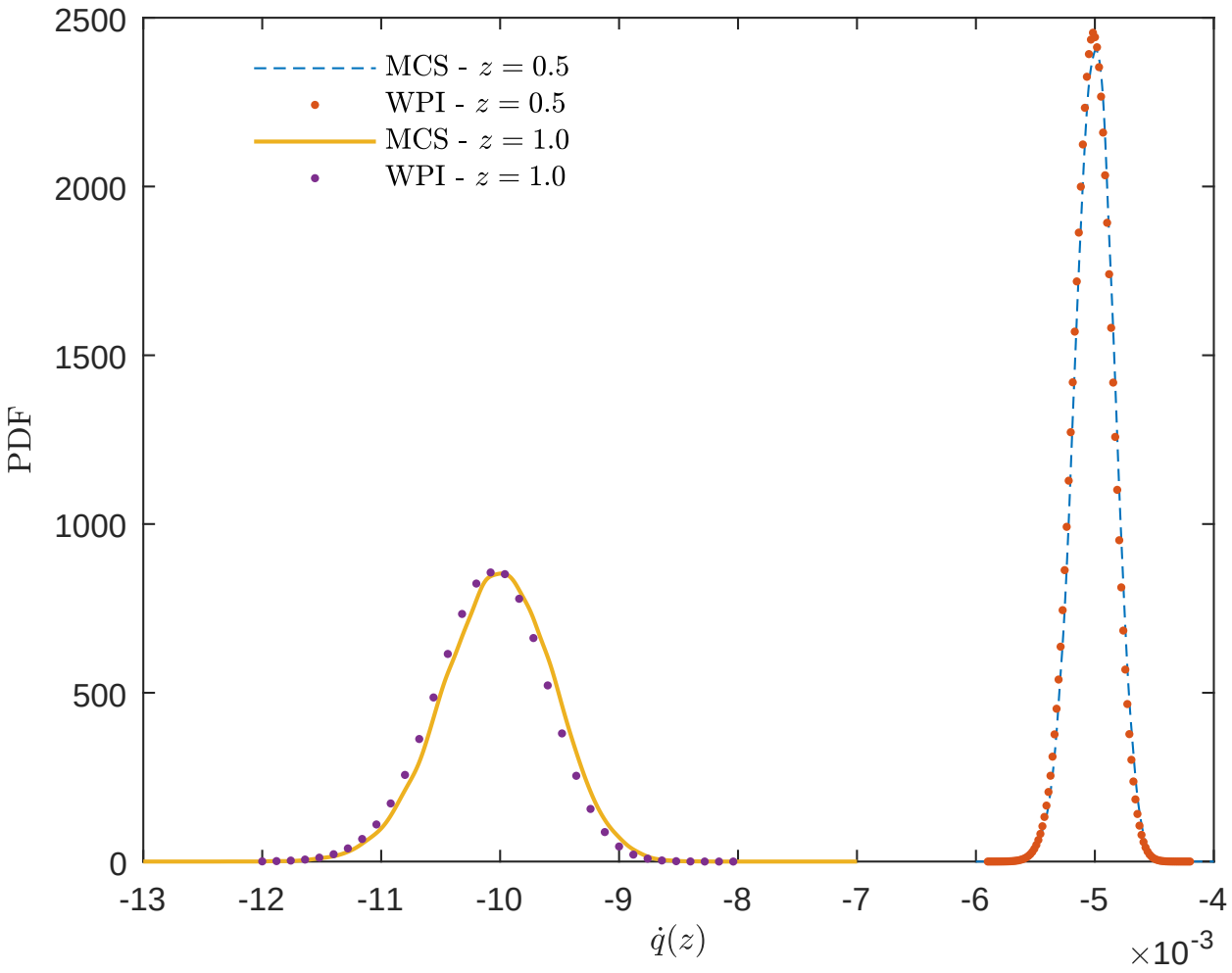

Figure 4.17: PDF of $\dot{q}(z)$ at positions $z = 0.5$ and $z = 1.0$, as obtained via the WPI technique; comparisons with MCS data (50,000 realizations).

Chapter 5

Concluding Remarks

An approximate WPI technique first proposed by [Kougioumtzoglou and Spanos, 2012] is generalized in this work to study non-Gaussian, non-white and non-stationary excitation processes. Combining the WPI formulation with the filter approximation technique utilizes modeling an excitation process as an output to the filter equation with a Gaussian white noise input and augmenting the response process vector to account for this additional equation. This results in an increased applicability of the technique to problems when the excitation power spectrum cannot be cast in a convenient form in the time domain; the filter approximation successfully facilitates these situations. Moreover, the technique can potentially model a larger variety of stochastic mechanics problems, including those with stochastic material/media properties represented by non-Gaussian and non-homogeneous stochastic fields [Kougioumtzoglou, 2017]. The corresponding example (Section 4.4) demonstrates a physically realistic modeling of the material properties.

Numerical validation using various SDOF and MDOF engineering systems have been performed, and the results obtained via the WPI technique have been compared to the pertinent MCS data. The comparison demonstrated high level of accuracy and reliability of the technique; the proposed method proves to be able to capture the salient features of the response PDF.

The computational effort associated with implementing the approximate WPI technique can

be sufficiently reduced via utilizing the localization property of the joint response PDF and coupling the WPI formulation with the recently developed computationally efficient PDF expansion schemes such as the one by [Kougioumtzoglou et al., 2015, Psaros et al., 2018b].

The future work in developing the WPI based technique can be directed at increasing the accuracy of the computations via exploring paths beyond the most probable one [Wio, 2013]. This can be achieved by considering fluctuations around the most probable (also deterministic) trajectory and higher order variations of the integral in Eqn. (3.15). In this regard, a scheme proposed by [Davison, 1954, Levit and Smilansky, 1985] utilizes an infinite orthogonal basis allowing to construct a Sturm-Liouville operator which is then used to take into account the fluctuations around the most probable path.

The work discussed in Part I has been published in [Psaros et al., 2018a].

Part II

Spectral parameter identification technique for nonlinear time-variant MDOF oscillators with fractional derivative elements subject to incomplete data

This page is intentionally left blank.

Chapter 6

Introduction

System identification has been an actively growing field for the past few decades with the focus on both developing new parameter identification techniques ([Hong et al., 2008, Prochazka et al., 1998, Reynders, 2012]) and assessing reliability of the existing methods under limited data ([Chatzi and Papadimitriou, 2016, Priori et al., 2018, Udwadia and Sharma, 1978]). Other challenges that require special consideration in this area of research are the non-stationary property of real-life signals and complex mathematical models of continua based on such tools as fractional calculus.

Most of the data obtained in real-life situations (e.g., environmental excitations, traffic loadings, vibration of operating machinery) exhibit time/space-varying behavior and, hence, can be best described as non-stationary processes, meaning that their statistics and potentially the frequency content vary with time. This makes traditional signal processing methods, such as Fourier analysis, unfit for studying such signals. The short-time Fourier transform, the Gabor transform, wavelets, chirplets, and the Wigner-Ville distribution are some of the most popular tools for analyzing the non-stationary spectral content of signals ([Cohen, 1995, Qian, 2002, Stephane, 2009]).

A range of reasons cause the data obtained from structural monitoring to be limited, incomplete and/or missing, for example, cost of data transfer and storage for wireless sensor networks, data corruption in harsh conditions or due to sensors failure/malfunction, frequency and unpre-

dictability of the effect. Various existing signal reconstruction techniques (e.g., Lomb-Scargle periodogram, iterative deconvolution method CLEAN, Auto-Regressive-Moving-Average model based techniques) can be applied to such situations to handle missing data; a review can be found in [Wang et al., 2006]. Most of the aforementioned techniques for signal reconstruction lack versatility and exhibit certain limitations, such as requiring strong a priori assumptions about the signal [Gudmundson et al., 2010], being computationally demanding [Comerford et al., 2015], performing well only in cases of few missed observations [Hung, 2008], or not being applicable to non-stationary data [Broersen, 2006].

Fractional calculus has recently become one of the advanced mathematical tools actively utilized in more accurate materials/media modeling ([Oldham and Spanier, 2006, Sabatier et al., 2007]). It can be interpreted as a generalization of classical calculus, which in turn provides with enhanced modeling flexibility and allows the concept to be employed in engineering mechanics for developing "non-local" continuum mechanics theories ([Di Paola et al., 2013, Tarasov, 2016]), as well as for modeling of viscoelastic materials [Di Paola et al., 2011]. Nonetheless, the majority of already existing system identification techniques have been based on the classical continuum (or discrete) mechanics theories and have been developed for treating conventional governing dynamics equations. Generalization of those techniques to fractional calculus models is not straightforward though.

A great number of researchers combine CS with time-frequency analysis when processing non-stationary sparse signals; an overview of these techniques can be found in [Sejdic et al., 2018]. However, there are not many system identification techniques that can address those challenges simultaneously, especially in applications to systems with fractional derivative terms. In this regard, an identification technique based on multiple-input/single-output (MISO) approach in the wavelet domain was originally proposed in [Kougioumtzoglou and Spanos, 2013], which allowed to account for non-stationary inputs and time-varying signal parameters. A treatment of nonlin-

ear oscillators with fractional derivative elements for response EPS determination was presented in [Kougioumtzoglou and Spanos, 2016], which was further utilized in [Kougioumtzoglou et al., 2017] to develop a parameter identification technique for such systems. In this work, the procedure is further extended to account for MDOF oscillators under incomplete/missing data. A nonlinear MDOF time-variant system with fractional derivative terms is used as numerical example to demonstrate reliability of the technique even in the presence of noise or under limited data.

This page is intentionally left blank.

Chapter 7

Treatment of Non-stationary and Incomplete Data

7.1 Non-stationary data: a harmonic wavelets approach

The family of generalized harmonic wavelets (GHW) [Newland, 1994] utilizes two parameters (m,n) to define the bandwidth at each scale level. One of the main advantages of this technique is that these two parameters decouple the time-frequency resolution achieved at each scale from the value of the central frequency, which is not the case with other wavelet bases. Moreover, GHW have proven to be particularly useful for structural dynamics applications due to their non-overlapping, box-shaped frequency spectrum, and their orthogonality properties.

A wavelet of (m,n) scale and k position in time attains a representation in the frequency domain in the form

$$\Psi^{G}_{(m,n),k}(\omega) = \begin{cases} \dfrac{1}{(n-m)\Delta\omega} \exp\left(-i\dfrac{\omega k T_0}{n-m}\right), & m\Delta\omega \leq \omega < n\Delta\omega \\ 0, & \text{otherwise} \end{cases}, \tag{7.1}$$

where m, n and k are non-negative integers, and

$$\Delta\omega = \frac{2\pi}{T_0}, \tag{7.2}$$

where T_0 is the total duration of the signal, and $m\Delta\omega \leq \omega < n\Delta\omega$ is the bandwidth of the box-shaped spectrum. The inverse Fourier transform of Eqn. (7.1) gives the time-domain representation of the wavelet which is

$$\Psi^G_{(m,n),k}(t) = \frac{\exp\left(in\Delta\omega\left(t - \frac{kT_0}{n-m}\right)\right) - \exp\left(im\Delta\omega\left(t - \frac{kT_0}{n-m}\right)\right)}{i(n-m)\Delta\omega\left(t - \frac{kT_0}{n-m}\right)}. \tag{7.3}$$

Next, it was shown in [Newland, 1994] that a collection of harmonic wavelets spanning adjacent non-overlapping intervals at different scales forms an orthogonal basis. The continuous generalized harmonic wavelet transform (GHWT) of an arbitrary signal $x(t)$ can be given by

$$W^G_{(m,n),k}[x] = \frac{n-m}{T_0}\int_{-\infty}^{\infty} x(t)\overline{\Psi^G_{(m,n),k}}(t)\mathrm{d}t, \tag{7.4}$$

whereas the inverse transform exactly reconstructs the target signal in the form

$$x(t) = \sum_{m,n}\sum_{k} W^G_{(m,n),k}[x]\Psi^G_{(m,n),k}(t) + \overline{W^G_{(m,n),k}[x]}\,\overline{\Psi^G_{(m,n),k}}(t), \tag{7.5}$$

where the bar over an expression denotes its complex conjugate. Considering Parseval's theorem and the non-overlapping quality of the different energy bands yields an estimate for the underlying stochastic process EPS in the form [Spanos and Kougioumtzoglou, 2012]

$$S_{xx}(\omega,t) = S^{xx}_{(m,n),k} = \frac{\mathbb{E}\left[\left|W^G_{(m,n),k}[x]\right|^2\right]}{(n-m)\Delta\omega}. \tag{7.6}$$

Note that the expectation operator in Eqn. (7.6) implies that an ensemble of realizations compatible with the underlying non-stationary stochastic process is readily available. Similarly, the cross-EPS

of the two processes $x(t)$ and $y(t)$ can be estimated as

$$S_{xy}(\omega,t) = S^{xy}_{(m,n),k} = \frac{\mathbb{E}\left[W^G_{(m,n),k}[x]\overline{W^G_{(m,n),k}[y]}\right]}{(n-m)\Delta\omega}, \tag{7.7}$$

where the bar over an expression denotes its complex conjugate.

In both Eqs. (7.6) and (7.7) the EPS is assumed to be constant over the intervals $m\Delta\omega \leq \omega < n\Delta\omega$ and $\frac{kT_0}{n-m} \leq t < \frac{(k+1)T_0}{n-m}$, in agreement with the theory of locally stationary processes (e.g., [Spanos and Kougioumtzoglou, 2012]).

7.2 Incomplete data: a compressive sensing approach

7.2.1 Preliminary remarks

CS is a signal processing technique that allows for signal reconstruction even if the maximum frequency in the recorded signal is greater than half the signal's sampling rate ([Candes et al., 2006a,b, Donoho, 2006, Eldar and Kutyniok, 2012]). Robust CS can be achieved utilizing several important properties, one being sparsity, i.e. the sampled signal being sparse in some known basis. Further, the sampling domain and the relatively sparse transformation domain must have high coherence. This results in a sparse signal in the transform domain having a non-sparse representation in the sampling domain (e.g., a single Fourier coefficient in the transform domain corresponds to a monochromatic signal in the sampling domain). Also, efficient CS requires the restricted isometry property (RIP) being satisified as well [Candes et al., 2006b].

If it is known that the signal is sparse in a certain basis, the aim of CS is to find the sparsest representation of the given data in that basis; this can be achieved via L_1-norm minimization. Given a sample record $\mathbf{y}$ of length $N_0 - N_m$, where N_0 is the original sample length, and N_m is the number of missing data points, and assuming the locations of the missing data are known, the

corresponding sampling matrix $\mathbf{B}$ ($N_0 - N_m$ by N_0) can be drawn from

$$\mathbf{y} = \mathbf{B}\mathbf{x}, \tag{7.8}$$

where $\mathbf{x}$ is the coefficients vector in the assumed sparse basis.

7.2.2 Minimization problem

Eqn. (7.8) represents an underdetermined system with infinite number of solutions. The sparsest solution occurs when the L_0-norm is minimized [Patel and Chellappa, 2013]. However, this minimization problem is non-convex, i.e. it does not have any known exact solutions. Nevertheless, a viable alternative exists in minimizing the L_1-norm instead, which promotes sparsity and often yields the same results as minimization of the L_0-norm. This way, the problem becomes convex and can be set in a convenient linear algebra form

$$\min |\mathbf{x}|_{L_1} \text{ subject to } \mathbf{y} = \mathbf{B}\mathbf{x}. \tag{7.9}$$

The problem can be then solved via, for instance, basis pursuit [Chen et al., 1998] or greedy algorithms [Tropp and Gilbert, 2007].

A more recent enhancement was proposed in [Zhang et al., 2018] through focusing on the L_p-norm minimization approach to estimating EPS of stochastic processes subject to incomplete/missing data. The L_p-norm can be defined as

$$|x|_{L_p} = \left(\sum_i |x_i|^p \right)^{\frac{1}{p}}, \; p > 0 \tag{7.10}$$

Since minimizing the L_1-norm does not guarantee the sparsest solution, reconstruction technique can be improved or accurately met with fewer sample data when $0 < p < 1$ is used. In this regard, it was shown in [Zhang et al., 2010] that $p = 1/2$ can yield the sparsest solution resulting in the

minimization problem of the form [Zhang et al., 2018]

$$\min |\mathbf{x}|_{L_{1/2}} \text{ subject to } \mathbf{y} = \mathbf{B}\mathbf{x}. \tag{7.11}$$

7.2.3 Applications in engineering dynamics

In general, CS has found a variety of applications in structural dynamics over the past few decades, especially when dealing with wireless sensor networks which require saving in data transmission and storage. These networks are widely used for real-time structural health monitoring, where relying on the sparsity of the signal and combining CS with an appropriate compression basis can not only be beneficial in terms of cost-efficiency ([Bao et al., 2017, Gkoktsi and Giaralis, 2017, Harley, 2016, Jayawardhana et al., 2017, Ji et al., 2018, Perez-Ramirez et al., 2017, Xu et al., 2018, Yang and Nagarajaiah, 2017, Yao et al., 2017], but can also provide reconstructed data series with a far higher resolution than that of the originally captured signals when data corruption occurs due to sensors failure or malfunction (e.g., [Chen et al., 2017]). These techniques can also be tailored for fault detection and damage identification/localization in various engineering structures (e.g., [Du et al., 2017, Sousa and Wang, 2018].

Nonetheless, most of the aforementioned applications deal with the problems of compressing an acquired signal, which is assumed to be complete, and avoiding the computational burden of compressing it locally at the sensor. Thus, applications of CS theory to the problems of missing data presents a major distinction in that missing data is not necessarily intentional. This removes control over the arrangement of the sampling/sensing matrix $\mathbf{B}$. Further, the works that address situations of data losses focus primarily on deterministic signal reconstruction. However, for many cases, the main objective may not be signal reconstruction but rather characterization and quantification of the underlying stochastic process/field statistics relying on an ensemble of available realizations (e.g., EPS estimation). In this regard, a CS based technique for determining the (evolutionary) power spectra of stochastic processes was recently developed for realizations with highly

incomplete/missing data [Comerford et al., 2014, 2016]. This work utilized the GHW basis (Eqn. (7.5)) and showed that the accuracy/robustness of the technique can be further enhanced by relying on an adaptive basis reweighting procedure based on the information provided by an available ensemble of realizations [Comerford et al., 2014].

Another application platform can be found in marine engineering. In this regard, a methodology based on CS has been proposed for efficient processing and joint-frequency analysis of relatively long water wave records by enabling reconstruction of data recorded at a very low sampling rate (sub-Nyquist) [Laface et al., 2017]. Another example demonstrates a CS technique developed for extrapolating in the spatial domain and estimating the space-time characteristics of a sea state based on data collected at very few spatially sparse points (e.g. wave buoys) [Malara et al., 2018]. A number of marine engineering applications involving three-dimensional waves interacting with marine structures, such as optimizing arrays of wave energy converters benefit from this novel technique.

For the non-stationary processes considered in the current work, the EPS is calculated from a mean square value of the GHWT over an ensemble of readily available time-histories (Eqn. (7.6)). A "partial" GHW basis is required for this purpose. First, wavelet scales must be defined, i.e. a set of non-overlapping frequency intervals corresponding to (m,n) in Eqn. (7.1) so that the desired trade-off between time and frequency resolutions is achieved. Next, the harmonic wavelet basis components can be generated efficiently via an inverse fast Fourier transform (FFT) algorithm. However, a single harmonic wavelet must be shifted $(n-m)$ times in the time domain to form an orthogonal basis. Finally, rows corresponding to the missing data must be removed, yielding a sampling matrix with more columns than rows. With the sampling matrix formed, solution of the underdetermined linear system of Eqn. (7.8) yields the GHWT coefficients $W^G_{(m,n),k}$. The coefficients can be used directly for estimating the underlying stochastic process EPS via Eqs. (7.6) and (7.7), allowing to circumvent the computationally demanding task of reconstructing the

signal in the time domain first. A detailed presentation of the CS based EPS estimation technique subject to missing data can be found in [Comerford et al., 2016].

This page is intentionally left blank.

Chapter 8

Identification Technique

8.1 Input-output relationships

Consider a MDOF linear time-variant (LTV) oscillator with a fractional derivative element governed by the following differential equation of motion

$$\ddot{\mathbf{x}} + \mathbf{C}(t)\mathrm{D}^q[\mathbf{x}(t)] + \mathbf{K}(t)\mathbf{x} = \mathbf{w}(t), \tag{8.1}$$

where $\mathbf{x}(t)$ is the oscillator response displacement; $\mathbf{C}(t)$ and $\mathbf{K}(t)$ are the time-varying damping and stiffness matrices, respectively; $\mathbf{w}(t)$ is a realization compatible with a Gaussian, zero-mean non-stationary stochastic excitation vector process, possessing a broad-band EPS $S_{\mathbf{w}}(\omega,t)$; and $\mathrm{D}^q[\cdot]$ denotes the Caputo's fractional derivative [Oldham and Spanier, 2006] defined as

$$\mathrm{D}^q[\mathbf{x}(t)] = \frac{1}{\Gamma(1-q)} \int_0^t \frac{\dot{\mathbf{x}}(\tau)}{(t-\tau)^q} \mathrm{d}\tau, \tag{8.2}$$

where $0 \leq q < 1$, and $\Gamma(z)$ is the gamma function.

Applying next the GHWT (Eqn. (7.4)) to the Eqn. (8.1) and assuming that the stiffness and damping elements are slowly varying functions in time, and thus, approximately constant over the

compact support of the GHW in the time domain ($\mathbf{K}(t) \approx \mathbf{K}_k$ and $\mathbf{C}(t) \approx \mathbf{C}_k$) yields

$$W^G_{(m,n),k}[\ddot{\mathbf{x}}] + \mathbf{C}_k W^G_{(m,n),k}[\mathrm{D}^q[\mathbf{x}(t)]] + \mathbf{K}_k W^G_{(m,n),k}[\mathbf{x}] = W^G_{(m,n),k}[\mathbf{w}]. \tag{8.3}$$

Further, relying on the time localization of the GHW, the linearity property of the fractional derivative, and assuming that the frequency band $[m\Delta\omega,\ n\Delta\omega]$ is small enough for the frequency dependent functions to be approximated constant over the compact support by their respective values at the localized central frequencies $\omega_{c,(m,n),k} = (n+m)\Delta\omega/2$, the following approximate expressions can be derived [Kougioumtzoglou and Spanos, 2016]

$$W^G_{(m,n),k}[\dot{\mathbf{x}}] = i\omega_{c,(m,n),k} W^G_{(m,n),k}[\mathbf{x}], \tag{8.4}$$

$$W^G_{(m,n),k}[\ddot{\mathbf{x}}] = -\omega^2_{c,(m,n),k} W^G_{(m,n),k}[\mathbf{x}], \tag{8.5}$$

$$W^G_{(m,n),k}[\mathrm{D}^q[\mathbf{x}(t)]] = \left(i\omega_{c,(m,n),k}\right)^q W^G_{(m,n),k}[\mathbf{x}]. \tag{8.6}$$

The approximate expression of Eqn. (8.6) for the GHWT of the fractional derivative term can be seen as a generalization of the standard result related to the Fourier transform $\mathrm{FT}[\mathrm{D}^q[\mathbf{x}(t)]] = (i\omega)^q \mathrm{FT}[\mathbf{x}(t)]$ [Oldham and Spanier, 2006].

Substituting Eqs. (8.4)-(8.6) into Eqn. (8.3) yields the input-output relationship

$$W^G_{(m,n),k}[\mathbf{x}] \left(-\omega^2_{c,(m,n),k} + \left(i\omega_{c,(m,n),k}\right)^q \mathbf{C}_k + \mathbf{K}_k\right) = W^G_{(m,n),k}[\mathbf{w}]. \tag{8.7}$$

Next, considering the complex conjugate of Eqn. (8.7) and manipulating the equation yields

$$\left|W^G_{(m,n),k}[\mathbf{x}]\right|^2 = \frac{\left|W^G_{(m,n),k}[\mathbf{w}]\right|^2}{\left|-\omega^2_{c,(m,n),k} + \left(i\omega_{c,(m,n),k}\right)^q \mathbf{C}_k + \mathbf{K}_k\right|^2}, \tag{8.8}$$

while applying the expectation operator on both sides leads to

$$\mathbf{S}^{\mathbf{x}}_{(m,n),k} = \mathbf{H}^G_{(m,n),k} \mathbf{S}^{\mathbf{w}}_{(m,n),k} \overline{\mathbf{H}^G_{(m,n),k}}^T. \tag{8.9}$$

Note that $\mathbf{H}^{G}_{(m,n),k}$ denotes the GHW frequency response function (GHW-FRF) given by

$$\mathbf{H}^{G}_{(m,n),k} = \left(-\omega^{2}_{c,(m,n),k} + \left(i\omega_{c,(m,n),k}\right)^{q}\mathbf{C}_{k} + \mathbf{K}_{k}\right)^{-1}. \tag{8.10}$$

In general, Eqn. (8.10) represents a time- and frequency-dependent GHW-FRF and Eqn. (8.8) can be viewed as a generalization of the Wiener-Khinchin spectral relationship of the linear stationary random vibration theory [Roberts and Spanos, 2003].

Note that the derivation of the approximate input-output relationship of Eqn. (8.8) relies on the "local stationarity" assumption; see [Kougioumtzoglou and Spanos, 2016] for a detailed discussion. Thus, for cases when this assumption does not hold, Eqn. (8.8) might not provide the adequate accuracy. In general, it can be argued that for relatively stiff systems and/or for systems with relatively high damping, the related impulse response function is short-lived, and thus, a locally stationary input-output relationship of Eqn. (8.8) exhibits satisfactory approximation. However, the "local stationarity" restriction was circumvented in [Spanos et al., 2016] where an enhanced GHW based excitation-response relationship was derived for systems with integer order derivative terms. Future research may encompass its generalization to account also for fractional derivative elements.

8.2 Multiple-input/single-output technique

In this section, a novel MISO system identification technique is developed that relies on knowledge of the measured excitation/response signals. The technique is based on the pioneering work by Bendat and coworkers [Bendat, 1998, Bendat et al., 1992, 1995]. The MISO technique has found applications in various fields (e.g., [Perreault et al., 1999, Raman et al., 2005, Selvam and Bhattacharyya, 2006, Spanos and Lu, 1995]). It was recently generalized to account for non-stationary inputs and time-varying system parameters using harmonic wavelets [Kougioumtzoglou and Spanos, 2013]. The method was further extended to account for incomplete/missing data

as well as for systems with fractional derivative elements [Kougioumtzoglou et al., 2017]. The current work is focused on generalizing the methodology developed in [Kougioumtzoglou et al., 2017] further, to nonlinear time-varying MDOF systems with fractional derivative terms under limited data.

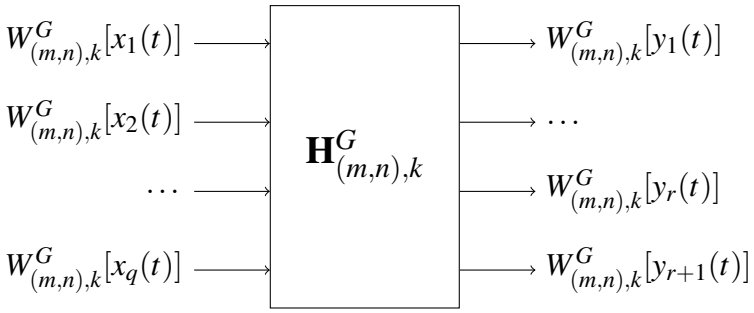

Figure 8.1: MIMO model with q inputs and $r+1$ outputs

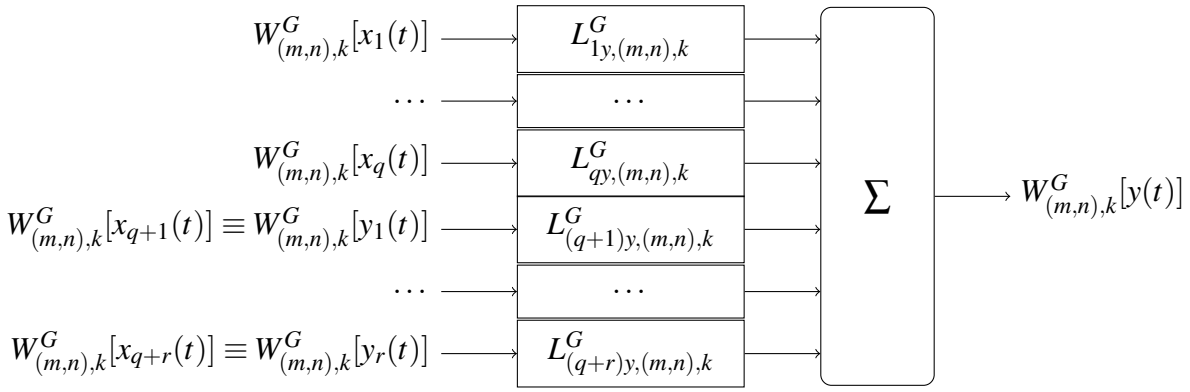

Figure 8.2: MISO model with $q+r$ inputs that can be correlated

Consider a general multiple-input/multiple-output (MIMO) system with q inputs and $r+1$ different outputs as illustrated by Fig. 8.1. When any correlation that exists between the different output records is due only to the fact that they come from the same set of input records, the MIMO problem can be readily considered as a set of MISO problems for each output separately. A general treatment of MISO systems is described in detail by [Bendat and Piersol, 1986]. However, when some correlation between the output signals exists after the effects of the q input records have been removed, the usual MISO problem should be extended to treat the additional contributions from

the correlated output records [Bendat and Piersol, 1993]. The problem is then recast as a MISO system with the $q+r$ inputs, which may be correlated (Fig. 8.2).

Each record allows us to define the auto-spectra $S_{ii} = S_{x_i x_i}$, S_{yy}, and the cross-spectra $S_{ij} = S_{x_i x_j}$, $S_{iy} = S_{x_i y}$, where $i, j = 1, 2, \ldots, q+r$. Note that $S_{ji} = \overline{S_{ij}}$. Next, the inputs are typically correlated, which requires that the original set of inputs is replaced by a set of uncorrelated ones. The decorrelation of the inputs can be performed via conditioning the EPS calculated from the measured signals. The conditioned EPS can be defined as

$$S_{ij}^c = S_{ij.(i-1)!}, \tag{8.11}$$

$$S_{iy}^c = S_{iy.(i-1)!}, \tag{8.12}$$

where

$$S_{ij.r!} = S_{ij.(r-1)!} - \frac{S_{rj.(r-1)!}}{S_{rr.(r-1)!}} S_{ir.(r-1)!},\ r < i,$$
$$S_{iy.r!} = S_{iy.(r-1)!} - \frac{S_{ry.(r-1)!}}{S_{rr.(r-1)!}} S_{ir.(r-1)!},\ r < i.$$

Note that for $r = 0$, $S_{ij.r!} = S_{ij}$ and $S_{iy.r!} = S_{iy}$.

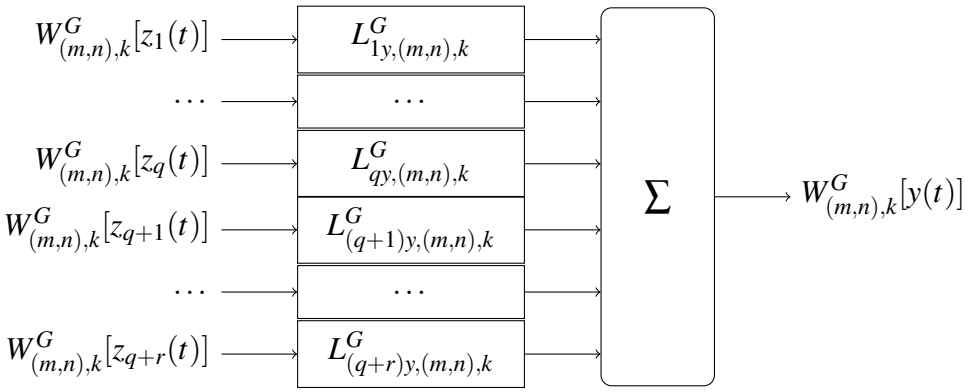

Figure 8.3: MISO model with $q+r$ inputs that are mutually uncorrelated

Using the conditioned power spectra calculated via GHWT, one can define the linear operators

$L^G_{iy,(m,n),k}$ (Fig. 8.3) that relate the conditioned input records $z_i(t)$ with a specific output $y(t)$:

$$L^G_{iy,(m,n),k} = \frac{S^{iy,c}_{(m,n),k}}{S^{ii,c}_{(m,n),k}}. \tag{8.13}$$

The total output EPS can then be calculated as

$$S^{yy}_{(m,n),k} = \sum_{i=1}^{q+r} \left| L^G_{iy,(m,n),k} \right|^2 S^{ii,c}_{(m,n),k}. \tag{8.14}$$

The current relationship does not take into account the presence of noise, which can be easily added to the above equations due to the fact that it is usually assumed uncorrelated to the other records.

Ordinary coherence functions between each of the inputs $z_i(t)$ and the total output $y(t)$ are given by

$$\left(\gamma^{jy}_{(m,n),k}\right)^2 = \frac{\left| S^{iy,c}_{(m,n),k} \right|^2}{S^{ii,c}_{(m,n),k} S^{yy,c}_{(m,n),k}}, \; i = 1,2,\ldots,q+r. \tag{8.15}$$

The ordinary coherence functions can be used to determine how much of the total spectral output $S^{yy}_{(m,n),k}$ at any frequency is due to any subset of the original q input records, or to any subset of the original r output records.

In the absence of noise, the GHW cumulative coherence function (GHW-CCF), or the total multiple coherence function, can then be defined by the sum

$$\left(\gamma^{y:z}_{(m,n),k}\right)^2 = \sum_{i=1}^{q+r} \left(\gamma^{jy}_{(m,n),k}\right)^2 \to 1. \tag{8.16}$$

This quantity is used as an indicator of the modeling error providing information about the "goodness-of-fit" of the model subject to the measured data [Kougioumtzoglou and Spanos, 2013] and should be equal to one if the model provides a good fit.

8.3 Implementation of the identification technique

Consider a MDOF nonlinear oscillator whose motion is governed by the following differential equation

$$\ddot{\mathbf{x}} + \mathbf{C}(t)\mathrm{D}^{q}[\mathbf{x}(t)] + \mathbf{K}(t)\mathbf{x} + \mathbf{g}(\mathbf{x},\dot{\mathbf{x}}) + \mathbf{z}(t) = \mathbf{w}(t), \tag{8.17}$$

where $\mathbf{g}(\mathbf{x},\dot{\mathbf{x}})$ is an arbitrary nonlinear vector function of the response displacement and velocity; and $\mathbf{z}(t)$ accounts for added extraneous noise [Bendat et al., 1992]. Next, it is assumed that $\mathbf{g}(\mathbf{x},\dot{\mathbf{x}})$ can be represented by a superposition of zero-memory nonlinear transformations and linear subsystems [Zeldin and Spanos, 1998] in the form

$$\mathbf{g}(\mathbf{x},\dot{\mathbf{x}}) = \sum_{i=1}^{M} \mathbf{A}_i \frac{\mathrm{d}}{\mathrm{d}t}\mathbf{p}_i(\mathbf{x}). \tag{8.18}$$

In the above, $\mathbf{A}_i$ are polynomial functions; $\mathbf{p}_i$ are zero-memory nonlinear transformations; and M is the total number of base functions in the representation of $\mathbf{g}(\mathbf{x},\dot{\mathbf{x}})$. Substituting Eqn. (8.18) into Eqn. (8.17) provides

$$\ddot{\mathbf{x}} + \mathbf{C}(t)\mathrm{D}^{q}[\mathbf{x}(t)] + \mathbf{K}(t)\mathbf{x} + \sum_{i=1}^{M} \mathbf{A}_i \frac{\mathrm{d}}{\mathrm{d}t}\mathbf{p}_i(\mathbf{x}) + \mathbf{z}(t) = \mathbf{w}(t). \tag{8.19}$$

Taking a GHWT of Eqn. (8.19) and grouping terms for the MISO identification technique yields [Kougioumtzoglou et al., 2017]

$$\sum_{i=1}^{M+1} \mathbf{A}^{G}_{i,(m,n),k} W^{G}_{(m,n),k}[\mathbf{x}_i] + W^{G}_{(m,n),k}[\mathbf{z}] = W^{G}_{(m,n),k}[\mathbf{w}], \tag{8.20}$$

where $\mathbf{A}^{G}_{i,(m,n),k}$ are unknown time- and frequency-dependent GHW-FRFs; and $\mathbf{x}_i(t) = \mathbf{x}(t)$. Note that each $W^{G}_{(m,n),k}[\mathbf{x}_i]$ provides n inputs $W^{G}_{(m,n),k}[x_{ij}]$, where n is the number of degrees of freedom of the oscillator. Thus, the total number of inputs is equal to $n(M+1)$.

Taking into account Eqn. (8.10), one can notice that

$$\mathbf{A}^{G}_{1,(m,n),k} = \left[\mathbf{H}^{G}_{(m,n),k}\right]^{-1} = -\omega^{2}_{c,(m,n),k} + \left(i\omega_{c,(m,n),k}\right)^{q}\mathbf{C}_k + \mathbf{K}_k. \tag{8.21}$$

However, $W^G_{(m,n),k}[\mathbf{x}_i]$ represent, in general, mutually correlated inputs. A decorrelation scheme based on conditioned spectra described above (see also [Bendat and Piersol, 1986, 1993, Rice and Fitzpatrick, 1988]) and generalized in [Kougioumtzoglou and Spanos, 2013] to account for time- and frequency dependent EPS is applied next. The GHW-FRFs are then

$$\mathbf{A}^G_{i,(m,n),k} = \mathbf{L}^G_{i,(m,n),k} - \sum_{j=i+1}^{n(M+1)} \mathbf{A}^G_{j,(m,n),k} \frac{S^{ij,c}_{(m,n),k}}{S^{ii,c}_{(m,n),k}}. \tag{8.22}$$

A more detailed treatment of correlated inputs is given in books by Bendat and Piersol [Bendat and Piersol, 1986] and [Bendat and Piersol, 1993].

The identification procedure can be outlined as the following algorithm:

i. Provided records of excitation and oscillator response time histories, apply the GHWT (Section 7.1) and estimate the auto- and cross-EPS $S^{x_i x_i}_{(m,n),k}$, $S^{w_i w_i}_{(m,n),k}$, $S^{x_i x_j}_{(m,n),k}$, $S^{w_i w_j}_{(m,n),k}$, $S^{x_i w_j}_{(m,n),k}$ for all input and output processes. In case of incomplete/missing data, apply the CS technique delineated in Section 7.2 to reconstruct the signals.

ii. Compute the GHW-CCF $\left(\gamma^{w:x}_{(m,n),k}\right)^2$ via Eqn. (8.16) and select an appropriate frequency range to perform an accurate system parameter identification.

iii. Determine the GHW-FRFs $\mathbf{A}^G_{i,(m,n),k}$ via Eqn. (8.22).

iv. Determine the unknown system parameters. Note that $\mathbf{K}_k$ can be readily determined from $\mathbf{A}^G_{1,(m,n),k}$ for $\omega_{c,(m,n),k} = 0$. Further, the same GHW-FRF can be rewritten as

$$\mathbf{A}^G_{1,(m,n),k} = \left[\omega^2_{c,(m,n),k} + \mathbf{K}_k + \mathbf{C}_k \omega^q_{c,(m,n),k} \cos\left(q\frac{\pi}{2}\right)\right] + i\left[\mathbf{C}_k \omega^q_{c,(m,n),k} \sin\left(q\frac{\pi}{2}\right)\right]. \tag{8.23}$$

The imaginary part of $\mathbf{A}^G_{1,(m,n),k}$ is then equal to

$$\mathrm{Im}\left[\mathbf{A}^G_{1,(m,n),k}\right] = \mathbf{C}_k \omega^q_{c,(m,n),k} \sin\left(q\frac{\pi}{2}\right), \tag{8.24}$$

from where $\mathbf{C}_k$ can be obtained. However, one has to identify the order of the fractional

derivative q first by manipulating Eqn. (8.23), which yields

$$q = \frac{2}{\pi} \frac{\text{Im}\left[\mathbf{A}^G_{1,(m,n),k}\right]}{\text{Re}\left[\mathbf{A}^G_{1,(m,n),k}\right] - \mathbf{K}_k + \omega_{c,(m,n),k}\mathbf{I}}. \tag{8.25}$$

The GHW-FRFs $\mathbf{A}^G_{i,(m,n),k}$, $i = 2,\ldots,M+1$ corresponding to the nonlinear terms of the equation of motion can be used to identify the specific nonlinearity parameters.

This page is intentionally left blank.

Chapter 9

Numerical Validation

9.1 Time-variant Duffing oscillator with fractional derivative elements

The following example considers a 2-degree-of-freedom (2DOF) time-variant Duffing oscillator with a fractional derivative element in the form of Eqn. (8.17). In this regard, $\mathbf{g}(\mathbf{x},\dot{\mathbf{x}}) = \varepsilon\mathbf{K}(t)\mathbf{x}^3$, the damping and stiffness matrices are

$$\mathbf{C}(t) = \begin{bmatrix} c_1(t)+c_2(t) & -c_2(t) \\ -c_2(t) & c_2(t) \end{bmatrix}, \quad \mathbf{K}(t) = \begin{bmatrix} k_1(t)+k_2(t) & -k_2(t) \\ -k_2(t) & k_2(t) \end{bmatrix}, \tag{9.1}$$

where the time-varying parameters are

$$c_1(t) = 8+0.003t^2, \quad c_2(t) = 1+0.002t^2, \tag{9.2}$$

$$k_1(t) = 100-0.05t^2, \quad k_2(t) = 10-0.005t^2. \tag{9.3}$$

The smoothly varying stiffness can be a reasonable model, for instance, of a degrading structure during a seismic event. The order of the fractional derivative is $q = 0.5$, and the nonlinearity parameters are $\varepsilon_1 = 10$ and $\varepsilon_2 = 5$. The corresponding MIMO identification model is shown in Fig. 9.1.

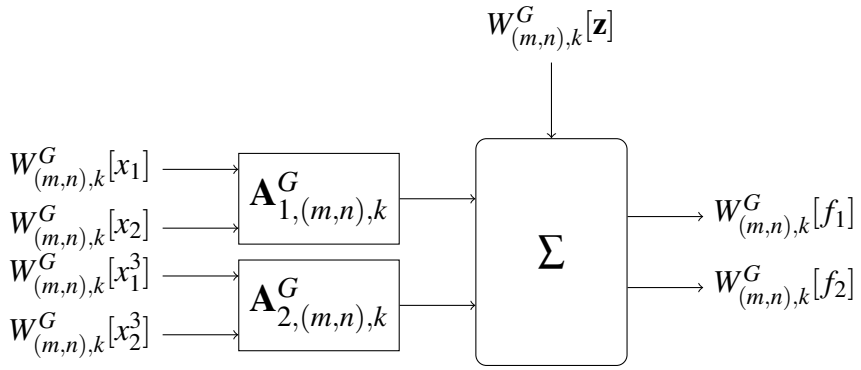

Figure 9.1: 2-DOF Duffing oscillator recast as a MISO problem for parameter identification

The excitation is modeled as a non-stationary stochastic vector process with a prescribed non-separable EPS of the form (Fig. 9.2)

$$S_{\mathbf{f}}(\omega,t) = S_0 \left(\frac{\omega}{p_1}\right)^2 \exp(-bt)\, t^2 \exp\left(-\left(\frac{\omega}{p_2}\right)^2 t\right), \tag{9.4}$$

where the parameters assume the values from Table 9.1. The EPS demonstrates some of the main characteristics observed in recorded seismic motions, such as the decreasing with time dominant frequency [Kougioumtzoglou and Spanos, 2009].

Table 9.1: System parameters pertaining to Eqn. (9.4)

S_0	p_1	p_2	b
5	30π	10π	0.15

Further, time-histories compatible with the excitation EPS are produced via spectral representation technique [Shinozuka and Deodatis, 1991] for each degree of freedom

$$f_i(t) = 2\sum_{j=0}^{m-1} \sqrt{S_f(j\Delta\omega,t)\Delta\omega}\cos\left(j\Delta\omega t + \phi_j\right), \tag{9.5}$$

where $\Delta\omega$ refers to the discretization in the frequency domain, and ϕ_j are independent random variables uniformly distributed over the interval $[0,2\pi]$ describing the phase. The total of 50 time-histories is available for each recorded signal, and the duration of the recorded signals is $T = 31.4\ s$. In applying the GHWT, the value $n-m=5$ is chosen to compromise between the time and

frequency resolutions.

The oscillator response is obtained for each sample path numerically via the linear L_1-algorithm utilizing discretization of the fractional derivative and a linear piecewise approximation when computing the derivatives; the algorithm is presented in detail in [Koh and Kelly, 1990].

The robustness of the technique is assessed through considering four differenet data scenarios:

i. complete excitation-response time histories,

ii. complete excitation-response time histories with added noise,

iii. incomplete excitation-response time histories,

iv. incomplete excitation-response time histories with added noise.

The added noise is modeled as a Gaussian white noise vector process with a signal-to-noise ratio of 40 dB; i.e. the standard deviation of the white noise is equivalent to 10 percent of the standard deviation of the signal. 20 percent missing data are imposed in uniformly distributed random locations in the signal records.

Fig. 9.3 shows sample realizations of system response (displacement) for the four data scenarios considered herein. The estimated EPS of the excitations f_1 and f_2 based on Eqn. (7.6) in combination with the CS treatment (Section 7.2) can be found in Figs. 9.4 and 9.5. The estimated EPS of the response vector process elements x_1 and x_2 calculated in a similar manner for all four data scenarios are demonstrated in Figs. 9.6 and 9.7.

The ordinary GHW-CCFs for the dominant inputs for each of the outputs are presented in Fig. 9.8 for the two time instances $t = 12.56\ s$ and $t = 31.4\ s$ for each of the four data scenarios. The effects of data loss and noise corruption on the technqiue's accuracy can be easily noticed in these figures. The total multiple GHW-CCFs are calculated and are equal to one ($(\gamma^{f_1:x}_{(m,n),k})^2 = (\gamma^{f_2:x}_{(m,n),k})^2 = 1$) which supports the validity of the identification model (Eqn. (8.16)).

All the parameters of the system are further estimated for all four data scenarios and compared to the target values. The identified damping, stiffness and nonlinearity parameters are plotted in Figs. 9.9-9.11, respectively. Additionally, the mean values of the nonlinearity parameters and the fractional derivative order are presented in Tables 9.2-9.4.

In Figs. 9.9 and 9.10, one can observe that the technique captures the main features of the time-varying parameters satisfactorily, even in the cases of noise and/or missing data. The constant parameters q, ε_1 and ε_2 are computed with satisfactory accuracy in average sense.

Table 9.2: Comparison between the target and the estimated mean values of the fractional derivative order q of the time-varying 2-DOF Duffing oscillator for four different data scenarios.

Target	Complete	Noise	Incomplete	Incomplete + Noise
0.5	0.5300	0.4515	0.5249	0.6078

Table 9.3: Comparison between the target and the estimated mean values of the nonlinearity parameters ε_1 of the time-varying 2-DOF Duffing oscillator for four different data scenarios.

Target	Complete	Noise	Incomplete	Incomplete + Noise
10	10.9773	9.8650	11.1273	13.4416

Table 9.4: Comparison between the target and the estimated mean values of the nonlinearity parameters ε_2 of the time-varying 2-DOF Duffing oscillator for four different data scenarios.

Target	Complete	Noise	Incomplete	Incomplete + Noise
5	5.2283	5.2222	4.1784	3.9839

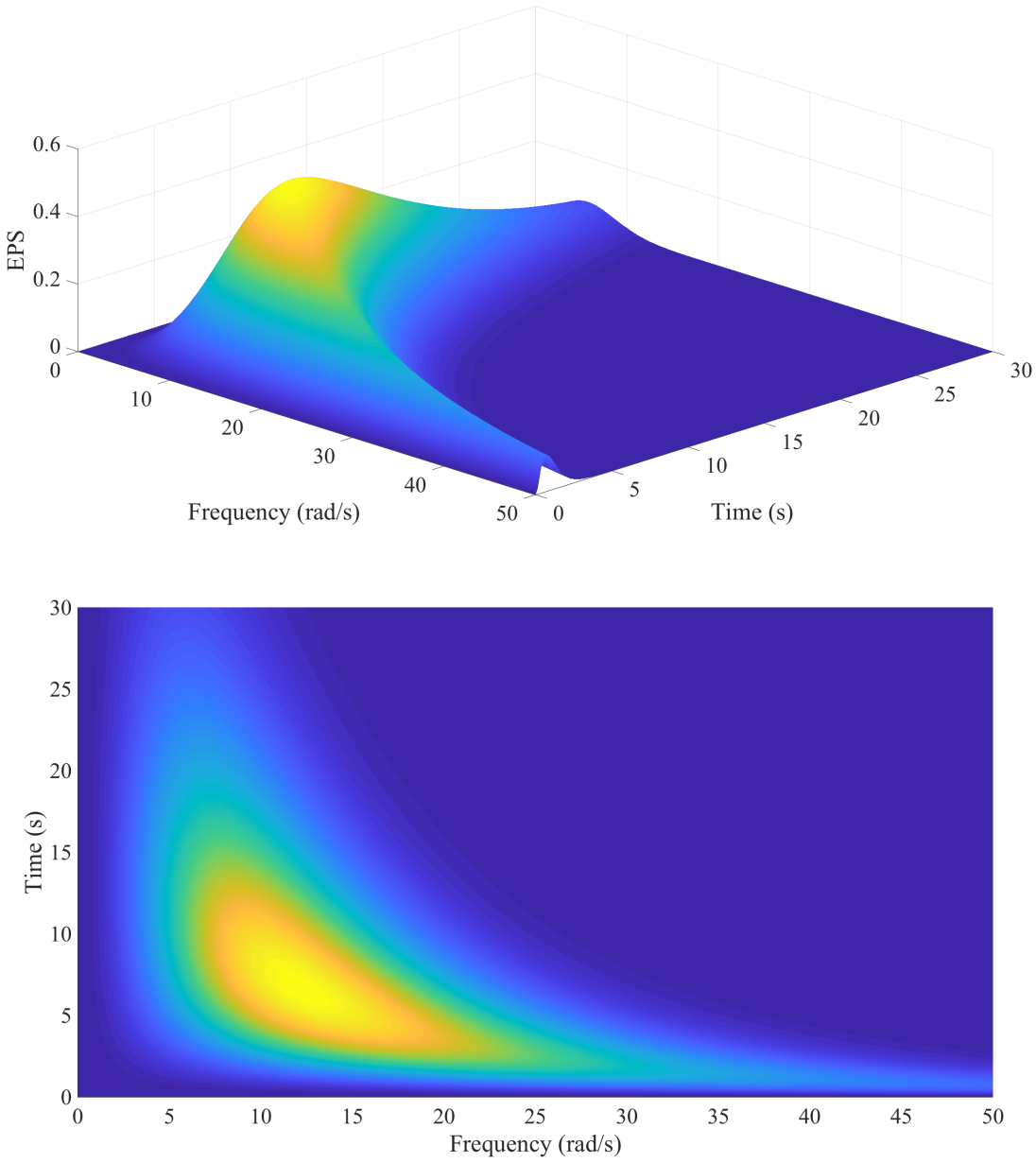

Figure 9.2: Non-separable excitation EPS used in Chapter 9.

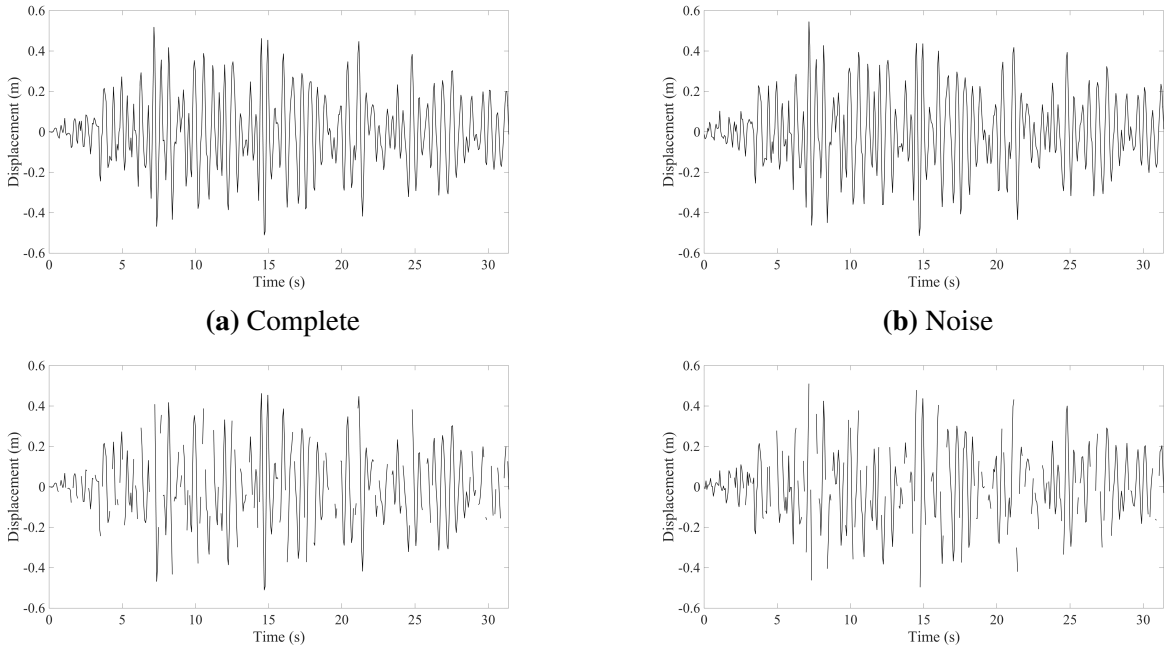

(a) Complete **(b)** Noise

(c) Incomplete **(d)** Incomplete + Noise

Figure 9.3: Typical response realizations of the time-varying 2-DOF Duffing oscillator for four different data scenarios.

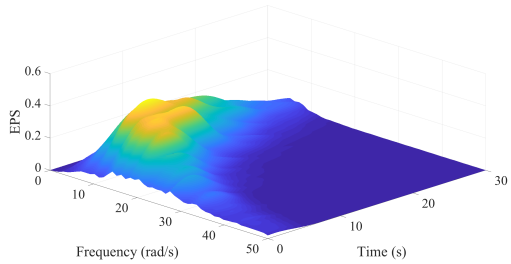

(a) Complete

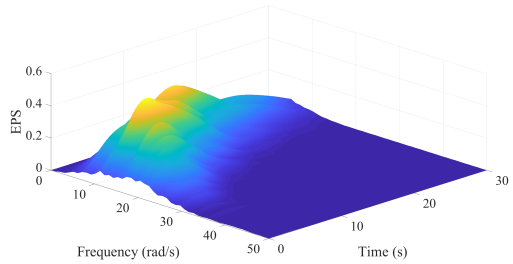

(b) Noise

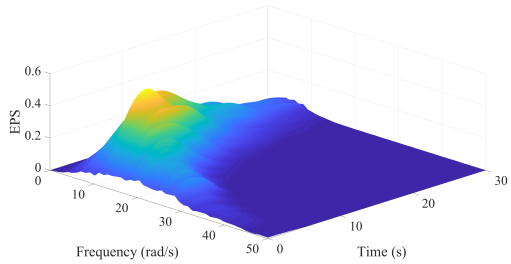

(c) Incomplete

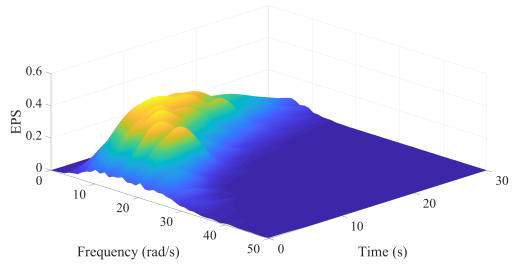

(d) Incomplete + Noise

Figure 9.4: Estimated EPS of the excitation applied to the first DOF (f_1) of the time-varying 2-DOF Duffing oscillator for four different data scenarios.

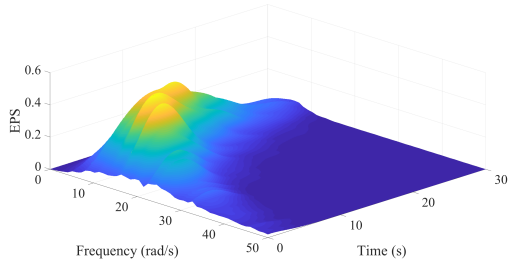

(a) Complete

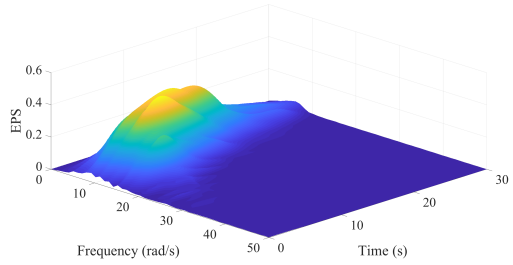

(b) Noise

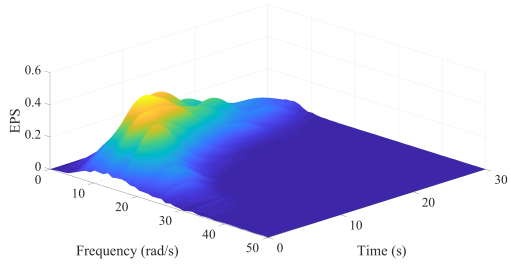

(c) Incomplete

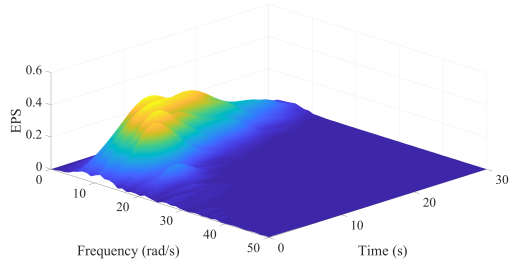

(d) Incomplete + Noise

Figure 9.5: Estimated EPS of the excitation applied to the second DOF (f_2) of the time-varying 2-DOF Duffing oscillator for four different data scenarios.

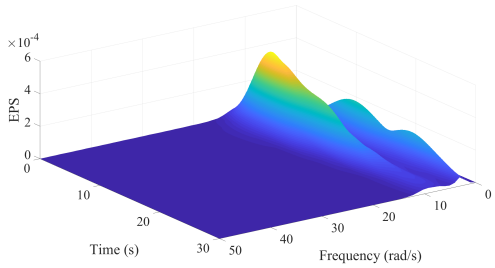

(a) Complete

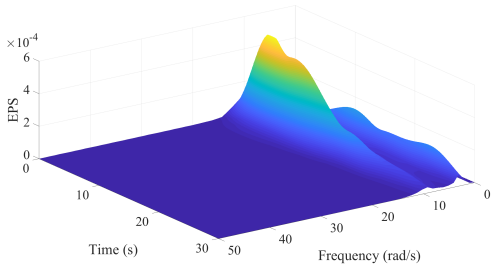

(b) Noise

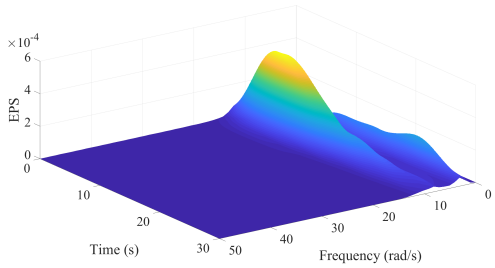

(c) Incomplete

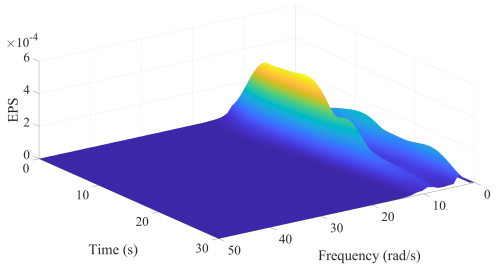

(d) Incomplete + Noise

Figure 9.6: Estimated EPS of the response of the first DOF (x_1) of the time-varying 2-DOF Duffing oscillator for four different data scenarios.

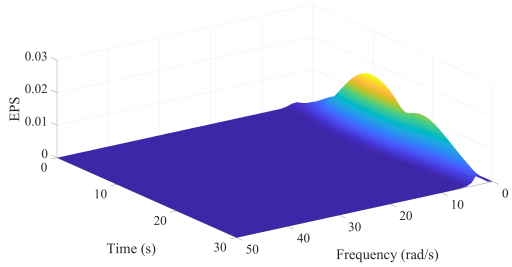

(a) Complete

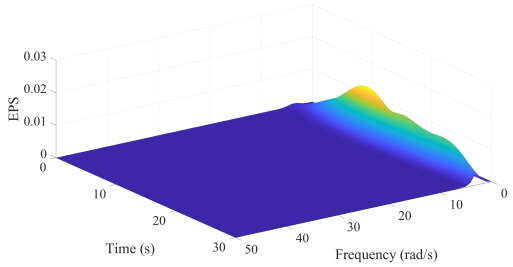

(b) Noise

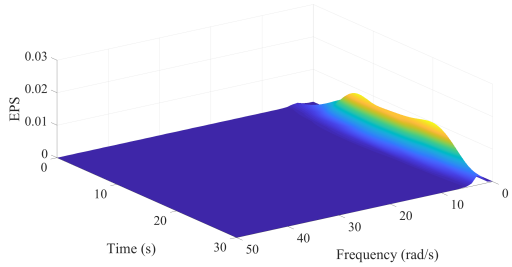

(c) Incomplete

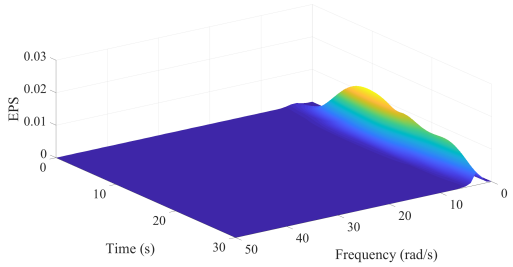

(d) Incomplete + Noise

Figure 9.7: Estimated EPS of the response of the first DOF (x_2) of the time-varying 2-DOF Duffing oscillator for four different data scenarios.

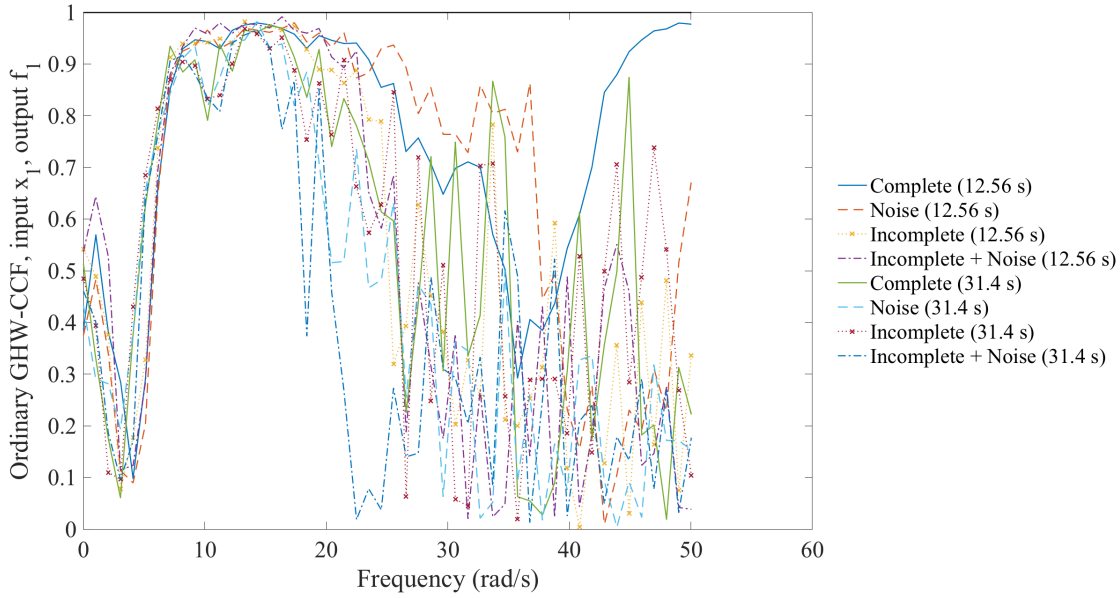

(a) $\left(\gamma^{1f_1}_{(m,n),k}\right)^2$

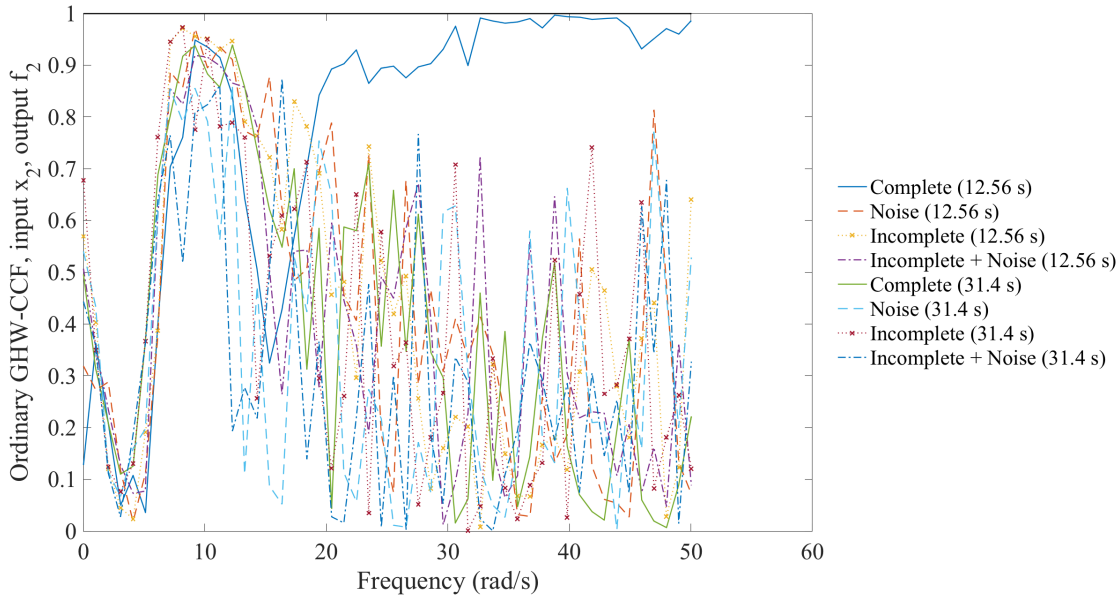

(b) $\left(\gamma^{2f_2}_{(m,n),k}\right)^2$

Figure 9.8: Estimated ordinary GHW-CCF of the dominating inputs for the time-varying 2-DOF Duffing oscillator for four different data scenarios at time instances $t = 12.56\ s$ and $t = 31.4\ s$.

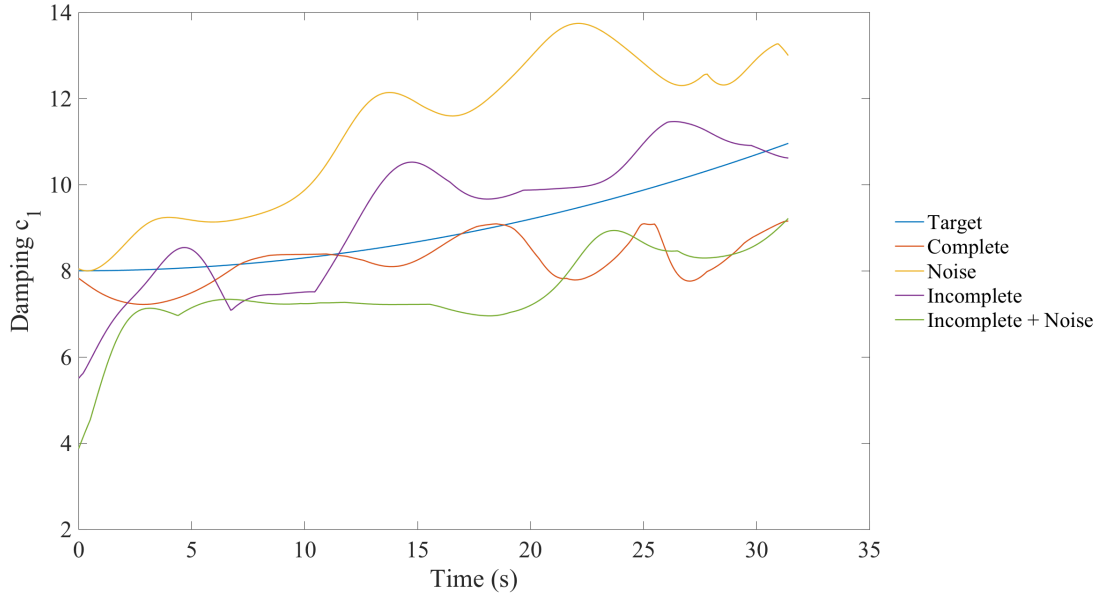

(a) Damping parameter c_1

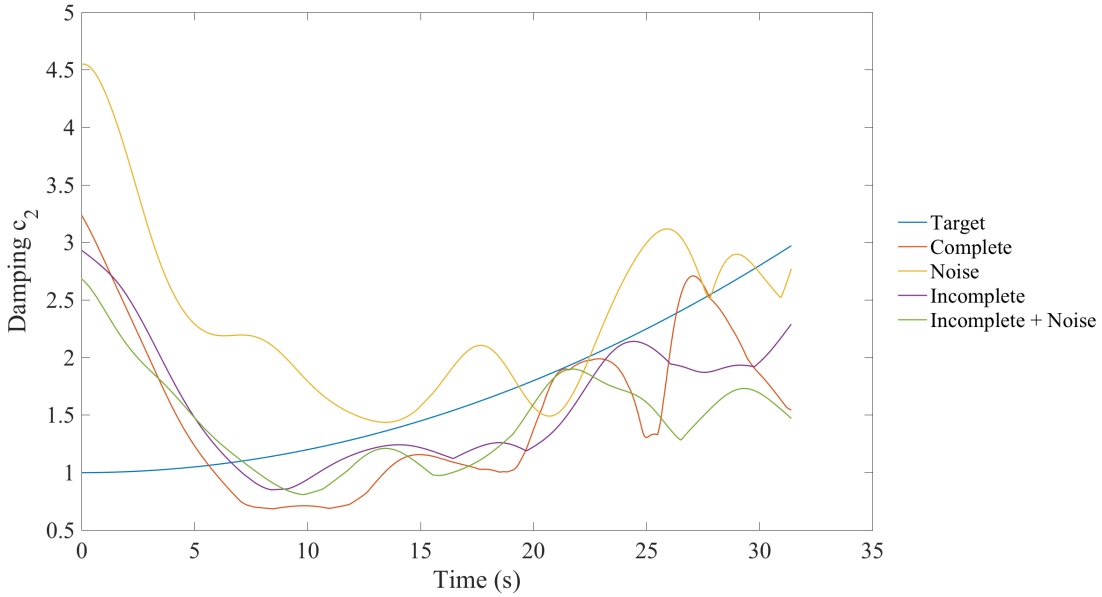

(b) Damping parameter c_2

Figure 9.9: Comparison between the target and the estimated damping parameters of the time-varying 2-DOF Duffing oscillator for four different data scenarios.

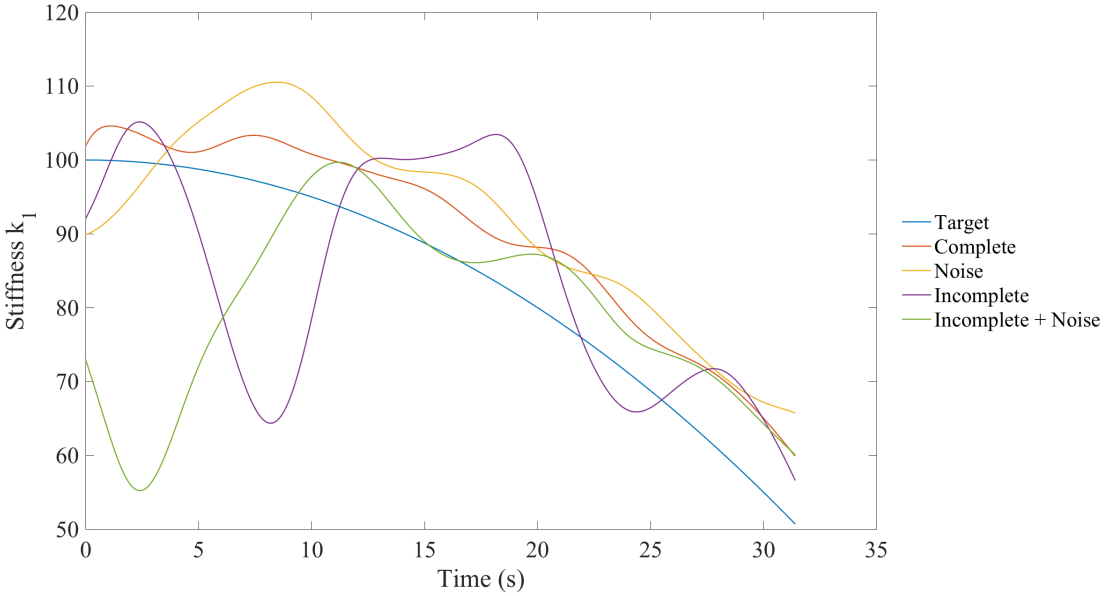

(a) Stiffness parameter k_1

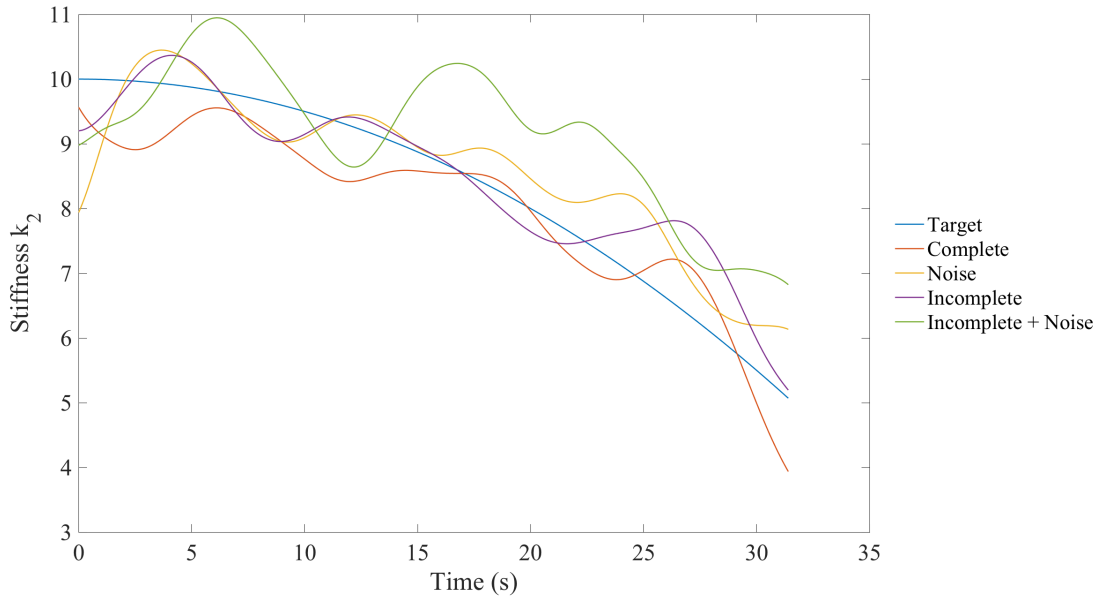

(b) Stiffness parameter k_2

Figure 9.10: Comparison between the target and the estimated stiffness parameters of the time-varying 2-DOF Duffing oscillator for four different data scenarios.

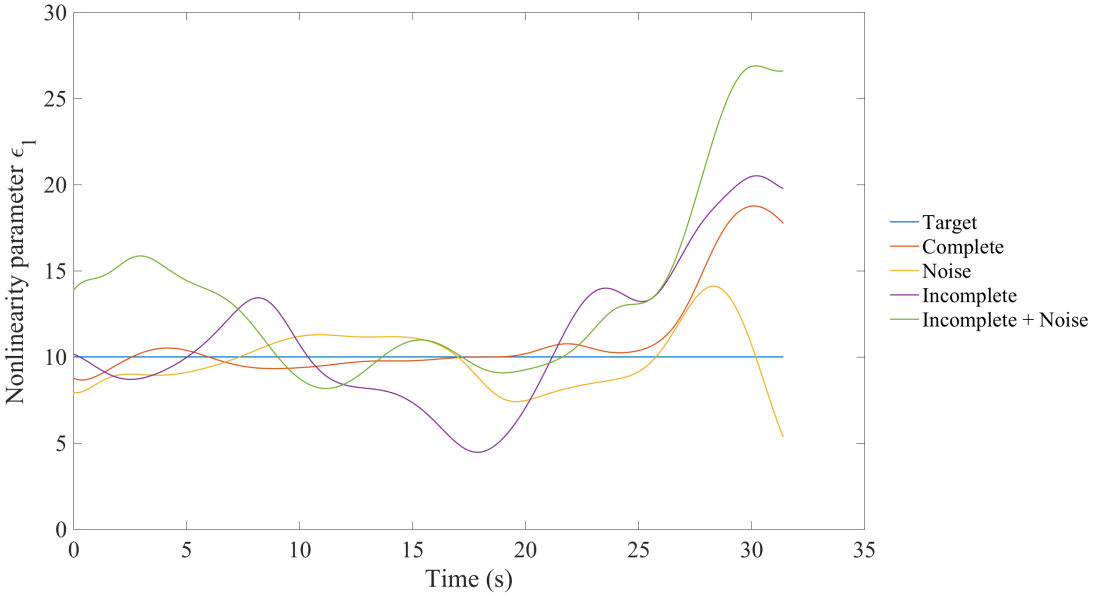

(a) Nonlinearity parameter ε_1

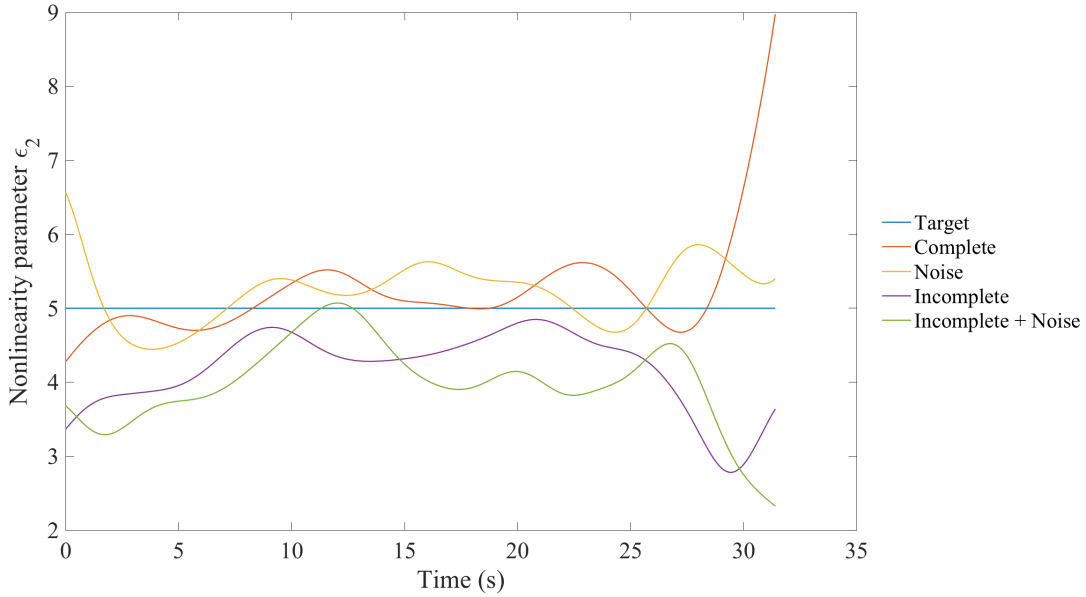

(b) Nonlinearity parameter ε_1

Figure 9.11: Comparison between the target and the estimated nonlinearity parameters of the time-varying 2-DOF Duffing oscillator for four different data scenarios.

Chapter 10

Concluding Remarks

Structural health monitoring and damage detection rely primarily on accuracy and robustness of the underlying identification techniques. Literature presents a variety of structural and mechanical system identification techniques capable of handling non-stationary time-histories, incomplete signal records, or advanced mathematical models like fractional derivative terms. Nonetheless, few of them can address all the aforementioned challenges simultaneously especially when applied to MDOF engineering systems.

The current research has focused on generalizing the recently developed MISO system identification technique for parameter identification of nonlinear and time-variant oscillators with fractional derivative terms subject to incomplete non-stationary data to MDOF systems. The MDOF problem has been recast in a way suitable for the MISO technique which was combined with a wavelet representation. Further, the L_1-norm minimization procedure based on CS theory has been utilized to determine wavelet coefficients in cases of incomplete/missing data. The wavelet coefficients are then used to calculate the time- and frequency-dependent GHW-FRFs and the unknown system parameters. Numerical validation of the proposed technique has been performed on the example of the 2-DOF Duffing oscillator with time-varying stiffness and damping, and a fractional derivative element. Numerical modeling has demonstrated robustness and reliability of the tech-

nique for different data scenarios, including noise corruption and limited availability of the data. Even though the technique fails to capture the details of the time-varying behavior of parameters, it succeeds in identifying their trend in average sense.

Future implementation of the technique may include problems of off-shore structures subject to flow-induced forces (e.g., [Raman et al., 2005, Selvam and Bhattacharyya, 2006, Spanos and Lu, 1995]). The governing equations for such structures account for various nonlinear terms of the Morison equation [Morison et al., 1950] and can potentially be capable of identifying time-varying system parameters. An improvement of the technique can be made in two regards:

i. CS minimization technique: L_p-norm minimization can be adopted to potentially improve reliability and accuracy of the MISO identification technique in cases of incomplete/limited data [Zhang et al., 2018];

ii. "Local stationarity" assumption: the technique developed herein relies on the "local stationarity" assumption, i.e. assuming that the impulse response function is short-lived. The assumption has been successfully circumvented for linear and non-linear SDOF oscillators through applying periodized GHWT in conjunction with a Galerkin scheme, and relying on the orthogonality properties of the GHW [Kong et al., 2016, Spanos et al., 2016].

Bibliography

R. P. Agarwal and D. O'Regan. *Ordinary and partial differential equations: with special functions, Fourier series, and boundary value problems*. Springer Science & Business Media, 2008.

P. Alevras and D. Yurchenko. GPU computing for accelerating the numerical path integration approach. *Comp. Struct.*, 171:46–53, 2016.

A. H.-S. Ang and W. H. Tang. *Probability Concepts in Engineering Planning and Design: Emphasis on Application to Civil and Environmental Engineering*. Wiley, New York, 2007.

L. Arnold. *Stochastic Differential Equations: Theory and Applications*. Wiley, New York, 1974.

Y. Bao, Z. Shi, X. Wang, and H. Li. Compressive sensing of wireless sensors based on group sparse optimization for structural health monitoring. *Struct. Health Monit.*, 00(0):1–14, 2017.

J. S. Bendat. *Nonlinear Systems Techniques and Applications*. John Wiley & Sons, 1998.

J. S. Bendat and A. G. Piersol. *Random Data. Analysis and Measurement Procedures*. John Wiley & Sons, 2nd edition, 1986.

J. S. Bendat and A. G. Piersol. *Engineering Applications of Correlation and Spectral Analysis*. John Wiley & Sons, 2nd edition, 1993.

J. S. Bendat, P. A. Palo, and R. N. Coppolino. A general identification technique for nonlinear differential equations of motion. *Prob. Eng. Mech.*, 7:43–61, 1992.

J. S. Bendat, R. N. Coppolino, and P. A. Palo. Identification of physical parameters with memory in non-linear systems. *Int. J. Non-Linear Mech.*, 30(6):841–860, 1995.

P. M. T. Broersen. Automatic spectral analysis with missing data. *Dig. Signal Proc.*, 16(6):754–766, 2006.

S. G. Brush. Functional integrals and statistical physics. *Rev. Modern Phys.*, 33:79–92, 1961.

E. J. Candes, J. K. Romberg, and T. Tao. Stable signal recovery from incomplete and inaccurate measurements. *Commun. Pure Appl. Math.*, 59:1207–1223, 2006a.

E. J. Candes, J. K. Romberg, and T. Tao. Robust uncertainty principles: exact signal reconstruction from highly incomplete frequency information. *Trans. Inf. Theory*, 52:489–509, 2006b.

W. Chai, A. Naess, and B. J. Leira. Filter models for prediction of stochastic ship roll response. *Prob. Eng. Mech.*, 41: 104–114, 2015.

M. Chaichian and A. Demichev. *Path Integrals in Physics: Stochastic Processes and Quantum Mechanics*. Institute of Physics Publishing, Bristol, U.K., 2001.

E. N. Chatzi and C. Papadimitriou. *Identification Methods for Structural Health Monitoring*. 2016.

S. S. Chen, D. L. Donoho, and M. A. Saunders. Atomic decomposition by basis pursuit. *J. Sci. Comput.*, 20:33–61, 1998.

Z. Chen, Y. Bao, H. Li, and B. F. Spencer Jr. A novel distribution regression approach for data loss compensation in structural health monitoring. *Struct. Health Monit.*, 00(0):1–18, 2017.

L. Cohen. *Time-Frequency Analysis*. 1995.

P. Colet, H. S. Wio, and M. San Miguel. Colored noise: A perspective from a path-integral formalism. *Phys. Rev. A*, 39(11):6094, 1989.

L. Comerford, M. Beer, and I. A. Kougioumtzoglou. Compressive sensing based stochastic process power spectrum estimation from incomplete records by utilizing an adaptive basis. *Symposium on Computational Intelligence for Engineering Solutions (CIES)*, pages 117–124, 2014.

L. Comerford, I. A. Kougioumtzoglou, and M. Beer. An artificial neural network approach for stochastic process power spectrum estimation subject to missing data. *Struct. Safety*, 52(B):150–160, 2015.

L. Comerford, I. A. Kougioumtzoglou, and M. Beer. Compressive sensing based stochastic process power spectrum estimation subject to missing data. *Prob. Eng. Mech.*, 44:66–76, 2016.

B. Davison. On Feynmann's 'integral over all paths'. *Proc. Roy. Soc. A*, 225(1161):252–263, 1954.

A. Di Matteo, I. A. Kougioumtzoglou, A. Pirrotta, P. D. Spanos, and M. Di Paola. Stochastic response determination of nonlinear oscillators with fractional derivatives elements via the Wiener Path Integral. *Prob. Eng. Mech.*, 38: 127–135, 2014.

M. Di Paola and R. Santoro. Path integral solution for non-linear system enforced by Poisson white noise. *Prob. Eng. Mech.*, 23(2-3):164–169, 2008.

M. Di Paola, A. Pirrotta, and A. Valenza. Visco-elastic behavior through fractional calculus: an easier method for best fitting experimental results. *Mech. Mater.*, 43(12):799–806, 2011.

M. Di Paola, G. Failla, A. Pirrotta, A. Sofi, and M. Zingales. The mechanically based non-local elasticity: an overview of main results and future challenges. *Philos. Trans. R. Soc. A: Math. Phys. Eng. Sci.*, 371:20120433, 2013.

D. L. Donoho. Compressed sensing. *Trans. Inf. Theory*, 52:1289–1306, 2006.

J. M. Donoso, J. J. Salgado, and M. Soler. Short-time propagators for nonlinear Fokker-Planck equations. *J. Phys. A: Math. Gen.*, 32(20):3681, 1999.

J. L. Doob. *Stochastic Processes*. Wiley, NY, 1953.

A. N. Drozdov and P. Talkner. Path integrals for Fokker-Planck dynamics with singular diffusion: Accurate factorization for the time evolution operator. *J. Chem. Phys.*, 109(6):2080–2091, 1998.

Z. Du, X. Chen, H. Zhang, and B. Yang. Compressed-sensing-based periodic impulsive feature detection for wind turbine systems. *IEEE Trans. Industr. Inform.*, 13(6):2933–2945, 2017.

S. J. B. Einchcomb and A. J. McKane. Use of Hamiltonian mechanics in systems driven by colored noise. *Phys. Rev. E*, 51(4):2974, 1995.

Y. C. Eldar and G. Kutyniok. *Compressed Sensing: Theory and Applications*. Cambridge University Press, 2012.

G. M. Ewing. *Calculus of Variations with Applications*. Dover, New York, 1985.

G. M. Feng, B. Wang, and Y. F. Lu. Path integral, functional method, and stochastic dynamical systems. *Prob. Eng. Mech.*, 7:149–157, 1992.

R. P. Feynman. Space-time approach to non-relativistic quantum mechanics. *Rev. Modern Phys.*, 20:367–387, 1948.

R. P. Feynman, A. R. Hibbs, and D. F. Styer. *Quantum Mechanics and Path Integrals, Emended Edition*. Dover Books on Physics, 2010.

V. C. Fragkoulis, I. A. Kougioumtzoglou, and A. A. Pantelous. Statistical linearization of nonlinear structural systems with singular matrices. *J. Eng. Mech.*, 142(9):04016063, 2016.

C. W. Gardiner. *Stochastic Methods: A Handbook for the Natural and Social Sciences*. Springer-Verlag Berlin Heidelberg, 2009.

I. M. Gelfand and A. M. Yaglom. Integration of functional spaces and its applications in quantum physics. *J. Math. Phys.*, 1:48–69, 1960.

I. I. Gihman and A. Skorohod. *Stochastic Differential Equations*. Springer-Verlag Berlin Heidelberg, 1972.

K. Gkoktsi and A. Giaralis. Assessment of sub-Nyquist deterministic and random data sampling techniques for operational modal analysis. *Struct. Health Monit.*, 16(5):630–646, 2017.

M. Grigoriu. *Stochastic Calculus: Applications in Science and Engineering*. Birkhäuser Basel, 2002.

E. Gudmundson, P. Stoica, J. Li, A. Jakobsson, M. D. Rowe, J. A. S. Smith, and J. Ling. Spectral estimation of irregularly sampled exponentially decaying signals with applications to RF spectroscopy. *J. Magn. Res.*, 203(1): 167–176, 2010.

P. Hänggi. Path integral solutions for non-Markovian processes. *Zeitschrift für Physik B Condensed Matter*, 75(2): 275–281, 1989.

J. B. Harley. Predictive guided wave models through sparse modal representations. *Proceedings of the IEEE*, 104(8): 1604–1619, 2016.

K. Hasselmann, T. P. Barnett, E. Bouws, H. Carlson, D. E. Cartwright, K. Eake, J. A. Euring, A. Gicnapp, D. E. Hasselmann, P. Kruseman, A. Meerburg, P. Mullen, D. J. Olbers, K. Richren, W. Sell, and H. Walden. Measurements

of wind-wave growth and swell decay during the joint North Sea wave project (JONSWAP). *Ergänzungsheft zur Deutschen Hydrographischen Zeitschrift*, A8:1–95, 1973.

X. Hong, R. J. Mitchell, S. Chen, C. J. Harris, K. Li, and G. W. Irwin. Model selection approaches for non-linear system identification: a review. *Int. J. Syst. Science*, 39(10):925–946, 2008.

J.-C. Hung. A genetic algorithm approach to the spectral estimation of time series with noise and missed observations. *Inf. Sciences*, 178(24):4632–4643, 2008.

M. Jayawardhana, X. Zhu, and R. Liyanapathirana. Compressive sensing for efficient health monitoring and effective damage detection of structures. *Mech. Syst. Signal Proc.*, 84:414–430, 2017.

S. Ji, C. Tan, P. Yang, Y.-J. Sun, D. Fu, and J. Wang. Compressive sampling and data fusion-based structural damage monitoring in wireless sensor network. *J. Supercomput.*, 74:1108–1131, 2018.

M. Kac. On distributions of certain Wiener functionals. *Trans. Amer. Math. Soc.*, 65:1–13, 1949.

K. Kanai. Semi-empirical formula for the seismic characteristics of the ground. *Bull. Earthq. Res. Inst.*, 35:309–325, 1957.

M. H. Kim, A. Tahar, Y. B. Kim, and et al. Variability of TLP motion analysis against various design methodologies/parameters. In *Eleventh Int. Offshore Polar Eng. Conf.* International Society of Offshore and Polar Engineers, 2001.

C. G. Koh and J. M. Kelly. Application of fractional derivatives to seismic analysis of base-isolated models. *Earthq. Eng. Struct. Dyn.*, 19:229–241, 1990.

A. N. Kolmogorov. Uber die Analytischen Methoden in der Wahrschein-lichkeitsrechnung. *Math. Ann.*, 104:415–458, 1931.

F. Kong, I. A. Kougioumtzoglou, P. D. Spanos, and S. Li. Nonlinear system response evolutionary power spectral density determination via a harmonic wavelets based Galerkin technique. *Int. J. Multiscale Comp. Eng.*, 14(3): 255–272, 2016.

I. A. Kougioumtzoglou. A Wiener Path Integral solution treatment and effective material properties of a class of one-dimensional stochastic mechanics problems. *J. Eng. Mech.*, 143(6):04017014, 2017.

I. A. Kougioumtzoglou and P. D. Spanos. An approximate approach for nonlinear system response determination under evolutionary stochastic excitation. *Current Science, Indian Academy of Sciences, (Special Issue, Invited)*, 97: 1203–1211, 2009.

I. A. Kougioumtzoglou and P. D. Spanos. An analytical Wiener Path Integral technique for non-stationary response determination of nonlinear oscillators. *Prob. Eng. Mech.*, 28:125–131, 2012.

I. A. Kougioumtzoglou and P. D. Spanos. An identification approach for linear and nonlinear time-variant structural systems via harmonic wavelets. *Mech. Syst. Signal Proc.*, 37:338–352, 2013.

I. A. Kougioumtzoglou and P. D. Spanos. Nonstationary stochastic response determination of nonlinear systems: A Wiener Path Integral formalism. *J. Eng. Mech.*, 140(9):04014064, 2014.

I. A. Kougioumtzoglou and P.D. Spanos. Harmonic wavelets based response evolutionary power spectrum determination of linear and non-linear oscillators with fractional derivative elements. *Int. J. Non-Linear Mech.*, 80:66–75, 2016.

I. A. Kougioumtzoglou, A. Di Matteo, P. D. Spanos, A. Pirrotta, and M. Di Paola. An efficient Wiener Path Integral technique formulation for stochastic response determination of nonlinear MDOF systems. *J. Appl. Mech.*, 82(10): 101005, 2015.

I. A. Kougioumtzoglou, K. R. M. dos Santos, and L. Comerford. Incomplete data based parameter identification of nonlinear and time-variant oscillators with fractional derivative elements. *Mech. Syst. Signal Proc.*, 94:279–296, 2017.

V. Laface, I. A. Kougioumtzoglou, G. Malara, and F. Arena. Efficient processing of water wave records via compressive sensing and joint time-frequency analysis via harmonic wavelets. *Appl. Oc. Res.*, 69:1–9, 2017.

C. Lanczos. *The Variational Principles of Mechanics*. New York: Dover Publications, 4th edition, 1986.

F. Langouche, D. Roekaerts, and E. Tirapegui. Functional integrals and the Fokker-Planck equation. *Il Nuovo Cimento B (1971-1996)*, 53(1):135–159, 1979.

S. Levit and U. Smilansky. *The path integral formulation of the semi-classical approximation and its application to nuclear reactions between heavy ions*. United States: World Scientific Pub Co., 1985.

J. Li and J. Chen. *Stochastic Dynamics of Structures*. Wiley, New York, 2009.

J. Liang, S. R. Chaudhuri, and M. Shinozuka. Simulation of nonstationary stochastic processes by spectral representation. *J. Eng. Mech.*, 133(6):616–627, 2007.

Y.-K. Lin. *Probabilistic Theory of Structural Dynamics*. Krieger Publishing Company, 1976.

M. Loéve. *Probability Theory*. Van Nostrand-Reinhold, Princeton, NJ, 1963.

S. Machlup and L. Onsager. Fluctuations and irreversible process. II. Systems with kinetic energy. *Phys. Rev.*, 91(6): 1512, 1953.

G. Malara, I. A. Kougioumtzoglou, and F. Arena. Extrapolation of random wave field data via compressive sampling. *Oc. Eng.*, 157:87–95, 2018.

A. J. McKane, H. C. Luckock, and A. J. Bray. Path integrals and non-Markov processes. I. General Formalism. *Phys. Rev. A*, 41(2):644, 1990.

A. T. Meimaris, I. A. Kougioumtzoglou, and A. A. Pantelous. A closed form approximation and error quantification for the response transition probability density function of a class of stochastic differential equations. *Prob. Eng. Mech.*, (54):87–94, 2018.

J. R. Morison, J. W. Johnson, S. A. Schaaf, and et al. The force exerted by surface waves on piles. *J. Petroleum Techn.*, 2(05):149–154, 1950.

A. Naess and J. Johnsen. Response statistics of nonlinear, compliant oshore structures by the path integral solution method. *Prob. Eng. Mech.*, 8(2):91–106, 1993.

A. Naess and V. Moe. Stationary and non-stationary random vibration of oscillators with bilinear hysteresis. *Int. J. Non-Lin. Mech.*, 31(5):553–562, 1996.

A. Naess, O. Gaidai, and S. Haver. Efficient estimation of extreme response of drag-dominated offshore structures by Monte Carlo simulation. *Ocean Eng.*, 34(16):2188–2197, 2007.

D. E. Newland. Harmonic and musical wavelets. *Proc. Roy. Soc. A*, 444(1922):605–620, 1994.

T. J. Newman, A. J. Bray, and A. J. McKane. Inertial effects on the escape rate of a particle driven by colored noise: An instanton approach. *J. Stat. Phys.*, 59(1):357–369, 1990.

B. Øksendal. *Stochastic Differential Equations*. Springer-Verlag, Berlin, 2003.

K. B. Oldham and J. Spanier. *The Fractional Calculus: Theory and Applications of Differentiation and Integration to Arbitrary Order*. Dover Publications, 2006.

V. M. Patel and R. Chellappa. *Sparse Representations and Compressive Sensing for Imaging and Vision*. Springer, New York, 2013.

C. A. Perez-Ramirez, M. Valtierra-Rodriguez, A. Moreno-Gomez, A. Domiguez-Gonzalez, R. A. Osornio-Rios, and J. P. Amezquita-Sanchez. Wavelet-based vibration data compression technique for natural frequencies identification of civil infrastructure. *IEEE Intern. Autumn Meeting Power Electron. Comput.*, 2017.

E. J. Perreault, R. F. Kirsch, and A. M. Acosta. Multiple-input, multiple-output system identification for characterization of limb stiffness dynamics. *Biol. Cybern.*, 80:327–337, 1999.

I. Petromichelakis, A. F. Psaros, and I. A. Kougioumtzoglou. Stochastic response determination and optimization of a class of nonlinear electromechanical energy harvesters: A Wiener path integral approach. *Prob. Eng. Mech.*, 53: 116–125, 2018.

W. J. Pierson and L. Moskowitz. A proposed spectral form for fully developed wind seas based on the similarity theory of S.A. Kitaigorodskii. *J. Geophys. Res.*, 69(24):5181–5190, 1964.

C. Priori, M. De Angelis, and R. Betti. On the selection of user-defined parameters in data-driven stochastic subspace identification. *Mech. Syst. Signal Proc.*, 100:501–523, 2018.

A. Prochazka, J. Uhlir, P. J. W. Rayner, and N. G. Kingsbury. *Signal Analysis and Prediction*. 1998.

A. F. Psaros, O. Brudastova, G. Malara, and I. A. Kougioumtzoglou. Wiener path integral based response determination of nonlinear systems subject to non-white, non-Gaussian, and non-stationary stochastic excitation. *J. Sound Vibr.*, 433:314–333, 2018a.

A. F. Psaros, I. A. Kougioumtzoglou, and I. Petromichelakis. Sparse representations and compressive sampling for enhancing the computational efficiency of the Wiener path integral technique. *Mech. Syst. Signal Proc.*, 111:87–101, 2018b.

S. Qian. *Introduction to Time-Frequency and Wavelet Transforms*. 2002.

S. Raman, S. C. S. Yim, and P. A. Palo. Nonlinear model for sub- and superharmonic motions of a MDOF moored structure, Part 1 - system identification. *J. Offshore Mech. Arctic Eng.*, 127:283–290, 2005.

E. Reynders. System identification methods for (operational) model analysis: review and comparison. *Arch. Comput. Methods Eng.*, 19:51–124, 2012.

H. J. Rice and J. A. Fitzpatrick. A generalized technique for spectral analysis of non-linear systems. *Mech. Syst. Signal Proc.*, 2:195–207, 1988.

H. Risken. *The Fokker-Planck Equation. Methods of Solution and Applications*. Springer-Verlag, Berlin, 1996.

J. B. Roberts and P. D. Spanos. Stochastic averaging: An approximate method of solving random vibration problems. *Int. J. Non-Lin. Mech.*, 21(2):111–134, 1986.

J. B. Roberts and P. D. Spanos. *Random Vibration and Statistical Linearization*. Courier Corporation, 2003.

R. Y. Rubinstein and D. P. Kroese. *Simulation and the Monte Carlo Method*. Wiley, Hoboken, NJ, 2nd edition, 2007.

J. Sabatier, O. P. Agrawal, and J. A. Tenreiro Machado. *Advances in Fractional Calculus: Theoretical Developments and Applications in Physics and Engineering*. 1st edition, 2007.

E. Sejdic, I. Orovic, and S. Stankovic. Compressive sensing meets time-frequency: an overview of recent advances in time-frequency processing of sparse signals. *Dig. Signal Proc.*, 77:22–35, 2018.

R. P. Selvam and S. K. Bhattacharyya. System identification of a coupled two DOF moored floating body in random ocean waves. *J. Offshore Mech. Arctic Eng.*, 128:191–202, 2006.

L. F. Shampine, I. Gladwell, and S. Thompson. *Solving ODEs with Matlab*. Cambridge University Press, 2003.

M. Shinozuka. Structural response variability. *J. Eng. Mech.*, 113(6):825–842, 1987.

M. Shinozuka and G. Deodatis. Simulation of stochastic processes by spectral representation. *Appl. Mech. Rev.*, 44: 191–204, 1991.

T. T. Soong and M. Grigoriu. *Random Vibration of Mechanical and Structural Systems*. Prentice Hall, New Jersey, 1993.

H. Sousa and Y. Wang. Sparse representation approach to data compression for strain-based traffic load monitoring: A comparative study. *Measurement*, 122:630–637, 2018.

P. D. Spanos. Filter approaches to wave kinematics approximation. *Appl. Ocean Res.*, 8(1):2–7, 1986.

P. D. Spanos and T. W. Chen. Random response to flow-induced forces. *J. Eng. Mech.*, 107(EM6):1173–1190, 1981.

P. D. Spanos and I. A. Kougioumtzoglou. Harmonic wavelets based statistical linearization for response evolutionary power spectrum determination. *Prob. Eng. Mech.*, 27(1):57–68, 2012.

P. D. Spanos and R. Lu. Nonlinear system identification in offshore structural reliability. *J. Offshore Mech. Arctic Eng.*, 117:171–177, 1995.

P. D. Spanos and B. A. Zeldin. Monte Carlo treatment of random fields: A broad perspective. *Appl. Mech. Rev.*, 51 (3):219–237, 1998.

P. D. Spanos, R. Ghosh, L. D. Finn, and J. Halkyard. Coupled analysis of a spar structure: Monte carlo and statistical linearization solutions. *J. Offshore Mech. Arctic Eng.*, 127(1):11–16, 2005.

P. D. Spanos, I. A. Kougioumtzoglou, and C. Soize. On the determination of the power spectrum of randomly excited oscillators via stochastic averaging: An alternative perspective. *Prob. Eng. Mech.*, 26(1):10–15, 2011.

P. D. Spanos, F. Kong, J. Li, and I. A. Kougioumtzoglou. Harmonic wavelets based excitation–response relationships for linear systems: A critical perspective. *Prob. Eng. Mech.*, 44:163–173, 2016.

M. Stephane. *A Wavelet Tour of Signal Processing*. 3rd edition, 2009.

R. L. Stratonovich. *Conditional Markov Processes and Their Applications to the Theory of Optimal Control*. Amer. Elsevier, New York, 1968.

H. Tajimi. Statistical method of determining the maximum response of building structure during an earthquake. *Proc. Second WCEE*, 2:781–798, 1960.

V. E. Tarasov. Fractional mechanics of elastic solids: continuum aspects. *J. Eng. Mech.*, 143(5):D4016001, 2016.

J. A. Tropp and A. C. Gilbert. Signal recovery from random measurements via orthogonal matching pursuit. *Trans. Inf. Theory*, 53:4655–4666, 2007.

F. E. Udwadia and D. K. Sharma. Some uniqueness results related to building structural identification. *J. Appl. Math.*, 34(1):104–118, 1978.

Y. Wang, L. Jian, and S. Petre. *Spectral Analysis of Signals: The Missing Data Case*. Morgan & Claypool, 2006.

M. F. Wehner and W. Wolfer. Numerical evaluation of path-integral solutions to Fokker-Planck equations. *Phys. Rev. A*, 27(5):2663, 1983.

F. W. Wiegel. Path integral methods in statistical mechanics. *Phys. Reports*, 16:57–114, 1975.

N. Wiener. The average of an analytic functional. *Proc. Natl. Acad. Sci.*, 7:253–260, 1921.

H. S. Wio. *Path Integrals for Stochastic Processes: An Introduction*. World Scientific, 2013.

H. S. Wio, P. Colet, M. San Miguel, L. Pesquera, and M. A. Rodriguez. Path-integral formulation for stochastic processes driven by colored noise. *Phys Rev. A*, 40(12):7312, 1989.

C. Xu, Z. Yang, X. Chen, S. Tian, and Y. Xie. A guided wave dispersion compensation method based on compressed sensing. *Mech. Syst. Signal Proc.*, 103:89–104, 2018.

Y. Yang and S. Nagarajaiah. Robust data transmission and recovery of images by compressed sensing for structural health diagnosis. *Struct. Control Health Monit.*, 24:1856, 2017.

R. Yao, S. N. Pakzad, and P. Venkitasubramaniam. Compressive sensing based structural damage detection and localization using theoretical and metaheuristic statistics. *Struct. Control Health Monit.*, 24:1881, 2017.

B. A. Zeldin and P. D. Spanos. Spectral identification of nonlinear structural systems. *J. Eng. Mech.*, 124:728–733, 1998.

Y. Zhang, L. Comerford, I. A. Kougioumtzoglou, and M. Beer. L_p-norm minimization for stochastic process power spectrum estimation subject to incomplete data. *Mech. Syst. Signal Proc.*, 101:361–376, 2018.

Z. Zhang, H. Wang, Y. Chang, X. Liang, and Y. Xu. L1/2 regularization. *Sc. China Inf. Sci.*, 6:1159–1169, 2010.

W. Q. Zhu. Recent developments and applications of the stochastic averaging method in random vibration. *Appl. Mech. Rev.*, 49(10S):72–80, 1996.